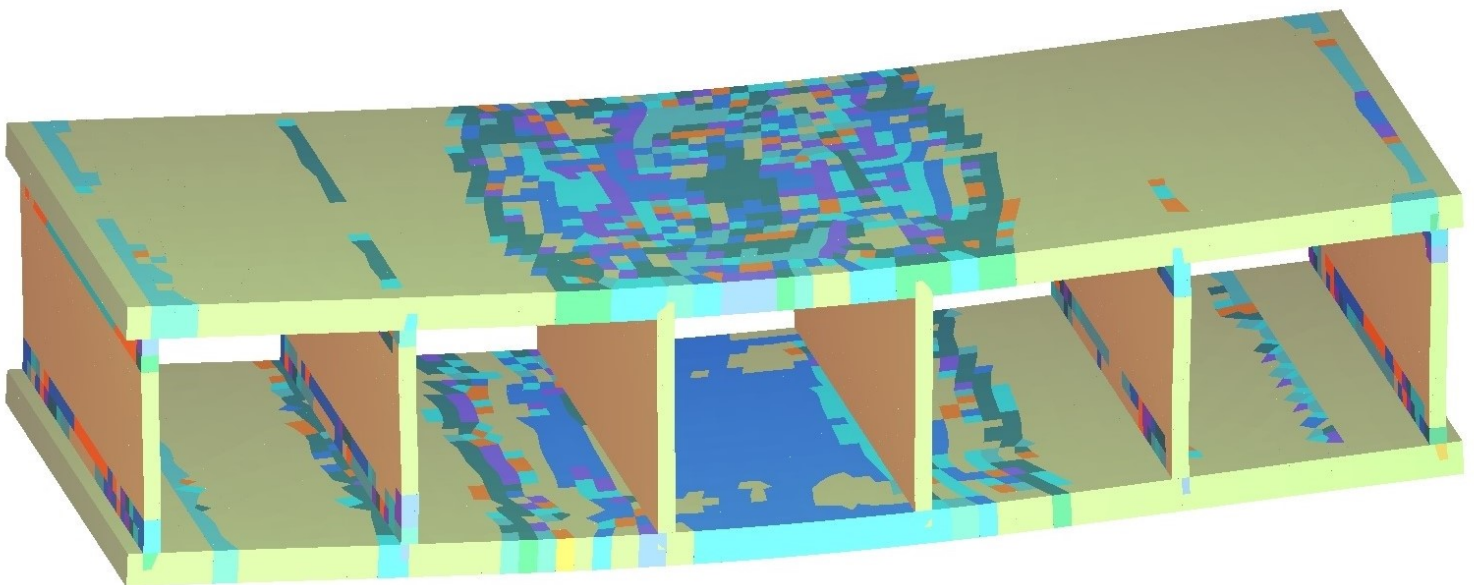


Virtual fatigue verification of Glass Fibre-Reinforced Polymer components for civil engineering applications

Mathieu Koetsier

Technische Universiteit Delft



Virtual fatigue verification of Glass Fibre-Reinforced Polymer components for civil engineering applications

by

Mathieu Koetsier

to obtain the degree of Master of Science
at the Delft University of Technology,
to be defended publicly on Monday August 2, 2021 at 9:30 AM.

Student number: 4583930
Project duration: November 9, 2020 – August 2, 2021
Thesis committee: dr. Marko Pavlovic, TU Delft, Chair of the committee
ir. Angeliki Christoforidou, TU Delft, supervisor
ir. Weikang Feng, TU Delft, supervisor
dr. ir. Frans van der Meer, TU Delft, supervisor
ir. Liesbeth Tromp, Royal Haskoning DHV, supervisor

An electronic version of this thesis is available at <http://repository.tudelft.nl/>.

Abstract

The increase in road traffic intensity and loading capacity of a truck over the last decades causes fatigue problems in existing bridges built in the 1960s and 1970s. For steel bridges, this means that the deck structure does not meet the current demands. A solution would be to replace these existing deck structures with [Glas Fibre-Reinforced Polymer \(GFRP\)](#) sandwich webcore deck panels. However, the ministry of infrastructure in the Netherlands has voiced its concern about the fatigue performance and displacements of these deck panels under the high traffic load and intensity. Furthermore, the knowledge about the fatigue performance of [GFRP](#) deck panels, applied in the main road network, is still limited. At the time of writing this report, the technical committee, CEN/TC 250 (responsible for developing structural eurocodes), establishes a technical design specification for [Fibre-Reinforced Polymer \(FRP\)](#) structures. This technical specification requires full-scale fatigue testing due to the complex failure modes that can occur. General fatigue damage summation methods like Palmgren-Miner [30, 41] are not allowed by this technical specification. This report discusses the development of [Virtual Fatigue Stiffness Simulation \(ViFaSS\)](#), a numerical non-linear fatigue stiffness reduction model that can predict the fatigue performance of in-plane stress dominated Glass Fibre-Reinforced Polymer components, with a wide range of lay-up compositions, based on existing knowledge and experiments, including the damage development under multi-axial stress states and stress redistribution. The damage development includes damage accumulation dependency on damage history and damage development dependency on the load type, e.g. [Tension-Tension \(T-T\)](#) or [Compression-Compression \(C-C\)](#). With the low utilisation of the material strength in civil engineering applications, the research is limited to the stiffness degradation of the material. The numerical model is coupled with the [Finite Element \(FE\)](#) software SOFiSTiK where the component is modelled with shell finite elements. The fatigue material response is characterised on a unidirectional ply level based on principal ply directions and based on experimental results from the Optidat program [36]. The coupon response predicted by [ViFaSS](#) for constant amplitude [T-T](#) and bending fatigue loading was in reasonable agreement with experimental results. For future work it is recommended to extend the model with the ability to use non-linear material behaviour and to include the strength degradation caused by fatigue.

Keywords:

- (a) Glass fibre-reinforced polymer
- (b) Fatigue
- (c) Virtual fatigue verification
- (d) Stiffness prediction

Preface

Dear reader,

The MSc thesis "Virtual fatigue verification of Glass Fibre-Reinforced Polymer components for civil engineering applications" laying in front of you represents a great deal of my knowledge and enthusiasm obtained during the inspiring five years at the Delft University of Technology. During my thesis, I explored multiple capabilities of myself, and it felt like a constant path of growth.

The support and collaboration with leading experts in the field of FRP was a grateful experience. Therefore, I would mention some of who have greatly supported me here by name. Starting with the committee members. First, I want to thank Marko Pavlovic for the time, guidance and judgement he provided, Liesbeth Tromp for sharing her knowledge and keeping me critical about the steps I made and how I wanted to proceed, Angeliki Christoforidou for her endless support and for providing me with all the information I needed, Frans van der Meer for the friendly and insightful discussions about the complex matter, Weikang Feng for the reviewing of my report. Besides my committee, I would like to thank Ton Boeters and Lieuwe Cornellisen from Royal Haskoning DHV for their input during our meetings.

During this thesis, I developed a fair amount of knowledge regarding the fatigue behaviour of GFRP. Despite that, there is no straightforward answer to my research question. However, this tells me that I did my research in the correct field of expertise and was able to contribute to future research.

*Mathieu Koetsier
Delft, June 2021*

Contents

Abstract	iii
List of Figures	ix
List of Tables	xi
1 Introduction	1
1.1 Project motivation	1
1.2 Problem statement	2
1.3 Scope	3
1.4 Research question	4
1.4.1 Main research question	4
1.4.2 Sub research questions	4
1.5 Aim and Objectives	6
1.6 Research method	7
2 Literature review	9
2.1 Fatigue behaviour of GFRP	9
2.1.1 Type of damage in fibre-reinforced polymers	9
2.1.2 Influence of load conditions	10
2.1.3 Constant amplitude loading	12
2.1.4 Variable amplitude loading	14
2.2 Fatigue life modelling approaches	17
2.2.1 Progressive fatigue damage modelling approaches in literature	18
2.3 Fatigue assesment according to design recommendations	22
2.3.1 CUR 96 recommendation 2019	22
2.3.2 Prospect for New Guidance in the Design of FRP Structures	22
2.3.3 Eurocode proposal prCENTS19101 based on draft version from 2020-11-04	23
2.3.4 Guideline for the Certification of Offshore Wind Turbines GL 2012	24
2.3.5 Conclusion	25
2.4 Conclusion	26
3 Numerical non-linear fatigue stiffness reduction model development	27
3.1 Implementation in the design process	28
3.2 Experimental input requirements	30
3.3 Model description	31
3.3.1 Module FE analysis and classical laminate theory	33
3.3.2 Module lifetime estimation of UD plies	34
3.3.3 Module element selection by a Artificial Neural Network	36
3.3.4 Module gradual stiffness degradation	38
3.3.5 Visualisation of results	46
4 Numerical non-linear fatigue stiffness reduction model validation	47
4.1 Model validation on MD laminate under T-T loading	47
4.1.1 Introduction	47
4.1.2 Computational procedure settings	50
4.1.3 Verification of FE model	50
4.1.4 Results and discussion	52
4.1.5 Conclusion	58

4.2	Model validation on MD laminate under bending fatigue	59
4.2.1	Introduction	59
4.2.2	Computational procedure	61
4.2.3	Verification of FE model	61
4.2.4	Results and discussion	62
4.2.5	Conclusion	66
4.3	Model limitations	67
5	Virtual stiffness based fatigue degradation of a sandwich webcore panel	69
5.1	Introduction	69
5.2	Computational procedure	72
5.3	Results and discussion	73
5.3.1	Results and discussion of virtual fatigue local bending analysis	73
5.3.2	Results and discussion of virtual fatigue equivalent design case analysis.	77
5.4	Description of validation procedure	80
6	Conclusions and Recommendations	81
6.1	Conclusions	81
6.2	Recommendations	84
A	Appendix CLT validation	87
A.1	Validation of the ABD matrix	87
A.2	Validation of the deformations	90
A.3	Validation of the ply stresses	93
B	Appendix constant life surface validation	99
C	Appendix S-N formulations	109
C.1	Parallel to fibres	109
C.2	Transverse to fibres	115
C.3	In-plane shear	119
D	Appendix Verification of primary stiffness degradation	121
E	Appendix degradation report	127
F	Appendix design webcore panel specimen	145
	Bibliography	149

List of Figures

1.1	Flow diagram ViFaSS analysis procedure tool	8
2.1	Crack propagation at interface [12].	10
2.2	Different failure mechanisms according to Talreja [56].	11
2.3	Debonding propagation.	11
2.4	Overview debonding influence glst-c and T-T [14].	12
2.5	Progressive buckling under cyclic compression load. [57]	12
2.6	constant life diagram (CLD) [44].	13
2.7	Deriving a CLD from S-N curve [5].	14
2.8	Overview of cycle counting [64].	14
2.9	"Schematic illustration of the evolution of damage and the sequence effect in block amplitude loading of cross-ply laminates, and the qualitative influence on the stress profile in the critical 0° plies." [15].	17
2.10	Overview Stiffness degradation stages [61].	18
2.11	Progressive damage model of Shokrieh and Lessard.	19
2.12	Progressive damage model of Passipoularidis et al..	20
3.1	Flowchart Fatigue assesment according to TS19101 and implementation of Progressive damage model.	29
3.2	Flow diagram numerical fatigue reduction model	32
3.3	Reference axis system used in this work, obtained from TS19101	33
3.4	Flowchart of the Classical Laminate Theory (CLT) module	33
3.5	Constant life surface construction.	34
3.6	S-N curve transverse to fibers for T-T	35
3.7	Visual representation of the Artificial Neural Network	36
3.8	FE model to compare Artificial Neural Network (ANN) configurations	37
3.9	Visual presentation of the damage interaction procedure, for the case $n_6 = n_2$	39
3.10	In-plane transverse modulus damage for compression load conditions for unidirectional (UD) glass-epoxy composite.	40
3.11	In-plane transverse modulus damage for tension load conditions for UD glass-epoxy composite.	40
3.12	In-plane shear modulus damage for UD glass-epoxy composite.	41
3.13	Damage summation high-low sequence UD ply.	42
3.14	Damage summation low-high sequence UD ply.	42
3.15	Marco-Starkey sequence effect, obtained from [15]	43
3.16	Stiffness reduction experiments used in the determination of α and β , obtained from [11]	43
3.17	Visualisation of the maximum allowable step size distribution	44
4.1	Geometrical representation of the coupon specimen [36]	48
4.2	Stiffness degradation measurements $[(\pm 45, 0)_4, \pm 45]$ [10]	48
4.3	Mechanical model	49
4.4	FE model verification	51
4.5	S-N formulation MD2 specimen	52
4.6	Stiffness degradation simulations (a) and stress distribution at $n/N=1$ (b)	54
4.7	Stiffness degradation simulations (a) and stress distribution at $n/N=1$ (b)	55
4.8	Visualisation of damage interaction relation, stiffness reduction versus \log_{10} of the number of cycles.	56
4.10	Simulation of block loading	57

4.11 Geometrical representation of the coupon specimen, $L=54[\text{mm}]$ and a is assumed to be $48[\text{mm}]$ after calibration of the force.	59
4.12 Force degradation measurements $[\pm 45]_8$ [62]	60
4.13 Mechanical model bending fatigue	60
4.14 Stress distribution close at the support.	62
4.15 Validation of force degradation simulation $[\pm 45]_8$, underlay from [62]	63
4.16 Stress distribution at the support after 1 cycle, in local ply coordinates.	63
4.17 Stress distribution at the support after 100 cycle, in local ply coordinates.	64
4.18 Stress distribution at the support after 1000 cycle, in local ply coordinates.	64
4.19 Stress distribution at the support after 10000 cycle, in local ply coordinates.	64
4.20 Stress distribution at the support after 100000 cycle, in local ply coordinates.	65
4.21 Stress distribution at the support after 400000 cycle, in local ply coordinates.	65
4.22 Shear stress-strain response of $[\pm 45^\circ]_s$ [63].	67
5.2 Tyre pressure distribution according to [29].	72
5.3 Finite element model local bending	73
5.5 Damage development of bottom and top face sheet. Colours represent different material properties. There is no related colour scale.	75
5.6 Deflection versus the number of cycles	76
5.7 Finite element model parallel	77
5.8 Damage development of bottom and top face sheet. Colours represent different material properties. There is no related colour scale.	78
5.9 Deflection versus the number of cycles	79
C.1 S-N curve parallel to fibers for T-T	113
C.2 S-N curve parallel to fibers for Tension-Compression (T-C)	113
C.3 S-N curve parallel to fibers for C-C	114
C.4 S-N curve transverse to fibers for T-T	117
C.5 S-N curve transverse to fibers for T-C	117
C.6 S-N curve transverse to fibers for C-C	118
C.7 S-N curve for in-plane shear $R=0.1$	119

List of Tables

3.1	Required static material properties	30
3.2	Comparison multiple ANN configurations	37
3.3	Stiffness degradation parameters obtained from [11]	40
4.1	Lay-up configuration Optidat GEV207 (MD2)	49
4.2	Material properties UD and multidirectional (MD) glass-epoxy laminate with V_f 52%	50
4.3	Lay-up configuration	61
4.4	Material properties UD and MD glass-epoxy laminate with V_f 48% (adjusted) and 52% (original)	61
5.1	Lay-up configuration face sheets GFRP anisotropic laminate $[90/0_3/45/-45/0_2]_s$	71
5.2	Lay-up configuration webs GFRP quasi-isotropic laminate $[0/90/45/-45]_s$	71
5.3	Determination of load application	72
6.1	Required static material properties	82
C.1	Fatigue life test results parallel to fibres for R=0.1	109
C.2	Fatigue life test results parallel to fibres for R=-1.0	110
C.3	Fatigue life test results parallel to fibres for R=10.0	112
C.4	Fatigue life test results transverse to fibres for R=0.1	115
C.5	Fatigue life test results transverse to fibres for R=-1.0	115
C.6	Fatigue life test results transverse to fibres for R=10.0	116
C.7	Fatigue life test results in-plane shear for R=0.1	119

Glossary

Symbols | [A](#) | [C](#) | [F](#) | [G](#) | [M](#) | [S](#) | [T](#) | [U](#) | [V](#)

Symbols

- $E_{1,c}$
parallel compression stiffness of UD plies. [30](#), [82](#)
- $E_{1,t}$
parallel tensile stiffness of UD plies. [30](#), [82](#)
- E_1
parallel modulus of UD ply. [50](#), [61](#)
- $E_{2,c}$
transverse compression stiffness of UD plies. [30](#), [82](#)
- $E_{2,t}$
transverse tensile stiffness of UD plies. [30](#), [82](#)
- E_2
transverse modulus of UD ply. [31](#), [50](#), [61](#)
- E_x
modulus of the laminate in x-direction. [50](#), [61](#)
- E_y
modulus of the laminate in y-direction. [50](#), [61](#)
- G_{12}
shear modulus of UD ply. [31](#), [61](#)
- G_{xy}
shear modulus of the laminate. [50](#), [61](#)
- V_f
Fibre volume. [xi](#), [50](#), [61](#), [62](#), [71](#), [80](#)
- ν_{12}
Poisson's ratio 12-direction. [30](#), [50](#), [61](#), [82](#)
- ν_{21}
Poisson's ratio 21-direction. [30](#), [50](#), [61](#), [82](#)
- σ_a
cyclic stress amplitude. [13](#), [15](#), [34](#), [35](#)
- σ_m
mean cyclic stress. [13](#), [34](#), [35](#)
- σ_x
Stress parallel to fibre direction. [52–56](#), [58](#), [81](#), [84](#)

σ_{11} longitudinal stress in a ply. [31](#), [40](#) σ_{22} transverse stress in a ply. [31](#), [40](#) σ_{max} maximum stress. [10](#), [13](#), [41](#), [62](#) σ_{min} minimum stress. [10](#), [13](#) τ_{12} shear stress in a ply. [31](#)**A****ANN**Artificial Neural Network. [ix](#), [xi](#), [31](#), [36](#), [37](#), [72](#)**ASTM**American Society for Testing Materials. [34](#)**C****C-C**Compression-Compression. [iii](#), [x](#), [11](#), [13](#), [39](#), [62](#), [66](#), [80](#), [83](#), [114](#), [118](#)**CA**constant amplitude. [4](#), [6](#), [12](#), [13](#), [15](#), [17](#), [26](#), [81](#)**CFRP**Carbon Fibre-Reinforced Polymer. [16](#)**CLD**constant life diagram. [ix](#), [13](#), [14](#), [19](#), [21–23](#), [26](#), [34](#)**CLS**constant life surface. [34](#), [35](#)**CLT**Classical Laminate Theory. [ix](#), [31](#), [33](#), [39](#), [49](#), [50](#), [60](#), [61](#)**F****FE**Finite Element. [vii](#), [31](#), [33](#), [71](#)**FE**Finite Element. [iii](#), [vii–ix](#), [7](#), [31](#), [36](#), [37](#), [44](#), [46](#), [49–51](#), [60](#), [61](#), [67](#), [72](#), [73](#), [77](#), [82](#), [84](#), [85](#)**FRP**Fibre-Reinforced Polymer. [iii](#), [v](#), [1](#), [2](#), [7](#), [9](#), [22](#), [23](#), [28](#)**G**

GFRP

Glas Fibre-Reinforced Polymer. [iii](#), [v](#), [xi](#), [1–4](#), [6](#), [7](#), [9](#), [24](#), [26–28](#), [31](#), [60](#), [69](#), [71](#), [81](#), [83](#), [85](#)

M**MD**

multidirectional. [xi](#), [35](#), [47](#), [49](#), [50](#), [52](#), [53](#), [58–61](#), [81](#), [83](#)

S**S-N**

Stress range vs. Number of load cycles. [ix](#), [x](#), [11–14](#), [17](#), [21](#), [23–26](#), [30](#), [31](#), [34](#), [35](#), [52](#), [62](#), [82](#), [109](#), [113–115](#), [117–119](#)

T**T-C**

Tension-Compression. [x](#), [11](#), [13](#), [113](#), [117](#)

T-T

Tension-Tension. [iii](#), [ix](#), [x](#), [10–13](#), [34](#), [35](#), [39](#), [47](#), [49](#), [58](#), [59](#), [62](#), [80](#), [81](#), [83](#), [84](#), [113](#), [117](#)

U**UCS**

ultimate compression stress. [13](#), [14](#)

UD

unidirectional. [ix](#), [xi](#), [18](#), [19](#), [22](#), [26](#), [27](#), [30](#), [31](#), [34](#), [40–44](#), [47](#), [49](#), [50](#), [52](#), [53](#), [56](#), [58–62](#), [66](#), [67](#), [75](#), [79](#), [80](#), [82](#), [84](#)

UTS

ultimate tensile stress. [13](#), [14](#)

V**VA**

variable amplitude. [4](#), [6](#), [12](#), [14](#), [15](#), [26](#), [27](#), [31](#), [81](#)

ViFaSS

Virtual Fatigue Stiffness Simulation. [iii](#), [ix](#), [8](#), [27](#), [28](#), [31](#), [33–36](#), [38](#), [44](#), [45](#), [47](#), [52](#), [53](#), [57–59](#), [62](#), [66](#), [67](#), [69](#), [73](#), [77](#), [80–85](#)

1

Introduction

1.1. Project motivation

Rijkswaterstaat, the ministry of infrastructure in the Netherlands, has several steel bridges in their management and a large part of these bridges are built in the 1960s and 1970s. For several decades road traffic has been increasing. The number of lorries is growing faster than cars and due to the developments in the truck industry, the loading capacity has increased. These heavy trucks are governing for the lifespan of the bridges. Also, the exceptional heavy transportation with exemptions has a large effect on the lifespan [19, 20]. Steel bridges are prone to fatigue, especially with an increase in loading magnitude and the number of cycles. For the steel bridges in the main road network, this means that they do not meet current demands. Rijkswaterstaat has 274 fixed and movable steel bridges in their domain. In 2008, 25 of those bridges coped with serious fatigue problems. Because of the increase in traffic intensity, all of the steel bridges will suffer from fatigue damage in the upcoming years. [19].

The current procedure Rijkswaterstaat uses to deal with the problem is to apply a high strength concrete topping on the existing steel deck structure. This results in lower stresses in the steel structure caused by local loading. However, the added concrete topping increases the permanent load on the structure and is not a valid option for movable bridges [48]. More desirable would be to use a material with a favourable weight to strength ratio.

An alternative solution to renovate these bridges is such a way that they fulfil the current requirements is to apply a fibre-reinforced polymer (FRP) deck on the main steel structure. However, Rijkswaterstaat has pointed out that they still have some concerns about the fatigue performance and displacements of these deck panels, especially with the high traffic load and intensity. The limited knowledge/data about the longterm behaviour of FRP applied in construction projects and their experience with the fatigue problems of the existing steel bridges is what causes these concerns. Noël and Jollivet et al. [26, 38] indicate that the increased loading results in more and more challenges in good fatigue performance of composites.

Royal Haskoning DHV is an engineering consultancy firm in the Netherlands. It has valuable expertise in the field of [Fibre-Reinforced Polymer \(FRP\)](#) for the design principle, the design review and quality control. Therefore, they are keen on developing a more thorough understanding of the fatigue performance of [Glas Fibre-Reinforced Polymer \(GFRP\)](#).

1.2. Problem statement

For a management body, as Rijkswaterstaat, asset management is an important aspect. Therefore, the predictability of the structure is of value to plan, e.g. maintenance and to minimise unforeseen effects [66]. To consider GFRP deck panels as a competitive alternative, it is desirable to understand the fatigue behaviour in more detail. The application of FRP panels is favourable due to their lightweight advantages. If the prediction of failure has a considerable uncertainty, this will result in large safety factors leading to extra self-weight [59]. With the application of FRP deck panels in the main road network, the material will be heavily loaded, with a large number of cycles. When designing these deck panels, it is of interest to predict the fatigue sensitive points in the structure. What type of failure can be expected in these details? What magnitude of damage is allowed? What is their lifetime? And is inspection and repair possible? These are questions that are of interest.

The knowledge of the fatigue performance of GFRP deck panels, applied in the main road network, is still limited. Unlike metals where the damage propagation mostly occurs in a single-mode, fatigue in FRP exists of multiple damage mechanisms. Fatigue failure, therefore, is mostly an effect of the accumulation of multiple damage mechanisms. Because the polymer matrix behaves like a viscoelastic material, the polymer is sensitive to temperature changes and creep effects [27]. The above-described aspects make it difficult to predict the fatigue behaviour.

At the time of writing this report, the technical committee, CEN/TC 250 (responsible for developing structural eurocodes), establishes a design specification for FRP structures. For the fatigue verification, the design specification requires qualification testing of new products and proof testing for the specific application of the product, e.g. a web core sandwich deck panel with project-specific geometry and boundary conditions.

It requires testing because members can exhibit several complex fatigue failure modes. In most cases, failure occurs in component connections, i.e. at singularities with stress concentrations. Those stress concentrations and the fatigue resistance of those connections are challenging to obtain. Therefore, testing on member level is required; stress concentrations and imperfections will be included in the verification. For the preliminary design, the design recommendation does not give any guidance.

Testing is a costly way of verifying the fatigue design resistance. Therefore, it is desirable to better predict the fatigue performance during the design stage. Focus on the fatigue behaviour of GFRP deck panels, applied in the main road network, can help increase the competitiveness of this alternative.

1.3. Scope

Some limitations and boundaries are set to achieve high-quality research in the prescribed amount of time. The research in this study will be focussed on fatigue verification in the predesign stage of civil engineering components, e.g. web core sandwich deck panels dominated by in-plane stresses. This study will make use of existing knowledge found in the literature and existing test results. Performing experiments is not within the scope of this study.

Research is limited to the fatigue behaviour of the **GFRP** material and the prediction on component level. Where the behaviour of the components can be described mainly by in-plane stresses.

1.4. Research question

From the problem statement, the following main research question and subquestions are drafted.

1.4.1. Main research question

How can the fatigue performance of in-plane stress dominated Glass Fibre-Reinforced Polymer components, with arbitrary lay-up compositions, be modelled based on existing knowledge and experiments, including the damage development under complex stress states and stress redistribution?

1.4.2. Sub research questions

To help answering the main question several sub questions are addressed.

1. How does damage due to cyclic fatigue loading influence GFRP stiffness properties?

When investigating the fatigue performance in more depth, a good understanding of the fatigue behaviour of glass fibre reinforced polymers is required. General fatigue behaviour of GFRP is investigated in the field of mechanical engineering, wind energy, and aerospace engineering [38]. Therefore a good understanding can be obtained with the help of a literature study.

2. What are relevant aspects for predicting damage initiation, damage growth in GFRP material dominated by in-plane stress caused by constant amplitude (CA) and variable amplitude (VA) fatigue loading and what are available prediction methods proposed in the literature?

Because the fatigue behaviour of composites exists of multiple interactive damage mechanisms, there is no straightforward failure mechanism or simple relation. To gain more insight into the behaviour of the fatigue sensitive properties, it is of interest to understand what type of damage can be expected under different load conditions. Much knowledge can be obtained from current research; [17] [16][15] [60].

In a civil engineering component such as a web core sandwich deck panel, multiple load configurations occur and therefore is loaded by a VA loading. Most of the time serviceability limit state governs in the design due to the low stiffness to height ratio. The GFRP's stiffness properties also decrease due to fatigue [39]. Therefore, stress redistributions can occur on a local scale. It is of interest to find the aspects, which are relevant to incorporate in the model to capture these effects.

Much research is performed on the development of models to predict material degradation due to cyclic loading of the GFRP material [40] [10]. Most of those models are used for small scale specimens and try to predict the complex damage accumulation. It is valuable to understand the proposed models and the theory that is incorporated. This gives insight into the contribution of different aspects and can help make choices regarding the model.

3. How can those relevant aspects be incorporated into a model such that engineers can incorporate those in the predesign?

Understanding the physical behaviour and the influence on the structural response and incorporating this in the model is challenging. Design choices should be made on how to capture these effects in the model. It is desired to model these effects as good as possible and to minimise the calculation time.

4. What are the minimum input requirements for such a model?

The fatigue material response will be needed to have the ability to model the fatigue behaviour of GFRP materials. It will be helpful to have an overview of the minimal required properties needed to indicate the experimental effort needed to use this model for a different material.

5. What does such a model predict when the local fatigue effects of wheel loading on a sandwich deck panel are simulated?

After the step of validation on coupon, experiments are performed. The expectation would be that the fatigue performance of large scale objects, such as sandwich deck panels, is predictable. To visualise this expectation, it will be valuable to simulate the fatigue degradation under local wheel loading and generate a virtual test outcome which can later be compared with experimental results.

1.5. Aim and Objectives

This study aims to predict and understand the **GFRP** fatigue performance in more detail by considering multiple relevant aspects like: damage development under multi-axial stresses, stress redistribution, etc. In an automated, iterative numerical tool that allows designers to consider more relevant elements, the designer can better predict the fatigue performance and increase the probability of passing the required qualification testing. The following objectives will contribute to the aim of this study.

1. Literature review of state-of-the-art fatigue in **GFRP**.
 - Fatigue behaviour of **GFRP**
 - Fatigue under **CA** and **VA** loading
 - Fatigue life modelling approaches
 - Review of current and new design codes
2. Numerical fatigue reduction model
 - Development of a fatigue damage algorithm that makes, where possible, use of existing knowledge and experiments.
 - Validate on existing experiments on coupon level
3. Possible numerical investigations for the fatigue performance of web core deck panels
 - Analyses that can be performed with the numerical fatigue reduction model.

1.6. Research method

Qualitative data from existing literature is collected to better understand the fatigue behaviour of FRP better. Analysing this existing knowledge will help understand the fatigue behaviour of GFRP in more detail, the influence on material properties and the possible damage mechanisms. Collecting this knowledge also gives insight into the relevant aspects that need to be considered to predict fatigue performance better.

Literature research will be done on the kind of fatigue degradation models/criteria currently developed, which are applicable to in-plane stress dominated structures. Which modelling procedures are available to analytical/numerical assess fatigue for complex loading will also be researched. Finite Element (FE) models will be created to identify stresses and strain ranges under fatigue load models. Qualitative research will be done on the fatigue failure criterium on panel level.

To reduce the complexity of incorporating multiple relevant aspects during the design, a fatigue degradation model will be suggested to model the degradation. A flow diagram of this model is given in figure 1.1. A linear analysis will result in membrane forces and model displacements. The pass criteria, which will be defined for the component of interest, are verified until they do not satisfy any more then the analysis is stopped. Transformation of the membrane forces to individual ply stresses gives insight to the stresses per individual ply. With the gradual stiffness degradation module, the ply stiffness will be degraded for each load cycle. Performing this procedure until the global or local fatigue failure criterium is reached will indicate the zones that will degrade/fail and the number of cycles to failure.

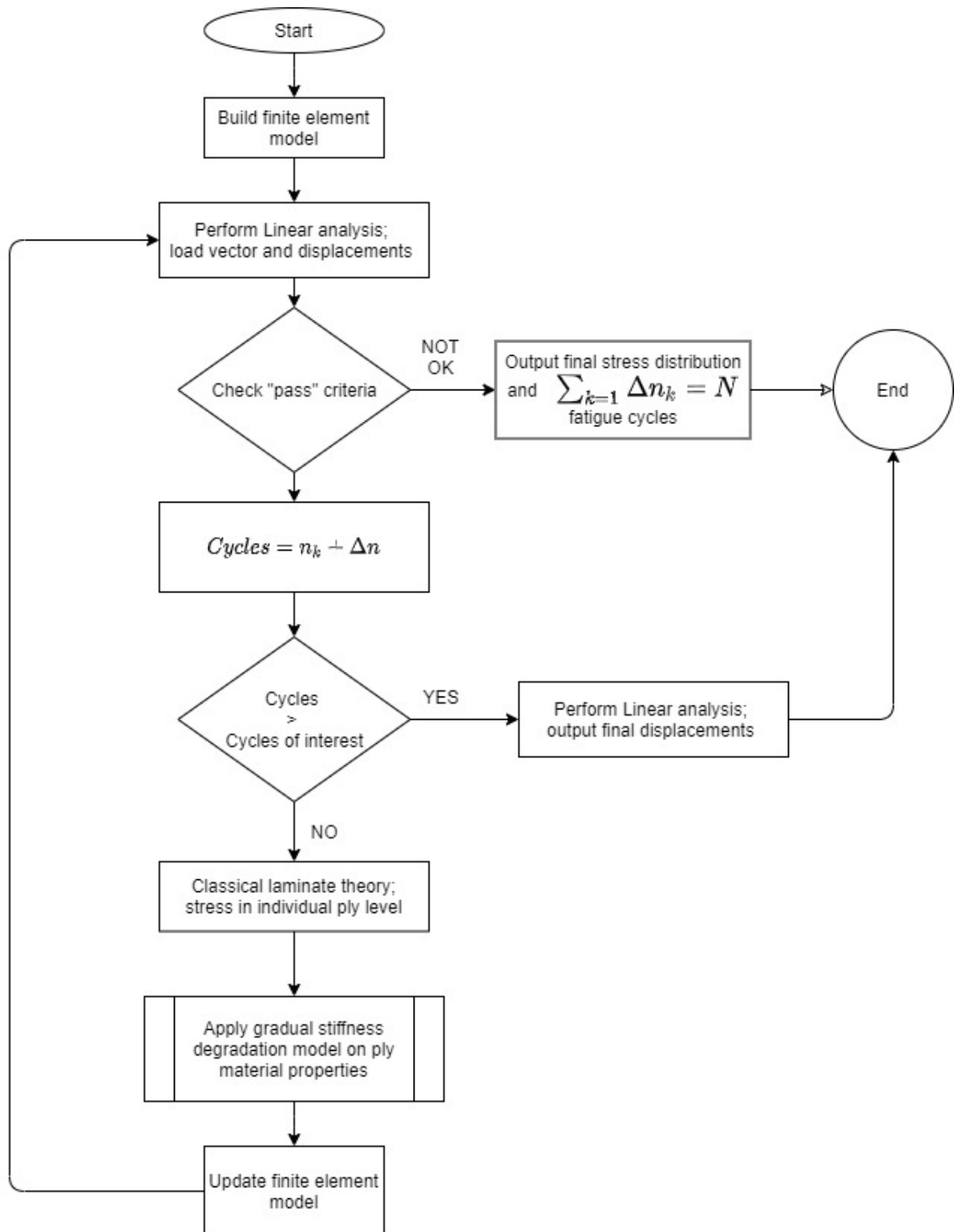


Figure 1.1: Flow diagram [Virtual Fatigue Stiffness Simulation \(ViFaSS\)](#) analysis procedure tool

2

Literature review

2.1. Fatigue behaviour of GFRP

Fatigue is a phenomenon that material properties degrade over time due to cyclic loads. These alternating loads result mainly in low stresses compared to the ultimate static strength. However, initiation of damage also occurs at a relatively low-stress range compared to the ultimate static stress. Fatigue failure in composites occurs when damage accumulation occurs in geometrical or material discontinuities, to a level that the resistance of the effective cross-section is reduced below the required static capacity.

Even though the fibre direction of composite materials is relatively fatigue insensitive, compared to traditional metallic materials, they also suffer under fatigue load cycles. The fatigue behaviour of composites is rather different from that of metallic materials. Metals are homogeneous and isotropic, whereas [Glas Fibre-Reinforced Polymer \(GFRP\)](#) is a composite. Existing knowledge of fatigue modelling can, therefore, not directly be applied [23]. In composites, considerable variability in material configurations is possible, fibre type, matrix type, material lay-up and different manufacturing methods. This variability makes it challenging to develop a commonly accepted procedure to validate the fatigue performance [22, 64].

2.1.1. Type of damage in fibre-reinforced polymers

In composites, multiple types of damage can occur. The order of occurrence depends on the stress state and the crack initiation and propagation energy of the different damage mechanisms [26]. [Hamidi et al. 2018](#) characterised the failure mechanisms of composites in four groups; fibre breakage, matrix cracking, fibre matrix shear out and delamination.

Matrix failure Damage starts to occur in regions with low strength, i.e. matrix and matrix fibre interfaces. Cracks occur mainly in the matrix of plies where the fibre direction is perpendicular to the load direction. Such damage, within plies, is called “intralaminar damage”. Cracking starts when the strain of the resin reaches the ultimate tensile strain. These cracks propagate until the next ply with different fibre orientation and stress concentrations at the cracktip arise. These stress concentrations can lead to crack propagation in the fibre direction between the plies, called “inter-laminar damage” resulting in delamination [57].

Delamination Delamination can occur due to the intralaminar cracks, due to significant stiffness differences between plies or due to local bending, resulting in interlaminar shear stresses. These interlaminar stresses can give rise to a crack development in the ply interface, which can lead to delamination. Cracks in the ply interface can also occur due to stress concentration caused by manufacturing defects in the interface [26]. The above-described situation is one of many situations where delamination can occur.

Interface failure In [Fibre-Reinforced Polymer \(FRP\)](#) fibres can act as crack stoppers. Where an intralaminar crack arrives at a fibre, see figure 2.1, interface failure between the fibre and matrix can

occur because the energy needed for interface failure is less than fibre failure. At the crack tip, the interface between the fibre and the matrix starts to fail due to large stress concentrations leading to debonding of the interface. Slip occurs between fibre and matrix, which causes the crack to propagate [12, 21].

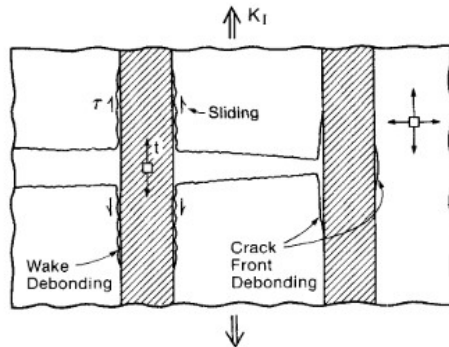


Figure 2.1: Crack propagation at interface [12].

Fibre failure The final stage of damage is a translaminal failure, i.e. fibre failure; this failure occurs where the fibre orientation is in load direction. Fibres can fail in tension and compression, and the fibres break in compression at a lower load than in tension due to misalignment and geometrical instability [21] [26]. The fibre properties of individual fibres are statistically distributed, caused by varying diameters, defects and scratched during production. This distribution in properties leads to the early breakage of weak fibres, causing a stress increase in surrounding fibres. When this increase in stress is considerable, progressive fibre breakage can occur. Besides fibre failure in tension or compression, fibre breakage can also occur due to stress concentrations caused by matrix cracking; instead of an interface failure, fibre breakage may occur [57].

2.1.2. Influence of load conditions

Composites are known for their different fatigue failure modes, as described in 2.1.1. The failure modes are dependent on the load conditions. In fatigue load, the load conditions are usually characterised by the ratio between tension and compression, the R-value; see eq 2.1. Fatigue life properties are usually determined for different applied mean stress and R-values resulting in different load types, e.g. $R = 0.1$ (tensile cyclic loading), $R = -1.0$ (tension-compression cyclic loading) and $R = 10$ (compressive cyclic loading). A description of the fatigue behaviour under the different load conditions is given in this paragraph.

$$R = \frac{\sigma_{min}}{\sigma_{max}} \quad (2.1)$$

σ_{min} = minimal normal stress due to cyclic load

σ_{max} = maximal normal stress due to cyclic load

Tension-Tension In **Tension-Tension (T-T)** fatigue, the behaviour of composites where fibres are mainly orientated in the load direction is driven by three damage mechanisms. Talreja proposed the fatigue life diagram, as shown in figure 2.2. Their underlining mechanisms can characterise three regions; region I represent fibre failure, region II indicates the progressive damage of fibre/matrix interface and fibre bridged matrix cracking. In region III, Gamstedt et al. indicates that there is a fatigue cut-off limit where cyclic loading does not result in damage. [17]. Other researchers did not found this cut-off limit [37].

Tension-Compression First, a short overview of the microscopic behaviour is given to better understand the macroscopic fatigue behaviour under compression-tension fatigue loading of multidirectional laminates.

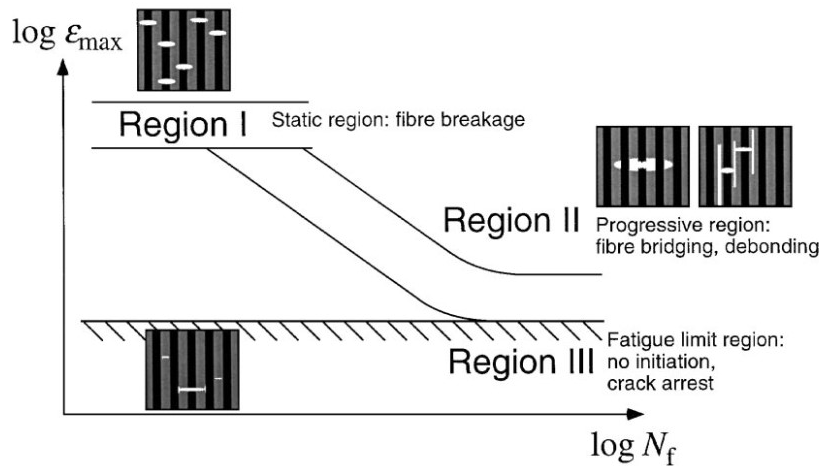


Figure 2.2: Different failure mechanisms according to Talreja [56].

Compression-Compression (C-C) loading can lead to debonding of the fibre-matrix interface. The debonding crack propagates to transverse cracks at a lower number of cycles compared to **T-T** loading. As seen in figure 2.3a the crack corner opens under a compression load, and the propagation leads to debonding. The propagation of the debonding eventually results in transverse cracking of the matrix. These transverse cracks can lead to delamination between two plies and eventually in fibre breakage, as shown in figure 2.3b.

Because this debonding is more severe for **Tension-Compression (T-C)** than for **T-T** the crack density in the material is larger than for **T-C**. Due to the larger crack density under compression, there are more stress intensities in the load-carrying plies, which lead to delamination and out-of-plane buckling. This effect also contributes to the steeper **S-N** slopes for **T-C** fatigue. Gamstedt and Sjögren[14] constructed an overview of the difference in this debonding behaviour and the propagation for tension-compression and tension-tension. See figure 2.4.

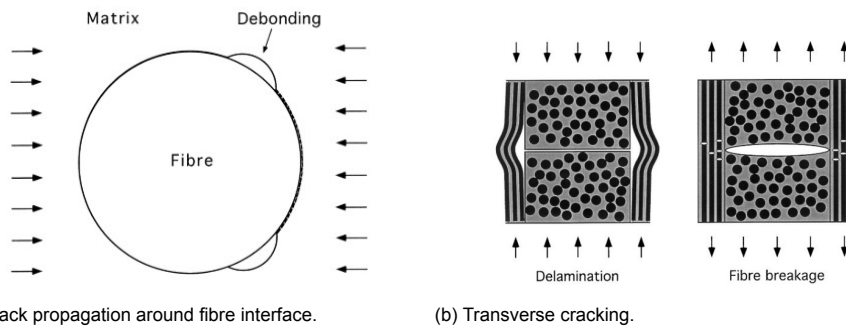


Figure 2.3: Debonding propagation.

Compression-Compression Under compression loading, fibre buckling is a possible damage mechanism. Fibres tend to buckle due to misalignments or stress concentrations caused by defects, like voids, in the matrix. The matrix supports the fibres; it is expected that when individual fibres buckle, the strain in the fibres is low, and the buckling is reversible due to their elastic properties and not sensitive to cyclic loading. However, the matrix that supports the fibre tends to deform inelastically, and therefore the buckling amplitude becomes progressive with the cyclic load. The deflection of the fibre increases, which initiates the buckling of surrounding fibres. This is illustrated in figure 2.5 [57].

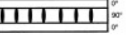
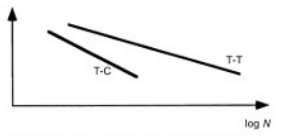
	<i>Tension-Compression</i>	<i>Tension-Tension</i>
Debond profile	 Crack tip opening in compression	 Contact zone in tension
Debond propagation	 High growth rate	 Low growth rate
Transverse cracking	 Accelerated initiation of transverse cracks	 Retarded transverse crack formation
Transverse crack density	 Many cracks	 Few cracks
Fatigue behaviour	 Shorter fatigue lives and more rapid degradation for fatigue with compressive load excursions	

Figure 2.4: Overview debonding influence glst-c and T-T [14].

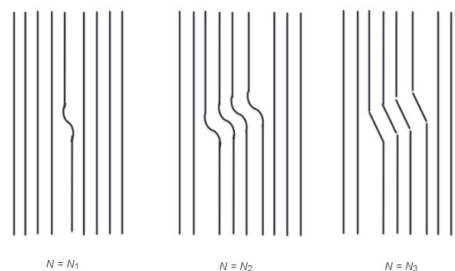


Figure 2.5: Progressive buckling under cyclic compression load. [57]

2.1.3. Constant amplitude loading

Constant amplitude (CA) loading is characterised as a sinusoidal wave with constant amplitude leading to a constant R-value, so one load type, and constant cyclic stress.

S-N diagram

A well-known representation of the fatigue life under CA is the S-N diagram, on the vertical axis stress, strain or displacement, on the horizontal axis the corresponding number of cycles. Mainly the slope of the S-N curve characterises the fatigue performance of the material. A 'steep' slope indicates a poor fatigue behaviour, i.e. a relatively low increase in the number of cycles to failure with a decrease in the stress range. 'Flat' slopes indicate a good fatigue behaviour, i.e. a rapid increase in the number of cycles to failure with a small decrease in the stress range [37]. These flat slopes also cause a large change in the number of load cycles to failure with a small stress change, which makes predictions more difficult.

Composites are known for their good fatigue behaviour, and applications can be found in areas where fatigue is dominant, e.g. wind turbine rotor blades. S-N curves of metals are characterised by a CA and variable amplitude (VA) cut-off limit, i.e. a stress range where no fatigue damage occurs. In

composite materials, this "cut-off" limit is not found [37]

S-N diagrams are obtained from experimental data for a CA load, i.e. one R-value, see equation 2.1. The S-N curve can be described analytically. Traditionally it is assumed that the logarithm of CA fatigue life N depends linearly on the logarithm of the stress/strain or displacement S .

$$\log N = a + b \cdot \log S \tag{2.2}$$

$N =$ Fatigue life time
 $S =$ Stress- strain or displacement
 $a - b =$ Constants

Equation 2.2 is equivalent to:

$$N = 10^a \cdot S^b \tag{2.3}$$

Equation 2.2 and 2.3 are known as a log-log or powerlaw formulations.

In the S-N curve formulation, the static strength, i.e. the failure strength of 1/2 load cycle, can be in- or excluded. There are some differences related to the coverage of fatigue behaviour when in or exclude the static strength. When including the static strength in the linear regression, the low-cycle region gives a more accurate prediction. An accurate prediction in this region can especially be relevant in variable amplitude loading, e.g. at exceptional loading. Also, simplification of the formulation is possible by only the static strength and slope of the linear S-N curve. However, high-cycle fatigue life predictions are less accurate. Nijssen [37] recommended to exclude the static strength in the S-N curve derivation when low-cycle fatigue is not of significant interest. The failure modes that occur in fatigue failure are different than in static failure.

Constant Life Diagram

The constant life diagram (CLD) is a representation method of the fatigue life where the effects of mean stress and anisotropy of the material are included. Parameters that describe the CLD are σ_m , σ_a and the R-ratio defined as $R = \sigma_{min}/\sigma_{max}$ [65]. Philippidis and Vassilopoulos 2002 constructed figure 2.6.

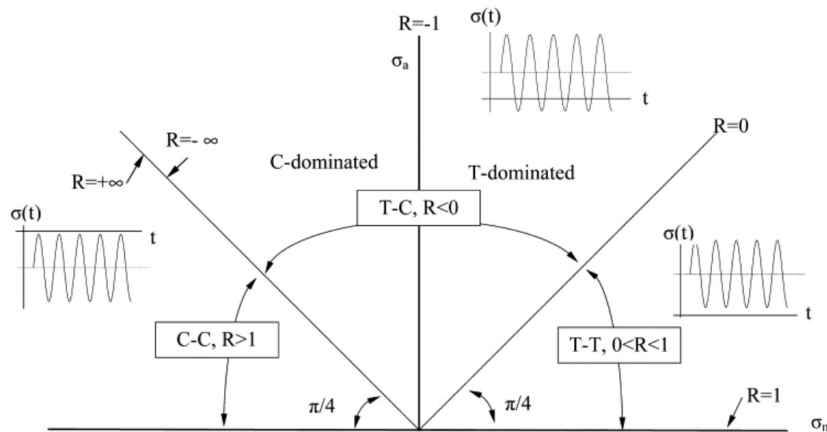


Figure 2.6: CLD [44].

The CLD indicates three zones; T-T, T-C and C-C. The radial lines represents the different R-values, i.e. load types, lines in the T-T zone have a symetric counter line for the C-C zone, R-values of the C-C zone are the inverse of the T-T.

Each radial line represents a single S-N curve, along these lines, the number of cycles to failure is marked, at the corresponding σ_a . Performing multiple S-N curves for different R-values, at least R=0.1, -1 and 10, and construct the constant lifelines, i.e. the lines connected by the same cycles to failure of different radial lines converged to the ultimate tensile stress (UTS) and ultimate compression stress

(UCS). Do give a reasonable prediction for non-tested S-N curves [65]. The translation of S-N curves to the CLD is shown in figure 2.7 from cur recommendation 96 [5]. The assumption that the lifelines converge to the UTS and UCS is a simplification because the strength degradation of long-term creep is ignored [65].

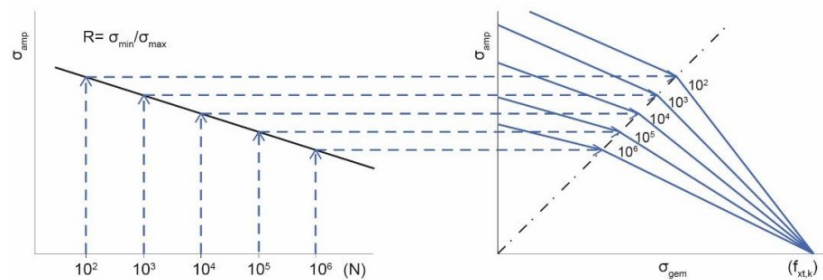


Figure 2.7: Deriving a CLD from S-N curve [5].

2.1.4. Variable amplitude loading

An estimation of the loading can be achieved, but modelling the random traffic load accurate is almost impossible. Therefore, approaches to model fatigue behaviour using block and random variable loading spectra are proposed. It is desired to model the fatigue behaviour under VA loading with fatigue models that are based on simple experiments. One of the methods to assess the fatigue behaviour of VA loading is to use damage accumulation rules. A more thorough description of these damage rules and their shortcomings is given further on under "Damage accumulation" [45]. In bridge design, traffic loads can result in multiple stress states. Transformation is required to assess the damage per cyclic content. Paragraph "Counting methods" will discuss transformation methods.

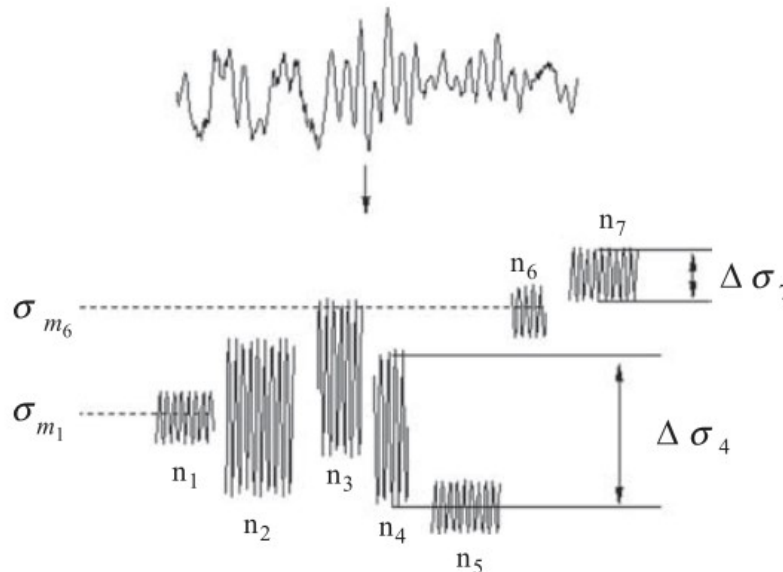


Figure 2.8: Overview of cycle counting [64].

Counting methods

Realistic load-versus-time history is irregular. In a bridge where one truck passes, multiple peaks and valleys can occur due to the nature of the structure, the number and type of axles on a truck and the location of interest. Cycle counting is used to transform these irregular load-time histories in cycles of multiple magnitudes and their occurrence, resulting in VA loads. Various methods have been proposed, of which rainflow counting is the most frequently used [64].

As described in subsection 2.1.2; the mean stress and stress range of the load are essential for the fatigue analysis of composites. One-parameter cycle counting methods are not applicable because the mean stress is then lost. Several methods can be used for the analysis of composite fatigue data [64]. These are described below.

Range-mean In the range-mean counting method, segments are extracted. These segments are characterised by their mean stress (R-value) and their stress range (σ_a). Segments are between a peak and valley, resulting in a half cycle. Corresponding segments can be combined and ordered at their time of occurrence, and this makes the method applicable to degradation models because the order of occurrence is needed.

A drawback of the range-mean counting method is that it obtains half cycles from peak to valley or vice-versa. Therefore, peaks and valleys of larger load cycles, e.g. temperature long-term load cycles, are not accounted for. Those superimposed traffic loads on the temperature load result in short-term cycles captured by the method. Therefore, in some situations, the range-mean approach can result in unconservative results due to the absence of potentially significant damaging load cycles.

Rainflow-counting As indicated above, the range-mean method does not take into account the long-term cycles. Rainflow-counting takes these cycles into account. For a description of the model, a reference is made to the work of de Jonge [7].

With the rainflow-counting method, the order of cycles is to some extent lost, some order is intact due to the way of storage, but the practical use of this information is limited. It is therefore not applicable for a cycle-by-cycle analysis [37].

Nijssen [37] proposed a rainflow-equivalent range-mean count. He modified the load spectrum with the help of the rainflow method such that the range-mean method gives very similar results as the original rainflow method while maintaining the load order.

Damage accumulation

Under VA loading accumulation of damage is rather complicated due to the multiple possible load types and different damage mechanisms. As described above, the damage development in composite materials is complex and depends on many parameters. The evolution also depends on the load and damage history due to the different failure modes in the laminate.

Palmgren-Miner's summation Palmgren-Miner [30, 41] assumed that damage could be accumulated stress independently and linearly, see their well-known equation 2.4. Where n_i is the number of cycles under the applied stress, N_i the cycles to failure under load cycle i [13, 37]. When D is equal to 1, failure of the structure is assumed. Several design guidelines allow the use of Palmgren-Miner's summation under spectrum load conditions.

$$D = \sum_{i=1}^n \frac{n_i}{N_i} \leq 1.0 \quad (2.4)$$

As described in the introduction of this paragraph, damage development is rather complex, and the Palmgren-Miner's summation, therefore, has some limitations;

- It is a binary failure criterion; the structure is failed or intact. There are no physical parameters included, and for composites, it is seen to give a wide variety in observed failure states [37].
- As can be seen from equation 2.4 the order of summation does not influence the damage. It, therefore, assumes that the damage per cycle is not dependent on the damage state of the structure before the load cycle. So the load sequence does not influence the damage. Damage mechanisms described in 2.1.1 suggest otherwise.

Van Delft et al. [60] compared VA test results with CA results on damage accumulation. They found a large over-estimation of the fatigue life. Schön and Nyman [49] found that miners rule underestimate the fatigue life time.

Factored Palmgren-Miner's summation

Factored Palmgren-Miner's summation In literature, modifications of Palmgren-Miner's summation are proposed. One of the simplest is the factored sum, i.e. reducing the failure level. Reducing is done by multiplying N with the factor K see equation 2.5. This has the same effect as shifting the S-N curves to the low cycle region over the x-axis. K then can be based on comparable experiments to correct for no conservative outcome [37].

$$D = \sum_i \frac{n_i}{N_i \cdot K} \leq 1 \quad (2.5)$$

Non-linear Palmgren-Miner's summation Owen and Howe [39] developed a non-linear stress independent fatigue damage accumulation. They include the damage evolution in the matrix of glass chopped strand mat/polyester resin laminate. See equation 2.6. Bond [6] adjusted the formulation for glass fibres by changing the exponent, see equation 2.7.

$$D = \sum_{i=1}^k \left[A \left(\frac{n_{oi}}{N_{fi}} \right) + B \left(\frac{n_{oi}}{N_{fi}} \right)^2 \right] \quad (2.6)$$

$$D = \sum_{i=1}^k \left[A \left(\frac{n_{oi}}{N_{fi}} \right) + B \left(\frac{n_{oi}}{N_{fi}} \right)^C \right] \quad (2.7)$$

Where n_{oi} , and N_{fi} are the operation of cycles and cycles to failure respectively of the i th cycle. A, B and C are constants determined by iteratively fitting to experimental data [6]. The curve fitted parameters are constants dependent on the R-value. However, they do not have any physical meaning [37].

Sequence effect

In composite materials, the damage states and damage mechanisms are interactive and dependent on existing damage, as described in 2.1.1. A sequence effect exists if the accumulation of the damage is dependent on the already induced damage [37].

Gamstedt and Sjögren [15] performed an experimental investigation on the sequence effect in Carbon Fibre-Reinforced Polymer (CFRP) material. They compared the physical reasons for the sequence effect, see figure 2.9. They found that the transverse cracking mechanism dominates the damage in high cycle fatigue and delamination in the low cycle fatigue. The matrix failure mechanism, described in 2.1.1, indicates that delamination starts to grow at the crack tip of transverse cracks. With high-low sequence loading, transverse cracks occur in the first load block. Therefore delamination in the second load block propagates faster. Due to this delamination, the composite interaction between layers decreases, resulting in higher average stresses in layers with stiffness in the load direction. The higher average stress in those layers result in shorter fatigue life, i.e. those layers become more sensitive than in the load cycle.

The described effect can also occur in unidirectional laminates, where the interface failure mechanism, described in 2.1.1, starts the fibre-matrix debonding and results in more considerable stresses in the fibres [15].

In metallic materials, the opposite is found. Large plastic zones at the crack tips are formed in high load cycles, leading to compressive stresses at the crack tip, making it more difficult for the lower tensile stresses at the crack tip to propagate under low load cycles [67].

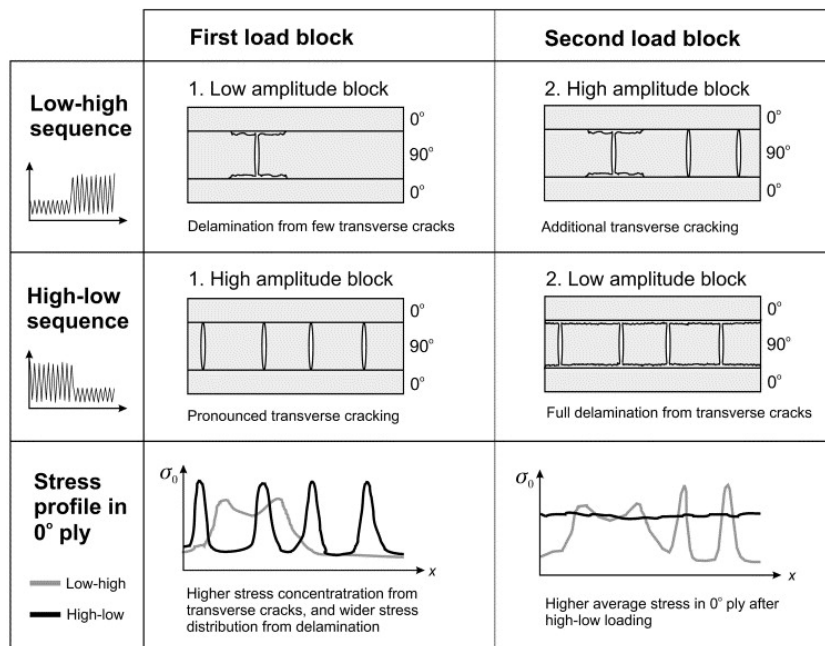


Figure 2.9: "Schematic illustration of the evolution of damage and the sequence effect in block amplitude loading of cross-ply laminates, and the qualitative influence on the stress profile in the critical 0° plies." [15].

2.2. Fatigue life modelling approaches

The methods found in the literature to describe the fatigue behaviour of composite laminates can be categorised into three categories [8]. 1: Fatigue Life Modeling and Prediction, 2: Phenomenological and Empirical Modeling and 3: Progressive Damage Modeling [18].

The first category are fatigue life models; these models use S-N degradation curves or Goodman-like diagrams. A criterion characterises failure. These models do not take into account any physical damage mechanisms. They only indicate at which number of cycles with a specific CA load the failure criterion is met [8]. The failure criterion of the stress-life for quadratic stress interaction is expressed for fibre failure, matrix failure and delamination.

Fatigue life prediction models usually consider one specific case of material, layup, loading and thickness. Interaction between failure mechanisms and a distinction in failure mode is to a limited extent included in some models. The authors of these models have assumed an in-plane stress state. Suitable for the prediction of in-plane fatigue behaviour of thin and thick laminates. However, for thick laminates, through-thickness normal and shear stresses and interlaminar shear stresses become more relevant [18].

The second category is phenomenological and empirical modelling. This approach tries to take material degradation due to the cyclic load into account. Models from this category describe the degradation of the specimen due to a reduction of stiffness, strength or stiffness and strength combined. Failure occurs when reduced strength is equal to the applied stress and the material is no longer able to bear the load [8]. When you only consider stiffness reduction, failure cannot be predicted. A stiffness reduction limit should be determined such that: stiffness reduction limit \leq strength reduction limit. This stiffness limit can be specified on engineering judgement or the stiffness reduction and corresponding damage development from other experiments. To determine the stiffness loss at a particular failure mode.

Strength reduction models can be distinguished by two types of models, the sudden death and wear out models. At low cycle fatigue, i.e. the high-stress low number of cycles, the residual strength is in the beginning mostly constant. When the number of cycles to failure is reached, the strength reduces abrupt. Models that describe this phenomenon are known as sudden death models. Opposite to the sudden death failure at high stress, more gradual degradation is observed at low stress. Models describing this behaviour are known as wear out models. The drawbacks of the strength reduction

method are that many experiments need to be performed to included load conditions. Current experimental data is only available for thin laminates.

Residual stiffness models describe the decrease in stiffness of the laminate, during fatigue loading. The stiffness degradation will mostly be described by the following equation $D = 1 - \frac{E}{E_0}$, where E_0 is the initial stiffness. The degradation growth $\frac{dD}{dN}$ is expressed in terms of observable properties. Schulte distinguished three stages in the reduction [18, 40, 61] see figure 2.10.

- The initial region (Stage I): the transverse matrix cracks dominate the stiffness reduction. A rapid reduction of 2-5% occurs.
- An intermediate region (Stage II): edge delamination and longitudinal crack along the 0 °fibres dominate the stiffness reduction. 1-5% reduction occurs in this stage.
- The final region (Stage III): damage progression from the first fibre failure leading to strand failure. Stiffness reductions progress abrupt and end with the failure of the specimen.

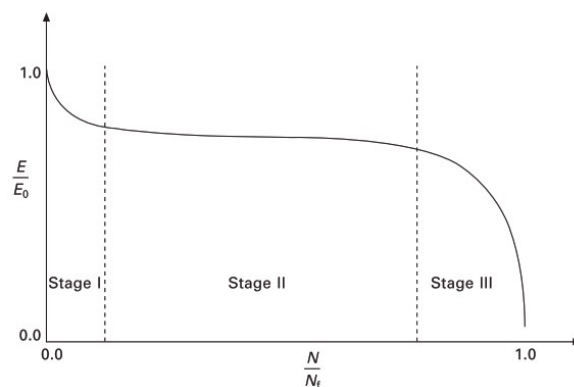


Figure 2.10: Overview Stiffness degradation stages [61].

The third category is the progressive damage modelling approach. This approach models the progression of damage in the laminate. This approach can predict the cycles to failure and model the degradation of the material properties. With these models, the damage growth and different residual mechanical properties are predicted. The essential components of this modelling approach are stress analysis, failure analysis, and material property degradation [53].

Models that predict the damage growth try to characterise the damage accumulation of matrix cracking and delamination. Models that predict residual mechanical properties are mostly developed based on mechanical properties and a pre-described damage variable, such as the Hashin failure criterion.

2.2.1. Progressive fatigue damage modelling approaches in literature

In this subsection, different progressive fatigue damage models are described. The focus is laid on methods that can be included in numerical models and use ply material properties as input. The models will be described in chronological order per author.

Shokrieh and Lessard [53] [54]

Shokrieh and Lessard proposed as one of the first an progressive damage model for fatigue analysis. They aimed to develop a general model, independent of geometry, lay-up, loading conditions, boundary condition, loading ratio, loading sequence and the ability to include stress concentrations. Their approach is based on results of **unidirectional (UD)** ply fatigue experiments. By simulating degradation cycle-by-cycle, the model can predict residual strength and life, failure mechanisms, propagation direction, and final failure life. In figure 2.11 the flow diagram of the algorithm is shown.

Non-linear shear stress-strain behaviour is included in the constitutive relations. For achieving realistic stresses, a 3D non-linear finite element technique is used. In earlier work, the authors developed a

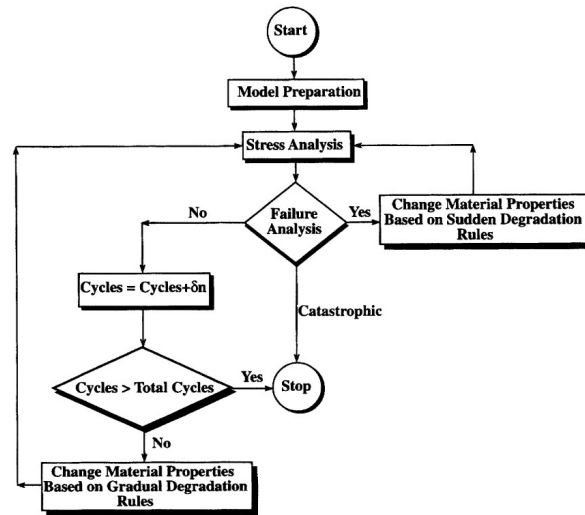


Figure 2.11: Progressive damage model of Shokrieh and Lessard.

three-dimensional finite element algorithm to describe the three-dimensional stress state [52]. They used a twenty-noded isoparametric quadratic solid element. The effect of the non-linear stress state near the edge is a critical location of failure initiation to cope with the edge effect, a refinement of the mesh at the sides of the model is applied[51].

They used seven failure modes for UD ply under multiaxial stress state; fibre tension, fibre compression, fibre-matrix shearing, matrix tension, matrix compression, normal-tension and normal-compression. The authors proposed quadratic polynomial failure criteria which are applicable for multiple stress states and ratios. An explanation is given in [52].

The material property degradation is divided into two sections; sudden material property degradation, e.g. one of the seven failure modes has occurred and gradual material property degradation, e.g. degradation of material strength and stiffness properties per applied cycle. With sudden material property degradation, the strength and stiffness properties of the ply are adjusted according to the type of failure. An example is given for fibre failure in tension or compression in equation 2.8a. When the failure criterion for fibre failure is met, the stiffness properties are reduced to zero.

$$\begin{aligned} & [E_{xx}, E_{yy}, E_{zz}, E_{xy}, E_{xz}, E_{yz}, \nu_{xy}, \nu_{xz}, \nu_{yz}, \nu_{yx}, \nu_{zx}, \nu_{zy}] \\ & \quad \downarrow \\ & [0, 0, 0, 0, 0, 0, 0, 0, 0, 0, 0, 0] \end{aligned} \quad (2.8a)$$

$$\begin{aligned} & [X_t, Y_t, Z_t, X_c, Y_c, Z_c, S_{xy}, S_{xz}, S_{yz}] \\ & \quad \downarrow \\ & [0, 0, 0, 0, 0, 0, 0, 0, 0] \end{aligned} \quad (2.8b)$$

For gradual material property degradation, the authors established a so-called generalized residual material property degradation technique. The technique uses experimental data from a unidirectional ply under uniaxial fatigue loading to simulate multiaxial fatigue behaviour. A more thorough description is given in [52]. Shokrieh and Lessard changed the strength degradation model proposed by [1] for the applicability on fatigue loading cycles. The prediction of fatigue life is based on an analytical representation of the Goodman type diagrams (CLD).

They validated their model on pin bearing connections in different laminate lay-ups. A good agreement with experimental results is obtained. For more information see [54].

Passipoularidis, Philippidis and Brondsted [43]

Passipoularidis, Philippidis and Brondsted proposed a progressive damage algorithm named FADAS. It performs a linear ply-by-ply stress analysis with the help of classical laminate theory. For the constitutive relations, a linear elastic behaviour is assumed. Out of plane shear and through-thickness stresses are not considered. A flow chart of the algorithm is given in figure 2.12. They considered two variations of

the algorithm; "FADAS" that degrades the properties after a complete cycle, and "FADAS INCR" that degrades the properties after each load increment, e.g. half cycle.

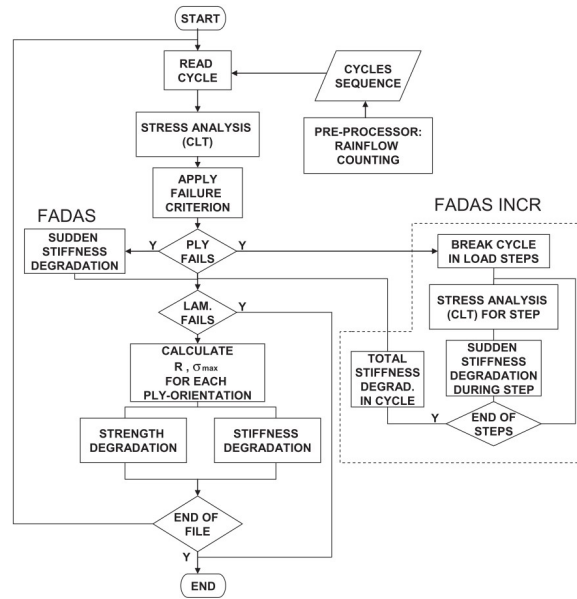


Figure 2.12: Progressive damage model of Passipoularidis et al..

Degradation of material strength and stiffness properties is included. Sudden and gradual material degradation are considered. For the failure criteria Puck's failure criteria are used [46, 47]. Strength degradation is based on a linear degradation and stiffness degradation is non-linear, see equations 2.9a and 2.9b.

$$\begin{aligned} X_{Tr} &= X_T - (X_T - \sigma_{1 \max}) \left(\frac{n}{N_1} \right) \\ Y_{Tr} &= Y_T - (Y_T - \sigma_{2 \max}) \left(\frac{n}{N_2} \right) \\ S_r &= S - (S - \sigma_{6 \max}) \left(\frac{n}{N_6} \right) \end{aligned} \quad (2.9a)$$

$$\frac{E_i}{E_{i0}} = 1 - (1 - \alpha_i) \left(\frac{n}{N} \right)^{\beta_i} \quad (2.9b)$$

X_{Tr} =	is the residual strength parallel to the fibres
Y_{Tr} =	is the residual strength transverse to the fibres
S_r =	is the residual shear strength
$\sigma_{i \max}$ =	maximum cyclic stress for n cycles
N_i =	corresponding fatigue life at $\sigma_{i \max}$
E_i =	reduced stiffness
E_0 =	initial stiffness
α_i =	experimental fitted parameter
β_i =	experimental fitted parameter

Stiffness degradation depends on the fatigue life fraction, so implicitly, the stress level and R-ratio are taken into account. The parameters α and β need to be fitted on corresponding experimental data. Stiffness degradation can vary between R-ratios, which means that the damage mechanisms are different for degradation and fatigue life. Therefore, the parameters need to be fitted per R-ratio.

Five different failure modes are considered in the algorithm; fibre failure in tension and compression, inter-fibre failure cracks parallel to the fibres, matrix cracks transverse to the principal direction and

wedge effect resulting in delamination or local buckling [46]. Each failure mode implies a degradation of material properties, comparable with the example of Shokrieh and Lessard, see 2.9b.

For the fatigue lifetime prediction use is made of the CLD formulation. Two variations are considered: an analytical description of the CLD with the BELL curve from [1] (BELL CLD), and a linearly interpolated CLD to safe calculation time (LCLD). The authors implemented the FADAS algorithm in MATLAB to perform the analysis. MATLAB is specialized software for mathematical applications. The algorithm is conservative in most cases. This is expected due to the assumption of linear strength degradation. The degradation is therefore overestimated, especially at the high-cycle fatigue life range. The authors compared their cycles to failure with Palmgren-Miner's summation and obtained that Palmgren-Miner is non-conservative for repeated block spectrum loading, regardless of the loading order. The difference was more considerable in the low-cycle fatigue range.

Obtained results are better in case the CLD is described with the BELL formulation. Improvement is expected when the behaviour predicted by the CLD formulation near $R=1$ is improved to include the creep behaviour.

Eliopoulos and Philippidis [11] [10]

Eliopoulos and Philippidis introduced a progressive damage algorithm for thick shell finite element formulations, where the damage model is based on unidirectional ply behaviour. The focus was laid on glass/epoxy composites used in the wind industry. Their algorithm relies on experimental data from the optiDAT database and is a modification of the above described FADAS algorithm.

The main difference is that material behaviour, which is assumed as non-linear, the same stiffness and strength degradations are used. Also, the same failure modes are assumed. The fatigue life prediction is made with LCLD (linear interpolation of the CLD), even though interpolation with the BELL CLD would lead to more accurate results. With the implementation of shell elements in the finite element model, delamination cannot be modelled nor can any other out of plane phenomenon [11].

In ref, [10] the implementation of the algorithm in ANSYS finite element software is described. Validation is performed on a specimen level. To speed up calculation time, degradation of material properties is done per step size of Δn load cycles instead of each load cycle separate. The authors performed a sensitivity analysis and concluded that the S-N definition and CLD formulations affected the precision of the prediction.

2.3. Fatigue assesment according to design recommendations

2.3.1. CUR 96 recommendation 2019

CUR Recommendation 96 is a dutch guideline that addresses recommendations for the design of FRP load-bearing structures in buildings and civil engineering structures [5].

General According to the CUR 96, recommendation fatigue must be considered when the structure is subjected to cyclic loading where the load cycles exceed 5000, or when the maximum cyclic load is greater than 40% of the maximum load.

Actions For traffic bridges CUR 96 prescribes the use of loadmodel 4b from NEN 1991-2 [35]. CUR 96 allows a cyclic load to be considered as a constant amplitude load if the range and mean stress do not vary more than 10%. If not, the load shall be considered as a variable amplitude load.

Verification The fatigue life needs to be determined using fatigue strength curves of the same type of material and load conditions, e.g. R-values. When the service life is not known for a specific R-value, use of a CLD is allowed. In the 2019 version, this is only allowed when it can be motivated that this is a conservative assumption. CUR 96 indicates to construct the CLD with R-values of; 0.1, -1.0 and 10.

CUR prescribes a double logarithmic relation for the load cycles and mean stress, see eq 2.10.

$$\log(N) = k \cdot \log\left(\frac{\gamma_{Mf} \cdot \gamma_M \cdot \sigma_{max}}{\eta_{cB}}\right) \quad (2.10)$$

$N =$	is the number of cycles to failure
$k =$	is a regression parameter, derived from tests
$B =$	is the characteristic strength of the laminate after 1 cycle, the characteristic static strength of the laminate can be assumed
$\sigma_{max} =$	maximum stress acting during a cycle
$\gamma_{Mf} =$	fatigue material factor = 1.0 if the variation of the measured stress for a specific number of cycles is no more than 10% to 20%

Table 6.7 from CUR 2019 gives values for k and B for UD plies; they may be used when the load carried by the UD ply in the direction of the load, this gives a conservative assumption. Otherwise, fatigue behaviour shall be derived from tests. It needs to be demonstrated that accumulation of damage over the service life will not lead to failure or loss of performance.

CUR 96 allows the use of Palmgren-Miner's summation for the accumulation of damage, as given in eq 2.4. Rainflow counting is recommended to convert variable amplitude loading to constant amplitude loads. When Palmgren-Miner's summation is ≥ 1 the component is failed.

2.3.2. Prospect for New Guidance in the Design of FRP Structures

Prospect for New Guidance in the design of FRP Structure [2], also called JRC document. A document prepared by JRC to establish European technical rules and standards for the design and validation of FRP structures, published in 2017.

General The prospect requires to consider fatigue when the expected load cycles exceed 5000 while the peak stress exceeds 15% of the design strength, or when the maximum cyclic load is greater than 40% of the full load.

Verification Like the CUR 96, the prospect allows, to consider a cyclic load with no more amplitude variation than 10% as a constant amplitude load. Fatigue life should be determined with S-N curves, constructed of the same material and load type, comparable with CUR 96. When no S-N curve is known for a specific R-value interpolation of a CLD is allowed. The prospect allows, same as CUR 96, the use of Palmgren-Miner's summation for the accumulation of damage, as given in eq 2.4. Rainflow counting needs to be used in order to convert variable amplitude loading to constant amplitude loads. Component failure is reached when $D \geq 1$.

Ageing and variation in material properties should be accounted for in test, or by including partial and conversion factors. JRC gives an explicit warning for the influence of interface cracks that can lead to local buckling, as described in 2.1.2 and indicated in figure 2.3b.

JRC describes the relation between load and number of cycles to failure with a double logarithmic equation, comparable with the CUR 96. The difference is in the fatigue material factor, which is prescribed by JRC at $\gamma_{Mf} = 1.10$. The static strength B is not precisely the static strength but the y-axis interception after linear regression of test results.

In complex geometries, tensile stresses normal and in-plane shear stresses in the interface can initiate cracks and propagate. If there is the uncertainty of these aspects in the design, testing should be performed on a component level.

2.3.3. Eurocode proposal prCENTS19101 based on draft version from 2020-11-04

prCEN/TS 19101 Design of Fibre-polymer composite structures is a technical specification prepared by the technical committee CEN/TC 250 "Structural Eurocodes", here called "TS19101". It establishes a technical design specification of FRP structures which is the preparation state towards a formal EuroCode design standard. The technical specifications apply to the design of buildings and civil engineering structures.

General Other than CUR 96 and JRC, TS19101 gives a mathematical condition. When fulfilled, an experimental fatigue verification needs to be performed. The condition is given in equation 2.11. This condition is derived for single-span bridges. Under normal loading conditions, those bridges exhibit tension-tension fatigue at the bottom and compression-compression fatigue at the top. This equation 2.11 excludes tension-compression, which can be more severe.

$$E_d (\gamma_{Ff} \cdot Q_{fat}) / R_d > 1,6 - 0,18 \cdot \lg N \quad (2.11)$$

$E_d (\gamma_{Ff} \cdot Q_{fat}) / R_d =$ is the design value of an action effect in the structural member or joint (an internal force and/or moment), caused by the fatigue action model;
 $\gamma_{Ff} =$ is the partial factor for the fatigue action (according to prEN 1990);
 $Q_{fat} =$ is the relevant constant amplitude fatigue action;
 $R_d =$ is the design value of the corresponding static resistance of the member or joint;
 $N =$ is the number of cycles of the fatigue action, i.e. the number of axle loads.

Actions The fatigue action model should include representative load conditions, i.e. R-value or mean stress. Fatigue actions caused by traffic loads should be derived from project specifications, and EN 1991-1 [34]. Fatigue actions caused by wind excitations should be considered in accordance with EN 1991-1-4 [32]. Also, fatigue actions due to thermal effects of the structure should be considered in accordance with prEN 1990 6.1.3.3(4). Fatigue models for traffic, wind and temperature should not be combined.

Verification Verification is based on internal force or moment, as shown in equation 2.12. The resistance of the member or joint needs to be obtained by testing. Palmgren-Miner's summation is

not allowed because it can lead to non-conservative results. The partial factor for fatigue resistance depends on inspection and fail-safe or not-fail-safe, i.e. does the failure of a local element lead to progressive failure or not.

$$E_d (\gamma_{FF} \cdot Q_{fat}) \leq \frac{\eta_c}{\gamma_{Mf}} \cdot R_{f,k} \quad (2.12)$$

$E_d (\gamma_{FF} \cdot Q_{fat}) =$ is the design value of an action effect in the structural member or joint (an internal force and/or moment), caused by the fatigue action model;

$R_{f,k} =$ is the design value of the corresponding static resistance of the member or joint, which should be obtained from member or joint testing, at constant amplitude

$\gamma_{Mf} =$ is the partial factor for the fatigue resistance, according to Table 10.1;

$\eta_c =$ is defined in 4.4.7 (corresponding to the material property which causes failure).

Testing TS19101 prescribes that qualification and proof testing should be performed; it gives protocols on how bridge decks and slab bridges should be tested. Further description of the test specifications is given in TS19101 draft version from 2020-11-04. An important aspect is that if the element is loaded by variable amplitude loading, a corresponding spectrum test load needs to be applied. Clause 10.4.2(6) states that qualification test is a pass if:

- the required number of cycles is completed without failure;
- the stiffness reduction is less than 5%, to prevent excessive micro-cracking;
- visible damage, i.e. macro-cracks, debonding, delamination, that could affect durability due to moisture ingress does not occur;
- the result of the post-fatigue static tests is within two standard deviations of the mean value of the static resistance achieved in the static tests.

Interpretation of these requirements is debatable.

TS19101 also prescribes proof testing of the product for project-specific applications, i.e. specific geometry and boundary conditions.

2.3.4. Guideline for the Certification of Offshore Wind Turbines GL 2012

Guideline for the Certification of Offshore Wind Turbines by Germanischer Lloyd Industrial Services GmbH [9]. Applies to the design, assessment and verification of offshore wind turbines, including GFRP components.

The verification of the fatigue resistance is based on Palmgren-Miner's summation when $D \geq 1$ the verification is not sufficient. The fatigue life time is determined with a Goodman diagram's help based on a characteristic S-N curve. If no S-N curve is present, the design recommendation prescribes a conservative value for m .

The allowable load cycles per load type are based on the design values obtained from the Goodman diagram with equation 2.13.

$$N = \left[\frac{R_{k,t} + |R_{k,c}| - |2 \cdot \gamma_{Ma} \cdot S_{k,M} - R_{k,t} + |R_{k,c}||}{2 \cdot (\gamma_{Mb}/C_{1b}) \cdot S_{k,A}} \right]^m \quad (2.13)$$

$S_{k,m}$	=	mean value of the characteristic actions
$S_{k,A}$	=	amplitude of the characteristic actions
$R_{k,t}$	=	characteristic short-term structural member resistance for tension
$R_{k,c}$	=	characteristic short-term structural member resistance for compression
m	=	slope parameter m of the S/N curve
N	=	permissible load cycle number
γ_{Ma}	=	partial safety factor for the material short-term
γ_{Mb}	=	partial safety factor for the material fatigue
C_{1b}	=	$N^{\frac{1}{m}}$ curve of high-cycle fatigue for the load cycle number N and slope parameter m.

Whereas in γ_{Mb} a reduction factor for; S-N curve, temperature effect, fabric type, post-cured or non-post-cured and local blade trailing edge is included.

An interesting observation, the ultimate load analysis is that Puck's failure hypothesis is used with design values. For inter-fibre failure, an extra reduction factor is included; $C_{IFF} = 1.25$ to account for material property changes due to temperature, ageing and other influences.

2.3.5. Conclusion

From the different design recommendations, multiple conclusions can be drawn.

- Where CUR 96 and JRC prospect gives a more general guidance area of fatigue load, the TS19101 gives a fixed mathematical condition, based on load levels, when a fatigue verification needs to be performed. This equation is explicitly derived from setting a conservative limit for bridges. An R-ratio of 0.1 is used to set the limits of this equation.
- CUR 96, JRC prospect and GL 2012 allow the use of Palmgren-Miner's summation, whereas TS19101 does not allow it because results could be non-conservative. Hence TS19101 cannot address VA without a further specification of either a load spectrum or damage summation method.
- For simple geometries, the fatigue verification according to CUR 96, JRC and guideline for wind turbines may be performed with S-N curves of the same material and load type and Palmgren-Miner's summation. TS19101 prescribes qualification testing of each product and proof testing for specific applications.
- The use of TS19101 can lead to higher design costs due to the tests that need to be performed.

2.4. Conclusion

The literature study showed that the fatigue damage in composites is complex, load-dependent and load-type dependent. For **constant amplitude (CA)** loading, suitable formulations of the fatigue lifetime can be obtained by **S-N curves** or **constant life diagram (CLD)**. Here the dependency of the mean and amplitude stress is incorporated. The main difficulty for designers arises when there is a need to consider a **variable amplitude (VA)** loading or a sequence of different **CA** loads. Then the damage accumulation becomes a relevant aspect. This accumulation is complex and depends on multiple parameters mainly due to the different possible damage mechanisms and variety in lay-up configurations. Multiple damage summations are proposed in the literature to estimate the lifetime to failure. However, there is no direct relation to the physical damage development in the composite.

In several design recommendations such as CUR 96 [5], JRC [2] and GL 2012 [9] fatigue strength curves need to be determined for the used laminate. Alternatively, CUR 96 [5] allows for the use of **unidirectional (UD)** ply fatigue curves when the load is mainly carried by these **UD** plies, where CUR 96 [5] give the S-N curve parameters.

When determining these S-N curves, mainly the local directions of the laminate is tested. However, in an actual structure, complex stress states can occur. This is currently disregarded in the above-mentioned design recommendations. Damage summations like Palmgren-Miner disregards the influence of damage dependency and load order and can give non-conservative results. Due to the lack of a better summation principle, Palmgren-Miner is allowed in some design recommendations, but not always.

From the literature study into the fatigue behaviour of **Glas Fibre-Reinforced Polymer (GFRP)** it can be concluded that multiple aspects influence the fatigue behaviour and that design recommendations do not cover these in detail. Therefore, the Eurocode proposal TS19101, requires testing on a component level to include damage accumulation, complex stress states and local defects in the verification.

The aspects relevant to simulate the fatigue behaviour of in-plane stress dominated components have to do with the damage development in the material and load configurations, which can vary for each design. Therefore, the aspects that should be incorporated in a more advanced model would be: progressive damage accumulation, damage development under complex stress states, redistribution of stress between layers, and redistribution of stress in the component when damage develops. The damage development should depend on damage history, the lifetime fraction and the type of loading.

3

Numerical non-linear fatigue stiffness reduction model development

This chapter aims to develop a method to predict the fatigue performance of in-plane stress dominated **Glas Fibre-Reinforced Polymer (GFRP)** components with existing knowledge and experiments from the Optidat Database [36]. One of the aims is to develop a numerical fatigue reduction model, later on, called: **Virtual Fatigue Stiffness Simulation (ViFaSS)**, to simulate the material's fatigue behaviour to obtain a more economical design. To reduce the experimental effort for determining the model input, the input information will be mostly based on simple experimental results, i.e. **unidirectional (UD)** ply behaviour as given in the Optidat Database [36]. Simultaneously, this model's applicability should be on an engineering scale, i.e. on component and structural level instead of material level. The primary goal of **ViFaSS** is to simulate the component and structure fatigue stiffness response. Where the material can be build up out of a wide range of **GFRP** lay-up configuration, i.e. ply orientations and thicknesses and where the component or structure is in-plane stress dominate. To incorporate damage effects that are not considered in current design recommendations.

From the literature study, it is obtained that when a component is loaded by a **variable amplitude (VA)** load, the damage accumulation becomes a relevant aspect because standard test results cannot capture the fatigue response. The damage evolution depends on; damage history, type of loading and stress state. Due to the damage development, strength and stiffness decrease, this stiffness decrease causes stress redistributions on laminate and component level.

The Eurocode proposal requires the designer to obtain the fatigue resistance of a member by testing. This test incorporates the aspects mentioned earlier and the influence of imperfections in the verification. Providing the designer with the ability to incorporate stiffness reduction and stress redistribution in the predesign will result in a more economical design that will most likely pass the prescribed test. **ViFaSS** is developed to reduce the complexity for the designer and implemented in a design procedure.

First, the model's implementation in the design process will be described in section 3.1. Section 3.2 gives the minimal input requirements that are needed for the model. Section 3.3 describes each module that is included in the model.

3.1. Implementation in the design process

When writing this report, the beginning of a technical specification for Fibre-polymer composite structures is prepared by the technical committee CEN/TC 250 "Structural Eurocodes", here called "TS19101". The expectation is that, when the TS19101 is finalised and available, it will become a widely used specification for designing **Fibre-Reinforced Polymer (FRP)** structures in combination with EuroCode 0 [33], which holds for the other "Structural Eurocodes". Therefore, the fatigue verification procedure of the TS19101 is used as a framework for decisions regarding the model.

Figure 3.1 presents the verification procedure in TS19101 as a flowchart, where the implementation of **ViFaSS** is shown in the highlighted box. For a more thorough description of the equations, see 2.3.3. The TS19101 requires to verify if the structural member does require a fatigue verification or not. A qualification test must verify the "pass" criteria (see list below) and the post fatigue resistance if a fatigue verification is needed.

The TS19101 does not provide any guidance for predesign of the member. There is where the **ViFaSS** provide the designer with the ability to improve the predesign and increase the probability of a positive test outcome. For most **GFRP** structures, the serviceability limit state, i.e. deflections, is governing, and partial material factors are still significant, factor 2-5, which will results in a relatively low-stress state in the components compared to the ultimate stress. Therefore, the expectation is that material failure will not occur under fatigue loading, and the fatigue response that is included in the **ViFaSS** is related to stiffness reductions. In the following section, design decisions are described.

Pass criteria from TS19101

- the required number of cycles is completed without failure;
- the stiffness reduction is less than 5%, to prevent excessive micro-cracking;
- visible damage, i.e. macro-cracks, debonding, delamination, that could affect durability due to moisture ingress does not occur;
- the result of the post-fatigue static tests is within two standard deviations of the mean value of the static resistance achieved in the static tests.

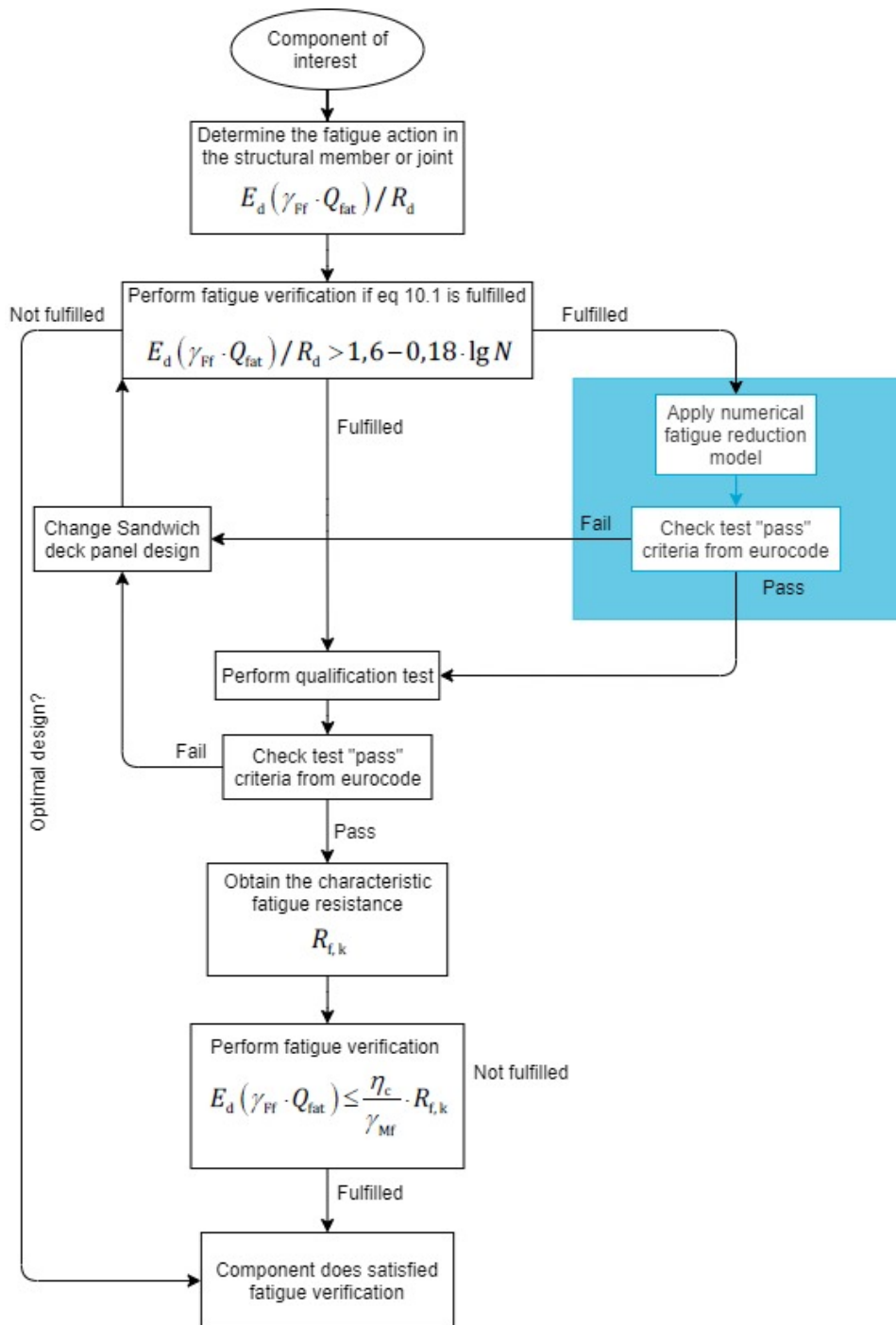


Figure 3.1: Flowchart Fatigue assesment according to TS19101 and implementation of Progressive damage model.

3.2. Experimental input requirements

All model input requirements are material related. As described in the chapter introduction, multiple properties of UD plies are needed. A complete set of UD data is required, existing of static material properties of the UD ply as indicated in table 6.1. Next to the static properties also fatigue properties are required on ply level in the form of S-N formulations. The minimum required S-N formulations needed are given below;

- UD 90°R=0.1
- UD 90°R=-1
- UD 90°R=10
- ±45°R=0.1
- ±45°R=-1

In section 3.3.2 a more thorough explanation is given on how the S-N curves are determined for the Optidat experimental results.

Table 3.1: Required static material properties

Property	Abbreviation	Test standard
Tensile modulus 1-direction	$E_{1,t}$	EN-ISO 527
Tensile modulus 2-direction	$E_{2,t}$	EN-ISO 527
Compressive modulus 1-direction	$E_{1,c}$	EN-ISO 14126
Compressive modulus 2-direction	$E_{2,c}$	EN-ISO 14126
Poisson's ratio 12-direction	ν_{12}	
Poisson's ratio 21-direction	ν_{21}	

3.3. Model description

In this section, a description of the model is given. In the subsections that will follow, a more thorough description of the modules is given.

From the literature study, it has become clear that the damage progression during VA loading is complex and that progressive damage models handle this better than proposed empirical relations, e.g. Palmgren-Miner summation. Therefore, a design procedure is developed that numerically performs the progressive fatigue damage accumulations, expressed in a reduction of the UD ply stiffness properties, and thus virtually verifies the fatigue response. The ViFaSS is designed to simulate the fatigue stiffness reduction of civil engineering components and structures build-out of GFRP material with a wide range of lay-up configurations. The mechanical component response under the fatigue load must be able to be characterised by in-plane material properties.

The ViFaSS uses the fatigue material response characterised on a UD ply level based on experimental results from the Optidat Database [36]. The stiffness degradation parallel to the fibre direction is not included in ViFaSS because it is in the order of 1 a 2% and neglectable compared to the transverse and shear reduction of around 25% and 32%, respectively.

The aspects that are incorporated in ViFaSS are progressive damage accumulation, damage development under multi-axial stress states, redistribution of stress between layers, and redistribution of stress in the component when damage develops. The damage development depends on damage history, the lifetime fraction and the type of loading.

The process of ViFaSS is given in figure 3.2 as a flow diagram and is fully programmed in Python. The full process is programmed in the programming language Python. The procedure starts with creating a Finite Element (FE) model in FE software SOFiSTiK of the structure with corresponding fatigue load models, support conditions and lay-up configurations. Performing a FE analysis of the structure will result in load vectors for each shell element. With the help of the Classical Laminate Theory (CLT) those load vectors are transformed into cyclic stresses: σ_{11} , σ_{22} and τ_{12} per individual ply. Together with the lifetime fraction, determined from the experimental results the ply stiffness properties: E_2 and G_{12} are degraded. To decrease the calculation time, a Artificial Neural Network (ANN) will filter the finite elements, which will experience no significant damage each even iteration. By repeating this process per fatigue load cycle step, a non-linear fatigue stiffness reduction model is formed. The virtually predicted material degradation gives insight into the material's damage development and stress redistribution between the layers and components.

The above-described considerations result in the following modules;

- classical laminate theory, to translate Finite Element (FE) results to ply stresses
- lifetime estimation from UD ply S-N curves
- element selection by an Artificial Neural Network (ANN)
- gradual stiffness degradation
- visualisation of results

Each of these modules is explained further on.

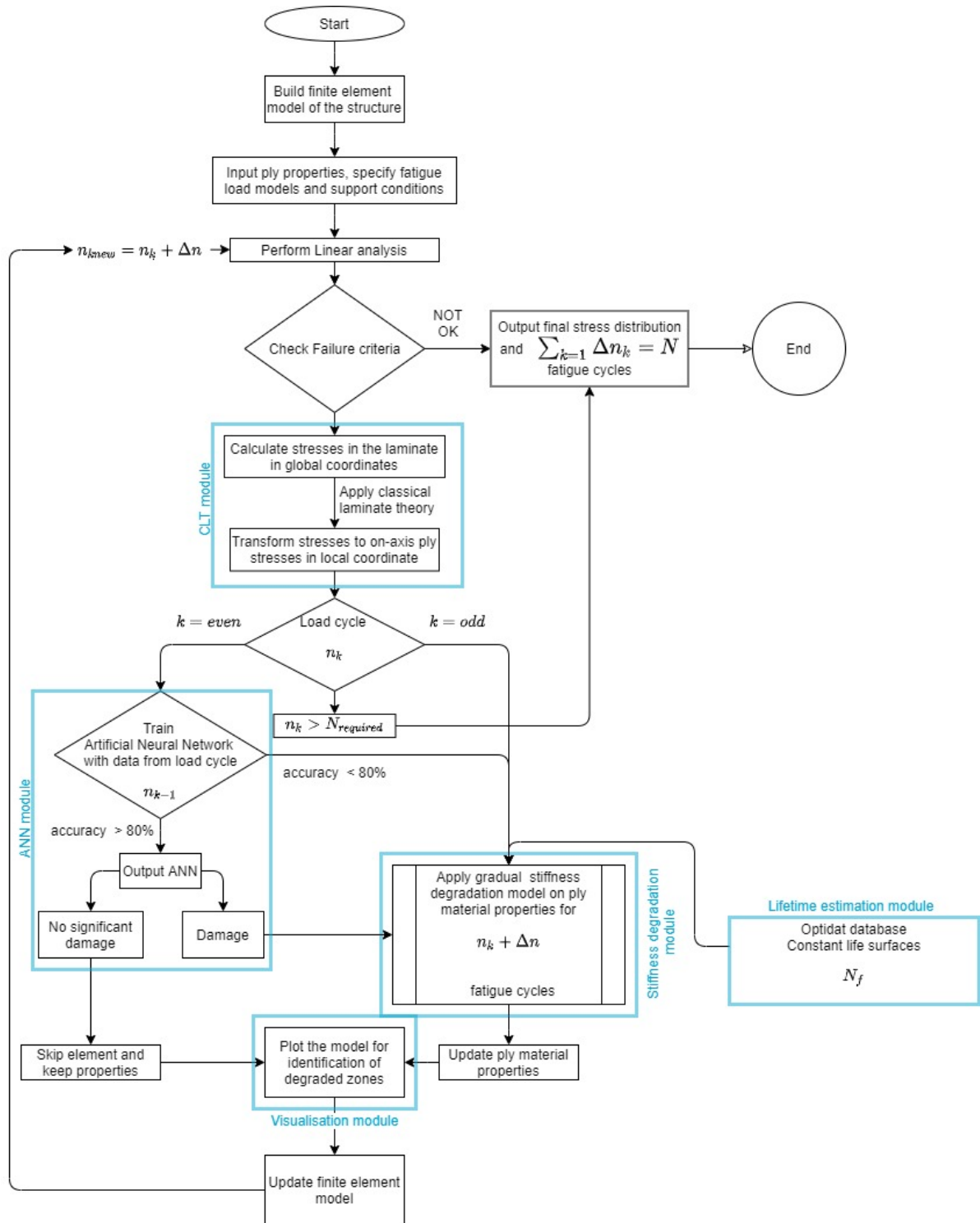


Figure 3.2: Flow diagram numerical fatigue reduction model

3.3.1. Module FE analysis and classical laminate theory

The basis of the fatigue damage analysis is the FE model, which calculates the membrane forces. Commercial FE software SOFiSTiK is implemented as FE module as engineering firms generally use it. In SOFiSTiK, the geometry is modelled as structural areas. For out of plane loading, SOFiSTiK uses Mindlin’s plate theory [55], and for in-plane loading, it uses membrane structural behaviour. Mindlin’s theory is used to obtain the plates’ bending moments and shear forces, respectively; $[m_{xx} m_{yy} m_{xy}]^T$ $[v_x v_y]^T$ and the membrane theory for the membrane forces; $[n_{xx} n_{yy} n_{xy}]^T$. For the used axis system, see figure 3.3.

The FE software exports, for each element and load case, a load vector consist of; $[n_{xx} n_{yy} n_{xy} m_{xx} m_{yy} m_{xy}]^T$. The CLT module of ViFaSS converts this load vector to in-plane stresses in the ply, i.e. normal stresses parallel and transverse to the fibre direction and the in-plane shear stress. Figure 3.4 presents the flowchart of the described procedure. Calculation of the ABD matrix, ply deformations and ply stresses are validated with eLamX2 [24]. This validation is given in appendix A.

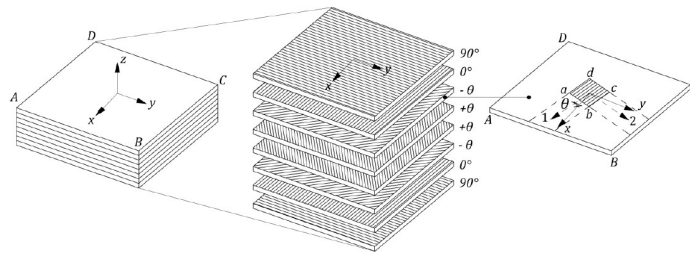


Figure 3.3: Reference axis system used in this work, obtained from TS19101

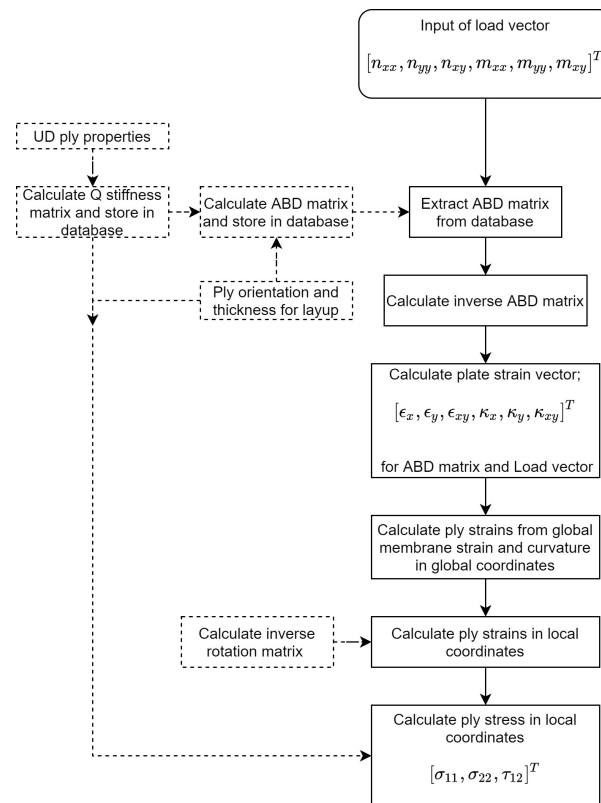
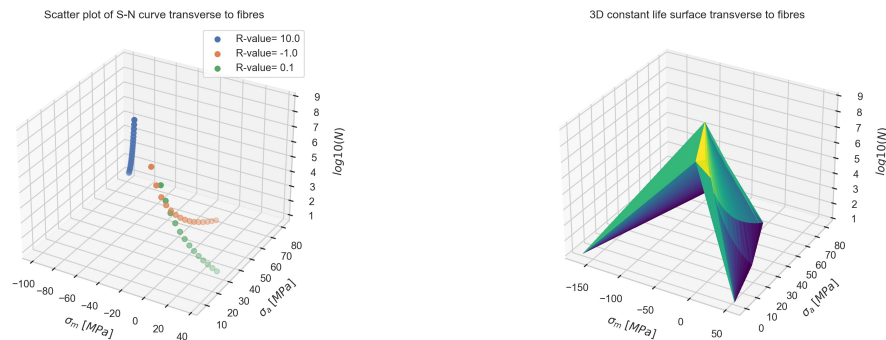


Figure 3.4: Flowchart of the CLT module

3.3.2. Module lifetime estimation of UD plies

To model the gradual stiffness degradation, the corresponding stress state's lifetime is required. See equation 3.2c and 3.2d. Because multiple stress states can occur in the structure, a lifetime envelope is required to determine the lifetime for each stress state. A **constant life diagram (CLD)** is a good example of such envelope describing the lifetime under different mean stress (σ_m) and alternating stress (σ_a). However, the interpolation of such a diagram is complex.

Therefore a different method is developed for obtaining the lifetime for the corresponding stress state. The **S-N** curves are projected in 3D space. On the XY plane, the mean (σ_m) and amplitude (σ_a) stress are projected, the Z-axis represents the cycles to failure. Figure 3.5a shows the **S-N** curves transverse to the fibres. Including the static strength on the mean-axis and linear interpolating between the 3D points will result in a **constant life surface (CLS)** as given in figure 3.5b. Construction of the **CLS** is done for in-plane, transverse and shear stress. For the construction of the **S-N** curves, in-plane experimental results from the OptiDAT database [36] are used.



(a) Scatterplot of S-N curves in 3D space, transverse to fibres. (b) **CLS** in 3D space.

Figure 3.5: Constant life surface construction.

S-N curve formulation

In this subsection, the **S-N** formulation for the mean and design value is described. As presented in section 2.1.3 the fatigue lifetime is represented in **S-N** diagrams. However, the relation of the dependent and independent variable, N and σ_{max} , respectively, is not fixed. In equation 2.2 a log-log relation between N and σ_{max} is suggested. However, there are more relations possible. Depending on the range of lifetime, the accuracy differs. In the **S-N** diagram it is possible to include the static data, i.e. σ_{max} at $N = \frac{1}{2}$. Including this data will influence the accuracy along the N-axis. Accuracy increases in the low-fatigue life region, i.e. near static strength, but decreases in the high-fatigue life region.

The **American Society for Testing Materials (ASTM)** standard for statistical analysis of fatigue data [4] allows a lin-log or log-log relation. Nijssen [37] showed that the log-log relation gives a higher accuracy in the high-fatigue life region than the lin-log relation when excluding the static strength. In figure 3.6 both relations are given for **Tension-Tension (T-T)** in the transverse direction of the **UD**-ply. The difference in fatigue life in the high cycle region is visible. The resulting figures are given in appendix C.

ViFaSS will be used for structures and components often designed on the serviceability limit state as indicated in the model description. Therefore, it is chosen not to include the static strength of the **UD**-ply in the **S-N** and to use the log-log formulation to have a higher accuracy in the predicted lifetime values of high cycle region.

For model validation, mean values are needed, and for design purposes, the 95 percentile lower confidence bound ($P \approx 0.95$) of the fatigue life is required. Therefore, the tolerance bound is determined with the help of ASTM E739 – 10 [4] see equation 3.1. To exclude the use of a table for $\sqrt{2F_p}$, $\sqrt{2F_p}$ is changed by the fifth percentile Student's t probability density function for the corresponding number of experiments. The use of the fifth percentile Student's t probability density function is validated with ASTM Special Technical Publication STP313 [3].

To use the tolerance bound, a similar relation as the S-N formulations should be determined, i.e. an a and b parameters should be fitted because the tolerance bound is not linear on a log-log scale. These parameters are given in the legend of the corresponding plot.

$$\hat{A} + \hat{B}X \pm \sqrt{2F_p\hat{\sigma}} \left[\frac{1}{k} + \frac{(X - \bar{X})^2}{\sum_{i=1}^k (X_i - \bar{X})^2} \right]^{1/2} \quad (3.1)$$

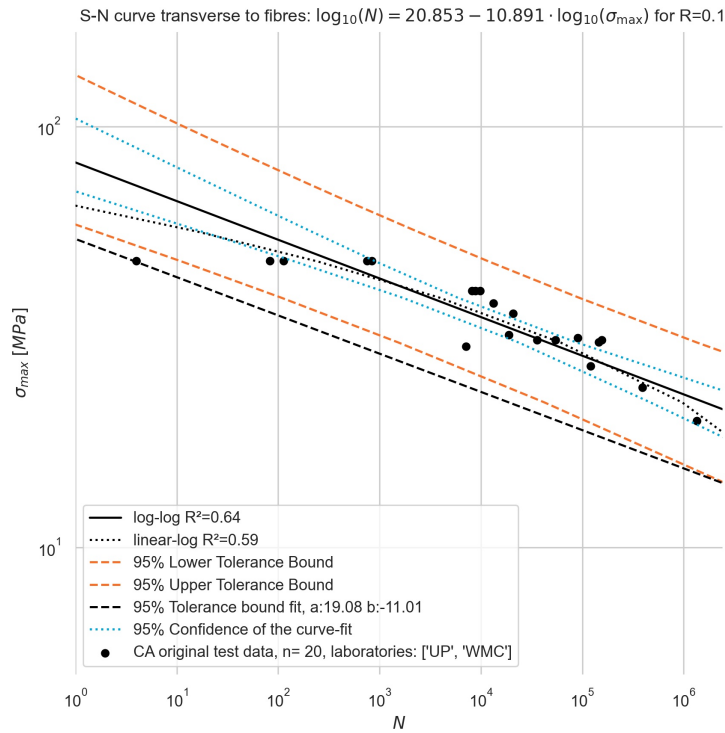


Figure 3.6: S-N curve transverse to fibres for T-T

Lifetime prediction with CLS

The purpose of the CLS is to give the fatigue lifetime of the corresponding stress state, i.e. σ_m and σ_a . ViFaSS will distinguish stress transverse to the fibres, shear stress and use the corresponding CLS to predict the number of cycles. In figure 3.6 the mean and 95 percentile tolerance bound is plotted, the CLS can predict the lifetime for both.

The OptiDAT database [36] consists of several experiments. There are multidirectional (MD) laminate types where fatigue experiments are performed for multiple R values 2, 10, -1, -0.4, 0.1, 0.5. The fact that multiple S-N formulations are known gives the possibility to use R 10, -1 and 0.1 to predict S-N curves for R 2, -0.4 and 0.5. Two methods were investigated, linear and cubic interpolation of the S-N curves, appendix B presents the validation of the method. All linear predicted values by the CLS are below the fitted S-N curves from experiments. Therefore, the validation of the method can conclude that linear interpolation of the surface gives conservative values.

In some cases, cubic interpolation can result in non-conservative results. The OptiDAT program [25] concluded that for a constant life diagram, at least the S-N curves for R values of 10, -1, 0.1 must be used. The validation also concludes this in appendix B.

Linear 3D interpolation is used because the difference between linear and cubic is minor, and for some R values, cubic overestimates the fatigue life.

3.3.3. Module element selection by a Artificial Neural Network

Letting ViFaSS degrade each layer's stiffness in every FE model's shell elements is memory and time-consuming. The shell elements that experience low stress will have no significant damage compared to those with higher stresses. Therefore, an ANN is used to reduce calculation time and by excluding elements with a low-stress state from the degradation module. The ANN improves the efficiency of the analysis. The selection of elements is made by training an ANN with results produced from the uneven load cycle. By using the results from the previous load cycle, the stress redistribution in the laminate is still included. The load vector from the FE analysis forms the input data, whereas the change in the material indicates failure. So when a shell element keeps its original properties during the odd cycle, no significant damage occurred.

The ANN is trained to predict if a shell element experiences damage based on the load vector. The accuracy of this prediction is essential to prevent mistakes in the analysis. It is known that a ANN gives better predictions within the range of the trained data. The expectation is that when in a component multiple complex stress states occur, the training data is representative for the next cycle. A visual representation of the neural network is given in figure 3.7.

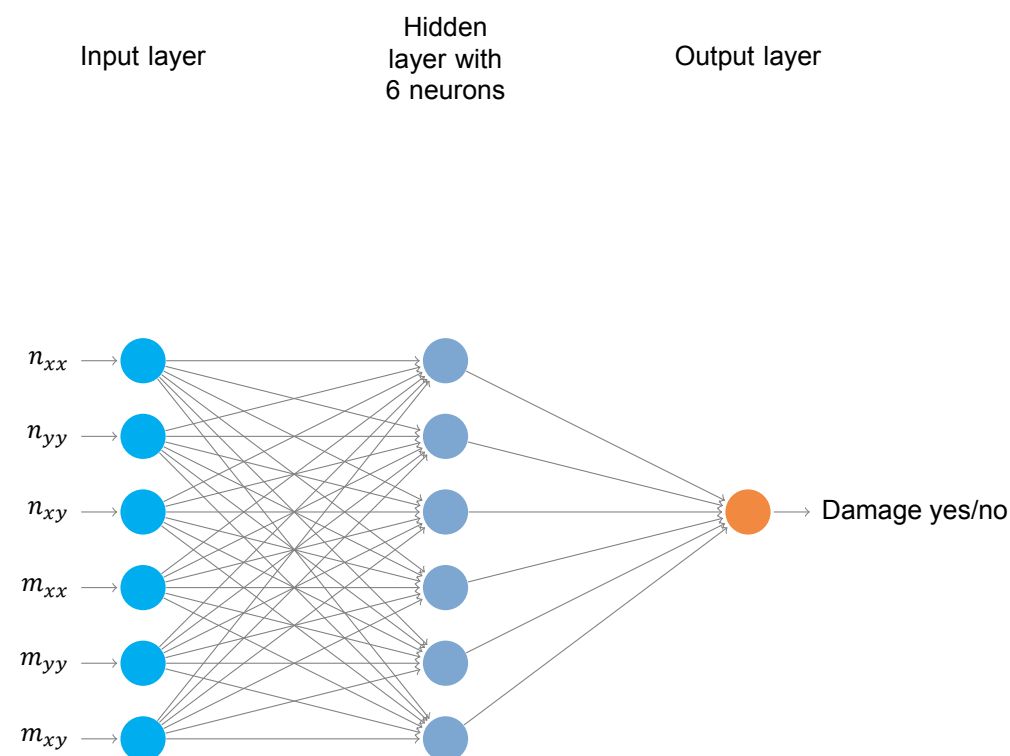


Figure 3.7: Visual representation of the Artificial Neural Network

Different ANN configurations, i.e. with changing the number of hidden layers and neurons per layer, are trained, ranging from 1 layer with 6 neurons to 3 layers with each 20 neurons. To simulate complex relations with a ANN more layers and neurons perform better. Most ideal is a ANN where the number of layers and neurons is reduced to limit the calculation time. The 6 best performing configurations, out of 42, are shown in table 3.2. The data used in comparing the different configurations is obtained from a simple sandwich deck panel test as seen in figure 3.8. Comparing the different configurations is done with a random sample of 10% of the data used for training the ANN and the other 90% for validation. In table 3.2 it can be seen that the differences in accuracy are minor. Therefore, to minimise training time, the configuration given in figure 3.7 is used, i.e. one layer with six neurons.

Table 3.2: Comparison multiple ANN configurations

Layers	Neurons	Accuracy	mse
2	13	0.993628919	0.006340144
1	16	0.993319452	0.006549608
2	16	0.993278623	0.006577705
2	19	0.993360102	0.006597224
1	10	0.993263066	0.006607056
1	6	0.993131042	0.006714792

SOFISTIK

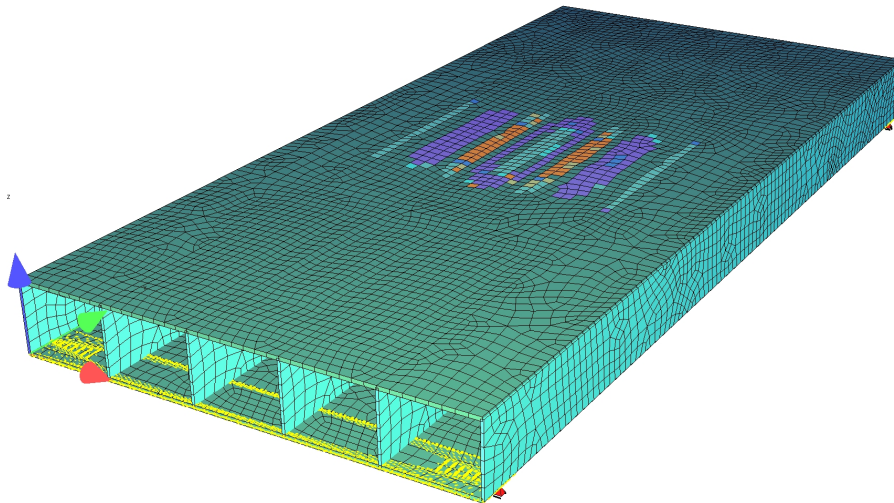


Figure 3.8: FE model to compare ANN configurations

3.3.4. Module gradual stiffness degradation

The stiffness degradation module is the core of ViFaSS where the material stiffness properties are degraded due to fatigue damage. In-plane transverse and shear stiffness will degrade due to fatigue. Degradation of the stiffness in the parallel direction to fibres is in the range of 1-2% and considered not significant [11]. The model assumes a linear stress-strain relation for all stiffnesses. This linear relation simplifies the incorporation of the degradation because only one parameter needs to be degraded instead of the non-linear stress-strain relation. Multiple types of stiffness degradation and their formulation are proposed in the literature for individual stiffness degradation.

ViFaSS considers only in the in-plane, transverse and shear stiffness due to damage development in the matrix. As described in section 2.2 the stiffness degradation is caused by the laminate's damage, e.g. matrix cracking, fibre-matrix debonding and debond propagation. It is assumed that by including only the stiffness reduction caused by matrix damage, in-plane dominated structures and components can be simulated properly. Excluding out of plane fatigue damage reduces the complexity and calculation time of the analysis.

For the stiffness degradation to be physically correct, there should be a relation between the transverse and shear modulus degradation. The matrix damage dependency suggests that the modulus reduction is proportional to the magnitude of damage, independent of the modulus direction. This quantification of moduli damage interaction relation's is complex due to multiple damage mechanisms and their unknown influence on the different moduli. In literature, there are some relations given for this interaction. Mohammadi et al. [31] proposed a continuum fatigue damage model. In their model, the interaction between matrix and shear damage was proposed in the damage increment and included the thermodynamic force variation within one load cycle. The proposed relation is not straightforwardly implementable in ViFaSS because the fibres and matrix are not modelled separately.

The relations given in equations 3.2c and 3.2d are proposed to incorporate the interaction between transverse and shear damage. These relations are a modification of the relation used by Pasipoularidis [42], the modification is inspired by the relation proposed by Mohammadi et al. for the continuum relation. The interaction is assumed to be in the damage increment per cycle step. Equation 3.2a describes the damage development when the interaction is not included, where equation 3.2b describes the numerical formulation of the increment. The interaction effect is visually presented in figure 3.9. The blue and green line represents the shear and transverse (tension) stiffness degradation, respectively. As shown in the figure, it is assumed that the secondary modulus degradation influences the primary modulus. It is assumed that the ratio of interaction depends on the equivalent number of cycles of the secondary modulus and primary modulus damage history.

For the shear damage, $D6_k$, the equivalent number of cycles is calculated, i.e. $n6_k$, the same is done for $D2_k$, resulting in $n2_k$. The slope of both damage curves is determined at $ni_k + \Delta n$, and normalised to the primary modulus with the ratio of the equivalent number of cycles, as explained above. The slope is normalised to ensure a stable interaction. When the slope is determined, the extrapolation is performed, shown by the inclined blue dashed line obtaining the new damage, $D6_{k+1}$ shown in figure 3.9.

The fatigue life fraction in 3.2c and 3.2d implicitly incorporates the dependency of the R-values. However, the α and β parameters are dependent on the type of damage that occurs. The damage development differs for different load conditions. Subsection 2.1.2 describes the damage developments due to the different load conditions.

$$Di_{k+1} = 1 - \frac{E_{i_{k+1}}}{E_{i_0}} = Di_k + \Delta n \cdot Di' \left(n + \frac{\Delta n}{2} \right) \quad (3.2a)$$

$$Di' \left(n + \frac{\Delta n}{2} \right) = f \left(n_k + \frac{\Delta n}{2}, Di_n + \frac{\Delta n}{2} f(n_k, Di_k) \right) \quad (3.2b)$$

$$D2' \left(n2 + \frac{\Delta n}{2} \right) = \frac{(1 - \alpha_2) \cdot \beta_2 \cdot \left(\frac{n_2 + \frac{\Delta n}{2}}{N_2} \right)^{\beta_2}}{n_2 + \frac{\Delta n}{2}} \cdot \frac{n_2 + \frac{\Delta n}{2}}{n_2 + \frac{\Delta n}{2}} + \frac{(1 - \alpha_6) \cdot \beta_6 \cdot \left(\frac{n_6 + \frac{\Delta n}{2}}{N_6} \right)^{\beta_6}}{n_6 + \frac{\Delta n}{2}} \cdot \frac{n_6 + \frac{\Delta n}{2}}{n_2 + \frac{\Delta n}{2}} \quad (3.2c)$$

$$D6' \left(n6 + \frac{\Delta n}{2} \right) = \frac{(1 - \alpha_6) \cdot \beta_6 \cdot \left(\frac{n6 + \frac{\Delta n}{2}}{N_6} \right)^{\beta_6}}{n6 + \frac{\Delta n}{2}} \cdot \frac{n6 + \frac{\Delta n}{2}}{n6 + \frac{\Delta n}{2}} + \frac{(1 - \alpha_2) \cdot \beta_2 \cdot \left(\frac{n2 + \frac{\Delta n}{2}}{N_2} \right)^{\beta_2}}{n2 + \frac{\Delta n}{2}} \cdot \frac{n2 + \frac{\Delta n}{2}}{n6 + \frac{\Delta n}{2}} \quad (3.2d)$$

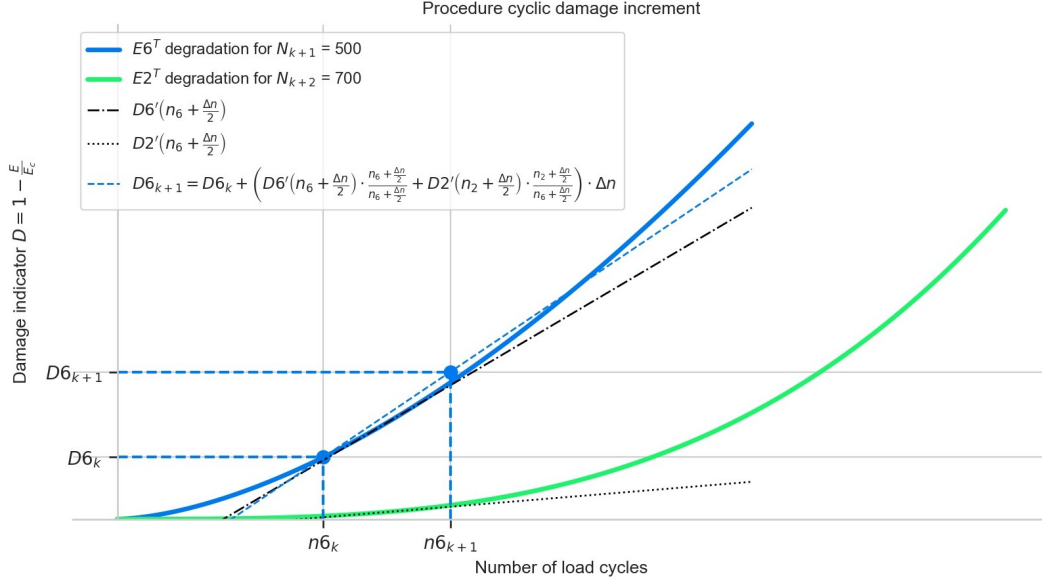


Figure 3.9: Visual presentation of the damage interaction procedure, for the case $n_6 = n_2$.

Three specific loading cases can experimentally characterise the material parameters α and β . Those load cases are; **Tension-Tension (T-T)** and **Compression-Compression (C-C)** loading in the transverse direction and pure shear loading. In all these loading cases, the interaction effect is assumed to be neglectable due to the large difference in fatigue life fraction for the different components. Additional to the difference in life fraction, the **Classical Laminate Theory (CLT)** theory indicates that the modulus of interest only determines the response of the laminate under those loading conditions. For these load conditions equation 3.2c and 3.2d simplifies to 3.3a and 3.3b.

$$D2' \left(n2 + \frac{\Delta n}{2} \right) = \frac{(1 - \alpha_2) \cdot \beta_2 \cdot \left(\frac{n2 + \frac{\Delta n}{2}}{N_2} \right)^{\beta_2}}{n2 + \frac{\Delta n}{2}} \quad (3.3a)$$

$$D6' \left(n6 + \frac{\Delta n}{2} \right) = \frac{(1 - \alpha_6) \cdot \beta_6 \cdot \left(\frac{n6 + \frac{\Delta n}{2}}{N_6} \right)^{\beta_6}}{n6 + \frac{\Delta n}{2}} \quad (3.3b)$$

Assuming these relations to be dependent on n and calculating the indefinite integral, with $Di(0) = 0$ an equation of the damage development is obtained; 3.4.

$$D_i = 1 - \frac{E_i}{E_{i0}} = (1 - \alpha_i) \left(\frac{n}{N} \right)^{\beta_i} \quad (3.4)$$

Pasipoularidis [42] used the same relation and performed experiments that satisfy the specific load conditions. The fitted parameters by **Pasipoularidis** are assumed in this work because the accuracy of the fit on the Optidat database's experiments is within the experimental scatter.

It is important to note that **Pasipoularidis** assumed that the shear modulus degradation is the same as the degradation of the $[\pm 45]_s$ laminate used in the test. This assumption is not entirely valid because

the layers also experience a low σ_{11} and σ_{22} component. Also, the measurements are based on the load-displacement measurements from the test rig.

Table 3.3 gives an overview of the used α and β parameters. Where α is the proportion of stiffness at failure, i.e. $\frac{E_{kfailure}}{E_0}$ and β is the concavity of the curve and has no direct physical relation. Figures; 3.10, 3.11 and 3.12 represents the in-plane modulus damage, calculated with; equation 3.4, for transverse compression, transverse tension and shear load conditions, respectively.

Table 3.3: Stiffness degradation parameters obtained from [11]

Modulus	D_i	α	β
Transverse tension stiffness	D_{2t}	0.75	3.17
Transverse compression stiffness	D_{2c}	0.95	0.62
Shear stiffness	D_6	0.68	1.65

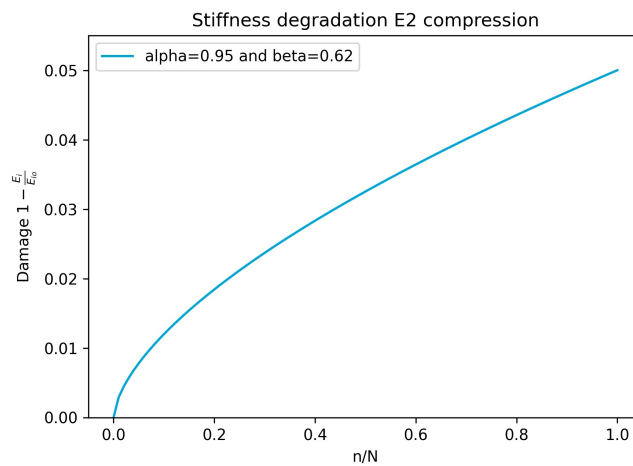


Figure 3.10: In-plane transverse modulus damage for compression load conditions for unidirectional (UD) glass-epoxy composite.

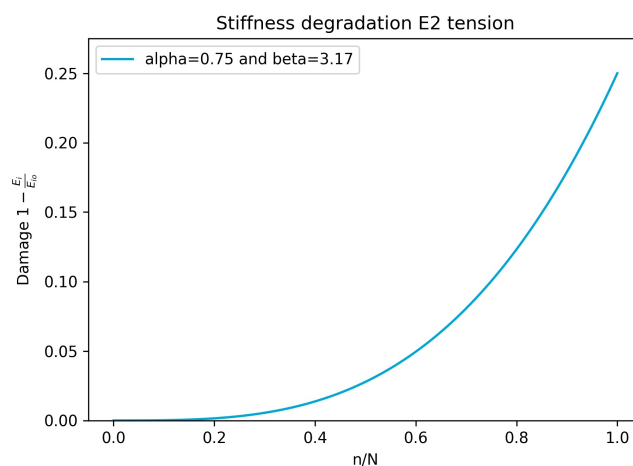


Figure 3.11: In-plane transverse modulus damage for tension load conditions for UD glass-epoxy composite.

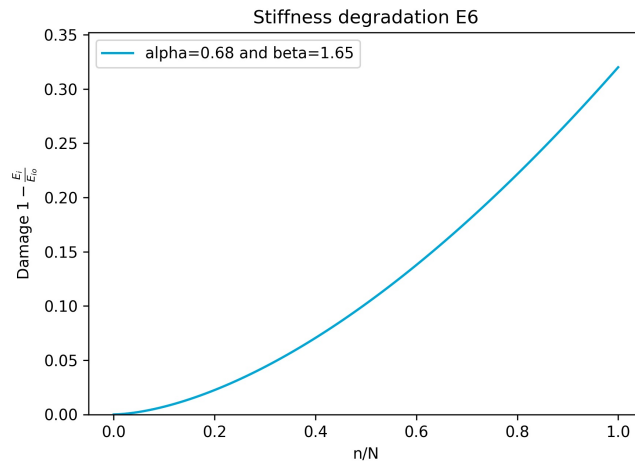


Figure 3.12: In-plane shear modulus damage for UD glass-epoxy composite.

Damage summation

As described in subsection 2.1.4 the damage state and damage mechanisms are interactive and dependent on the already induced damage. Thereby, the locally induced damage can result in a stress redistribution in the component, leading to a decreasing fatigue life during the lifetime. Therefore the damage summation is not that straightforward.

From the work of Gamstedt and Sjögren[15], see figure 3.15, it is shown that there is only a sequence effect if the damage progression is different for the high and low amplitude loading. Mathematically this occurs when the concavity, caused by the β parameter, differs per curve. In the work of Eliopoulos and Philippidis[11], the extensive experimental scatter in the results caused that the influence of σ_{max} on the concavity could not be quantified. In this work, the assumption is made that the parameter β is constant and not dependent on σ_{max} . This assumption is based on the presented results in [11], see figure 3.16. Results for the same R-value with different σ_{max} are close together. In the following, the damage summation of the model is explained.

Figure 3.13 is a graphical representation of the damage summation procedure. The damage of cycle k is obtained from the database, the degradation curves for transverse and shear damage are established with the calculated fatigue life $N2_{k+1}$ and $N6_{k+1}$ respectively. Rewriting equation 3.4 for n will give the corresponding number of cycles where the same damage occurs; ni_k , i.e. n_2 and n_6 in equation 3.2c and 3.2d. Using these equations to determine the increment at $ni_{k+\frac{\Delta n}{2}}$ and applying equation 3.2a gives Di_{k+1} , the "new" degraded stiffness. The different colours in the figure represent the damage curves for different fatigue lives, e.g. caused by stress redistribution or different applied loading. For example, the orange line represents a high load cycle and the blue line a low load cycle. Figure 3.13 and 3.14 illustrates the influence of a high-low and low-high loading sequence on the stiffness damage respectively. The relation given in equation 3.4 suggests that the maximum damage and the damage progression are independent of the applied stress because the shape parameters, i.e. α and β are constant per load type. However, according to the literature, as described in subsection 2.1.4, the interaction effect would also be expected in a UD laminates due to interface failure, which starts the fibre matrix debonding and results in higher stresses in the fibres [15]. From the figures can be concluded that there is no sequence effect included in the stiffness degradation due to the independence of the maximum applied stress.

For now, the used stiffness damage formulation is assumed to be applicable. Investigation on the stress dependency can result in a formulation where the sequence effect in UD plies is included.

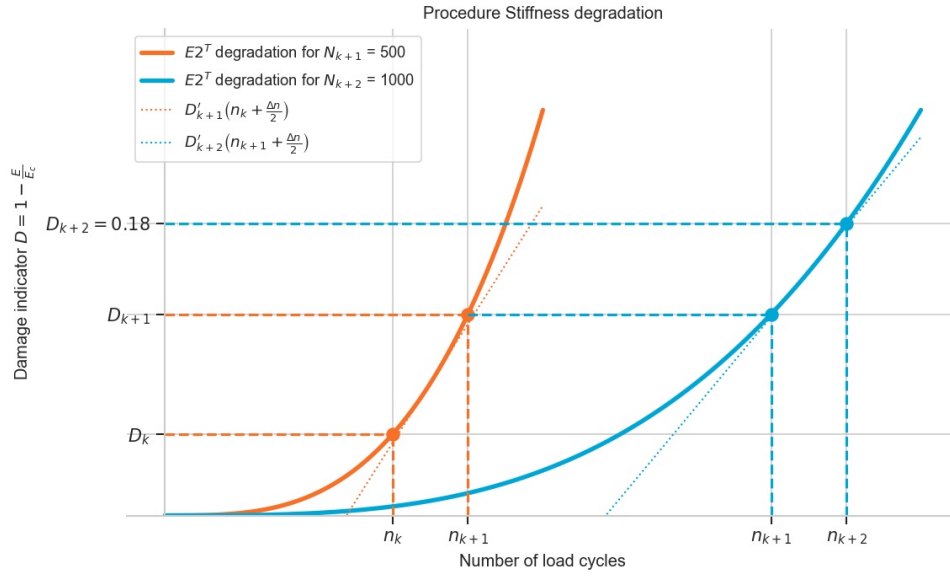


Figure 3.13: Damage summation high-low sequence UD ply.

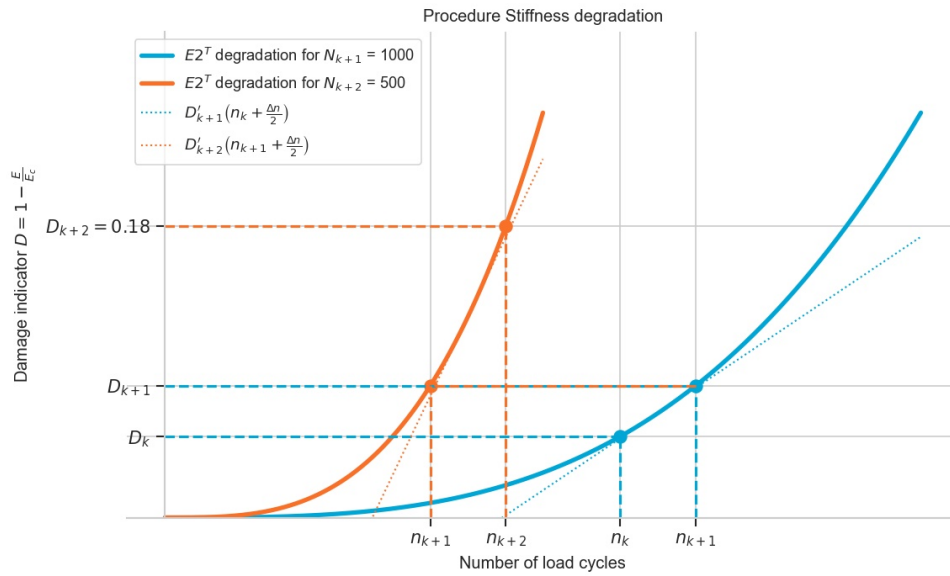


Figure 3.14: Damage summation low-high sequence UD ply.

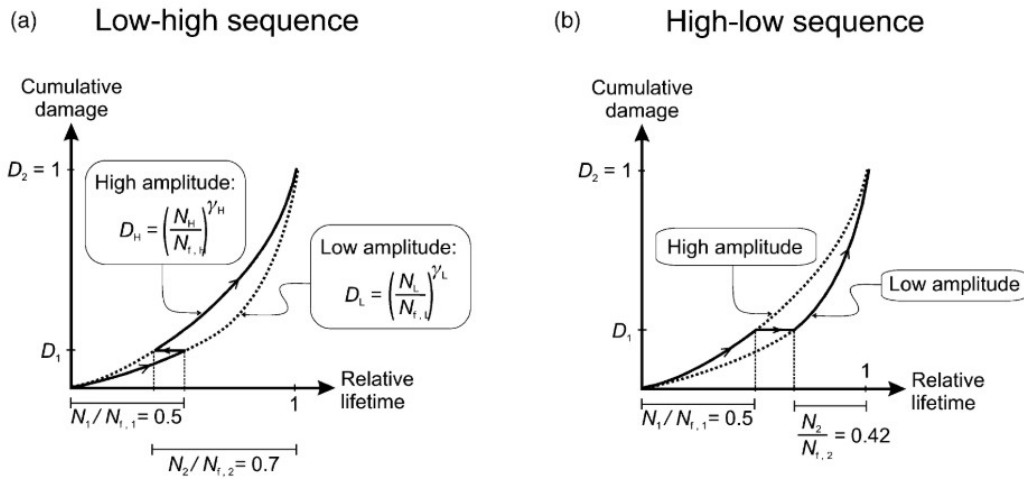


Figure 3.15: Marco-Starkey sequence effect, obtained from [15]

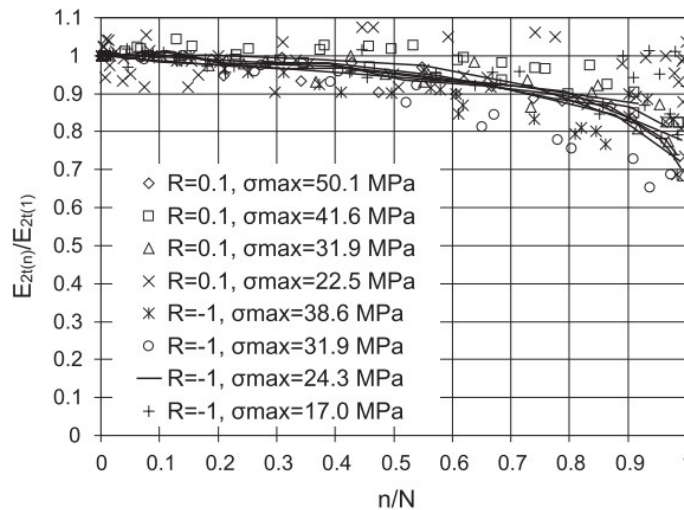


Figure 3.16: Stiffness reduction experiments used in the determination of α and β , obtained from [11]

Cycle step determination

The step size must be selected to be applicable for all shell elements. When determining the step size, i.e. Δn , several criteria are relevant:

- The stress redistribution due to gradually degrading ply stiffness should be captured accurately to model the component's fatigue response.
- The simulation of a component should not take too much time. Simulating each load cycle will predict the stress redistribution accurately; however, the computational efficiency of the model will be low.

An possible solution is to limit the damage increment per simulated cycle, i.e. when $\Delta n \cdot Di' \left(n + \frac{\Delta n}{2} \right)$ in equation 3.2a is limited. If the damage increment is limited to e.g. 1%, the stress redistribution is still simulated accurately. With the known analytical formulation of the UD stiffness degradation given in equation 3.4 the maximum step size can be calculated.

Figure 3.17 gives the distribution of the maximum step size per shell element per layer associated with 1% damage increase. The small step sizes result from heavily damaged layers, which eventually take a low portion of the stress. Taking the minimum step size will be over conservative and results in low computational efficiency. The optimal applied step size, used for all elements, can best be chosen

in such a way that is optimal for a large number of elements. The 5% percentile of the data is used as an appropriate step size. The proposed method is in line with the work of Van Paepegem [61], where also the damage increment is limited per simulated cycle.

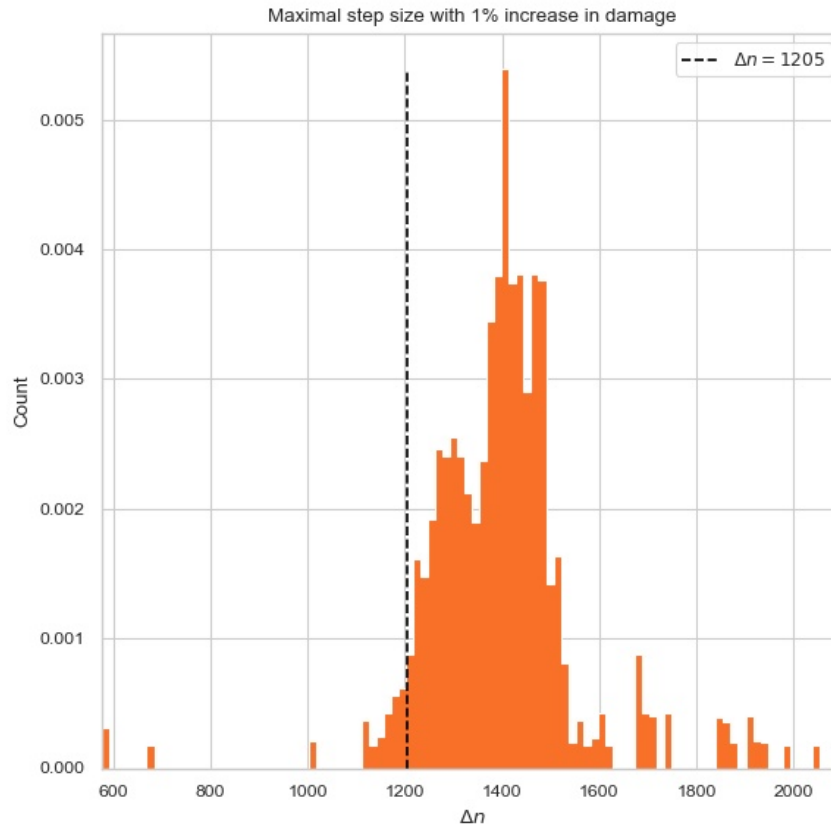


Figure 3.17: Visualisation of the maximum allowable step size distribution

Finite Element (FE) implementation

When **Virtual Fatigue Stiffness Simulation (ViFaSS)** has determined the ply damage in the current cycle, this information has to be incorporated into the **FE** model. These properties are implemented by defining new **UD** and layered materials in the material database with the help of a script using **TEDDY**, i.e. the text editor of the **FE** software. The coding language is **CADINP**.

However, there are some limitations in **SOFiSTiK** regarding the maximum allowable number of materials. The number of unique materials is limited to 999 different material definitions. To cope with this limitation, it is chosen to update the material properties in steps. For a new material definition to the following procedure is followed:

1. The existing **UD** materials are consulted, and when a difference of, e.g. 1%, occurs, a new **UD** material is created.
2. A new layered material is created if the specific composition does not exist until the database is full.
3. New layered materials replace unused layered materials until all the materials are present in the **FE** model.
4. The least used material number is replaced. The element that loses its layered material will get the same layered material as the element with the most similar load vector. The determination of the nearest load vector is based on the distance between the two vectors. See equation 3.5.

$$D_{ij}^2 = \sum_{V=1}^n (X_{vi} - X_{vj})^2 \quad (3.5)$$

Module verification

The above-described stiffness degradation module of ViFaSS is verified by a comparison of the predicted primary stiffness reduction and the analytical expression given in equation 3.2c and 3.2d. In appendix D this verification is reported in detail. The implemented procedure works correctly for all three stiffnesses. A 0.2% difference is caused by the numerical extrapolation between the analytical expression and the numerical simulation.

3.3.5. Visualisation of results

The visualisation of the stiffness degradation during the fatigue loading is critical for design validation. Therefore each time when a FE analysis is performed, a report is generated by SOFiSTiK, where the preferred output can be selected. This report contains information about the used materials, applied load conditions, reaction forces and visualisation of the following results per structural area, e.g. face sheets and webs ;

- applied fatigue load case
- material designation
- global deformation of the structure
- membrane forces
- membrane bending moments
- maximum compressive and tensile stress in the layered material

An example of such a report can be found in the appendix E.

4

Numerical non-linear fatigue stiffness reduction model validation

In this chapter, the applicability of [Virtual Fatigue Stiffness Simulation \(ViFaSS\)](#) is validated. For accuracy with in-plane stress dominated components, two types of loading can be characterised: in-plane loading and out of plane loading. Therefore, a validation is performed on two experiments that each include one type of loading. In section [4.1](#) the model is validated for in-plane [Tension-Tension \(T-T\)](#) fatigue loading, and in section [4.2](#) the model is validated for out of plane loading with a R-value of 0.1.

4.1. Model validation on MD laminate $[(\pm 45/0)_4/\pm 45]_T$ under T-T loading

To validate the proposed stiffness degradation relations in equations [3.2c](#) and [3.2d](#) an experiment is needed where transverse and shear stresses occur simultaneously in the plies. Also, the ply material properties used in the [multidirectional \(MD\)](#) laminate need to correspond with the material input used in [ViFaSS](#), i.e. [unidirectional \(UD\)](#) experiments from the Optidat database [\[36\]](#), so that the fatigue material response is similar. An experiment that fulfils the above requirements is also performed within the Optidat program; fatigue test of $[(\pm 45/0)_4/\pm 45]_T$ laminate under T-T loading [\[28\]](#). A more detailed description of the experiment is given under [4.1.1](#).

4.1.1. Introduction

Various aspects of the experiment are addressed in this subsection regarding the geometry, loading, mechanical model and material.

General The lay-up of the multi-directional laminate consists of 9 layers in total; five $\pm 45^\circ$ layers with a thickness of 0.61 mm and four 0° layers of 0.88 mm thickness. The unidirectional material is the same as is used in the model input. The laminate is fabricated with epoxy resin by vacuum-assisted resin transfer moulding and is post-cured at 80°C for a duration of 4 hours [\[28\]](#). Figure [4.1](#) represents the geometry of the coupon specimen. See table [4.2](#) for the [UD](#) and [MD](#) properties.

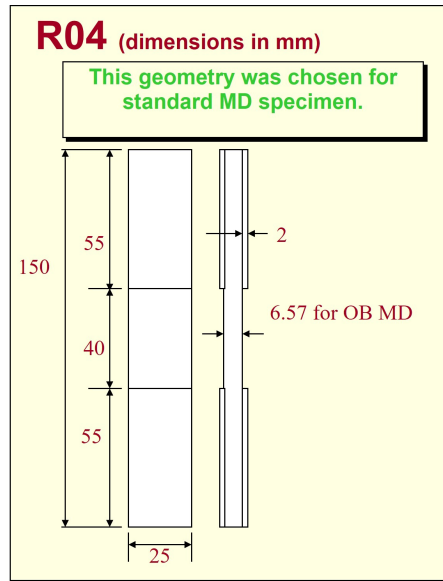


Figure 4.1: Geometrical representation of the coupon specimen [36]

Loading The experiment is performed on three different stress levels; 317, 252, 186 [MPa] and is also used to validate the FADAS algorithm [10]. See figure 4.2. The initial stiffness of the coupon specimens is measured after the first load cycle [10]. Within this first load cycle, some static damage occurs. At a high-stress level, the ± 45 layers damage more significantly. This damage causes the 0° layers to attract more stress after the first cycle. The higher stress in the 0° plies results in a higher measured stiffness related to the original cross-section than the measured stiffness after one low-stress cycle. The above-described effect can be observed in figure 4.2 where the high-stress degradation is "less" compared to the low-stress experiments.

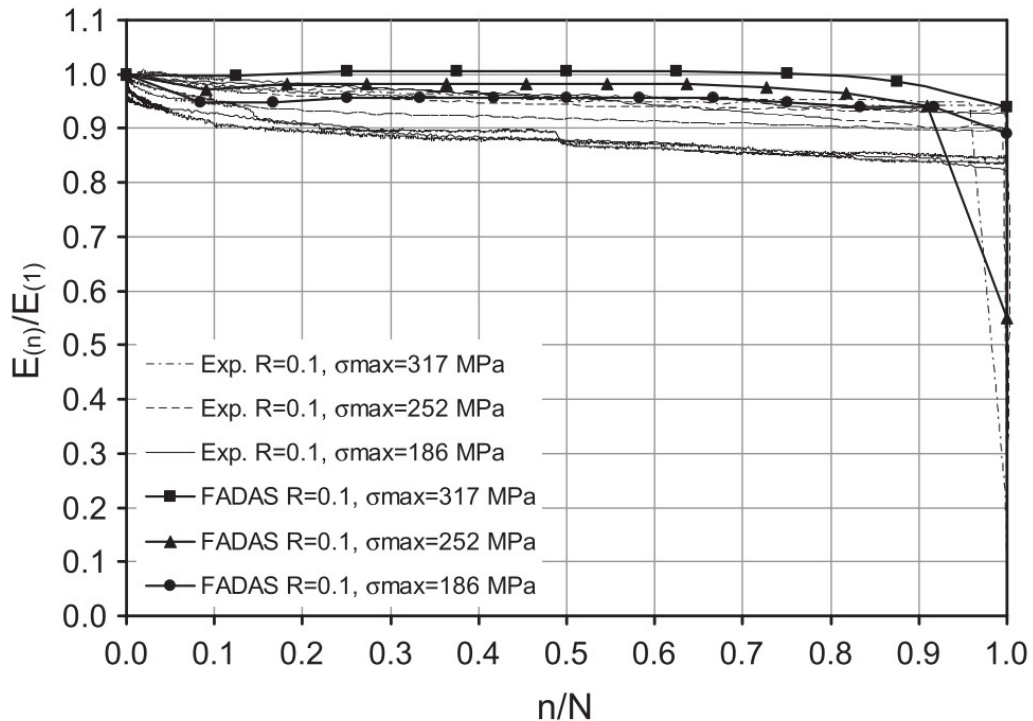


Figure 4.2: Stiffness degradation measurements $[(\pm 45, 0)_4, \pm 45]$ [10]

Mechanical and Finite Element (FE) model For a correct representation of the test conditions, the mechanical model given in figure 4.3 is used. For the top boundary condition, the z-direction is constrained, and only for the most left node, the x-directions is constrained for kinematic stability. At the bottom edge, only the y-direction is constrained. It is assumed that this will represents the mechanical behaviour for a T-T load condition because stress concentrations are excluded in this manner. The stiffness degradation is determined by the increase in displacement between the top and bottom middle node. The FE results are derived based on the use of layered shell elements.

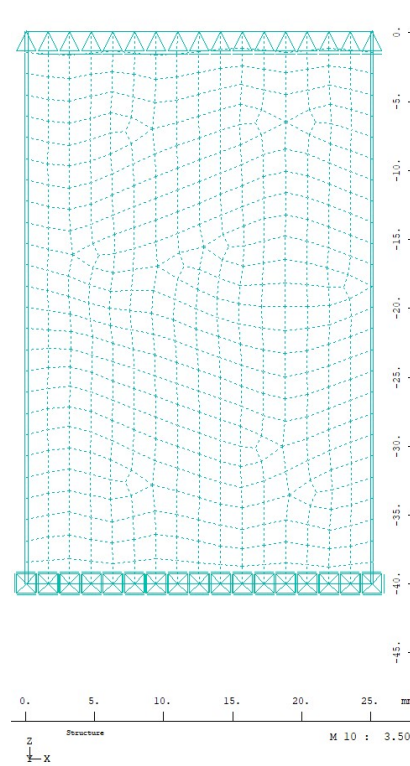


Figure 4.3: Mechanical model

Material The lay-up configuration of the composite material used is given in table 4.1, where the $\pm 45^\circ$ layers are modelled separately with each half of the $\pm 45^\circ$ thickness. This is correct because the $\pm 45^\circ$ layer consist out of a +45 and -45 layer stitched together [28]. Table 4.2 shows the experimental results of the UD ply and of the MD laminate. At the last 3 rows, the analytical stiffnesses, obtained with the Classical Laminate Theory (CLT) method, and the experimental stiffnesses of the MD laminate is shown. The CLT method shows a good comparison with the experimental results. Therefore, it is expected that the stress distribution is determined correctly.

Table 4.1: Lay-up configuration Optidat GEV207 (MD2)

Lay-up nr.	Thickness [mm]	UD ply name	angle [°]	Layer title
301	0.305	Optidat GEV206	45	[(+45,0)4,+45]
301	0.305	Optidat GEV206	-45	[(+45,0)4,+45]
301	0.880	Optidat GEV206	0	[(+45,0)4,+45]
301	0.305	Optidat GEV206	45	[(+45,0)4,+45]
301	0.305	Optidat GEV206	-45	[(+45,0)4,+45]
301	0.880	Optidat GEV206	0	[(+45,0)4,+45]
301	0.305	Optidat GEV206	45	[(+45,0)4,+45]
301	0.305	Optidat GEV206	-45	[(+45,0)4,+45]
301	0.880	Optidat GEV206	0	[(+45,0)4,+45]

301	0.305	Optidat GEV206	45	[(+45,0)4,+45]
301	0.305	Optidat GEV206	-45	[(+45,0)4,+45]
301	0.880	Optidat GEV206	0	[(+45,0)4,+45]
301	0.305	Optidat GEV206	45	[(+45,0)4,+45]
301	0.305	Optidat GEV206	-45	[(+45,0)4,+45]

Table 4.2: Material properties UD and MD glass-epoxy laminate with v_f 52%

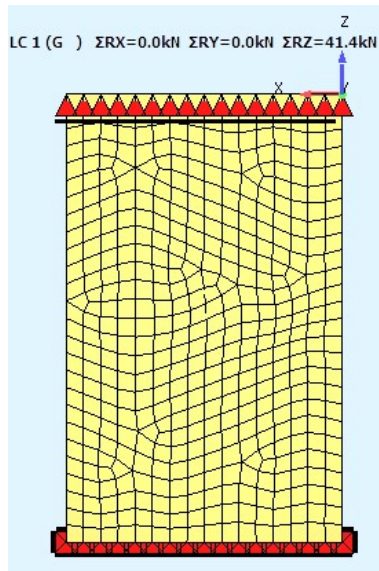
Properties		Unit	Optidat GEV206	Optidat GEV207 (MD2)
parallel modulus UD ply	E_1	[MPa]	37950	
Transverse modulus UD ply	E_2	[MPa]	13880	
Shear modulus UD ply	v_{12}	[MPa]	4000	
Poisson's ratio 12-direction	v_{12}	[-]	0.36	0.47
Poisson's ratio 21-direction	v_{21}	[-]	0.13	0.28
Laminate properties			CLT method	Experimental results
Modulus of the laminate in x-direction	E_x	[MPa]	26823	28700
Modulus of the laminate in y-direction	E_y	[MPa]	15040	15150
Shear modulus of the laminate	G_{xy}	[MPa]	4000	-

4.1.2. Computational procedure settings

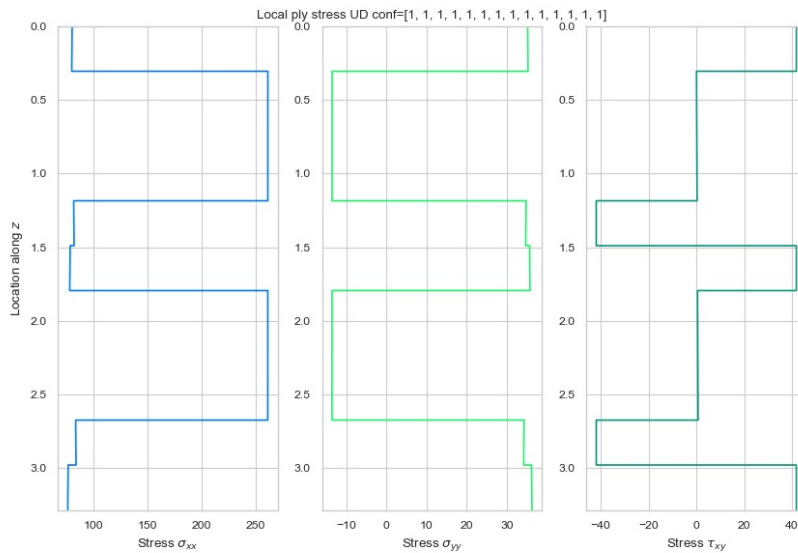
For the simulation of this coupon test, the cycle step is determined with the 5% percentile of a 3% damage increase per ply. Ply properties in the FE model are updated with a step size of 1% damage increase.

4.1.3. Verification of FE model

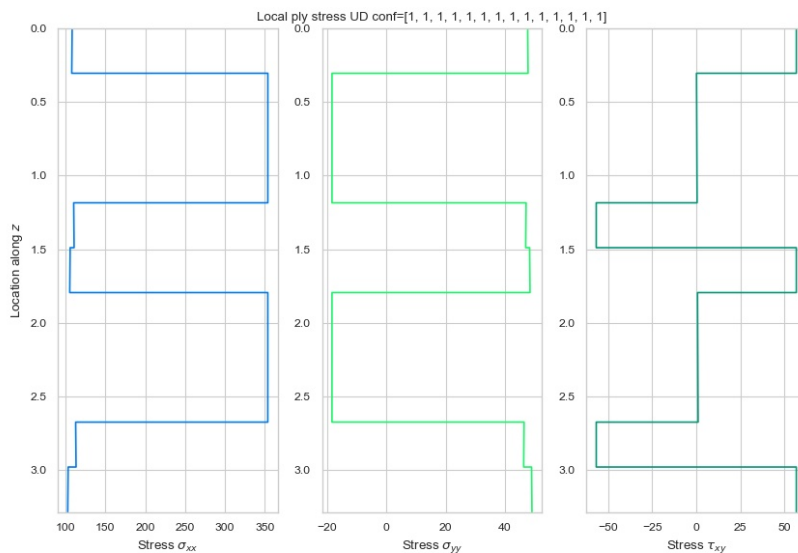
To verify the FE model support reactions are compared with a hand calculation. The reaction force, obtained with the FE analysis, are given in figure 4.4a for the first load case. The reaction force should be equal to: $\sigma = 252[MPa]$. $R_z = 25[mm] \cdot 6.57[mm] \cdot 252[N/mm^2] = 41391[N]$ which is the case. Also, the ply stresses are plotted for an FE element in the centre of the specimen. This gives the possibility to visualise the stress development in the specimen.



(a) Reaction force for $\sigma = 252[MPa]$.



(b) Ply stresses in local ply coordinates, as given in figure 3.3 for $\sigma = 186[MPa]$.



(c) Ply stresses in local ply coordinates, as given in figure 3.3 for $\sigma = 252[MPa]$.

Figure 4.4: FE model verification

4.1.4. Results and discussion

The validation here represents two parts:

1. stiffness degradation prediction of the MD $[(\pm 45, 0)_4, \pm 45]$ laminate
2. influence of the damage interaction relation described in 3.3.4.

In figure 4.4c the stress parallel and transverse to fibre direction and shear stress are shown. The transverse and shear stress in the ± 45 layers are significant, and interaction damage is expected. Therefore multiple simulations are performed, with and without interaction for: σ_x 186 MPa and σ_x 252 MPa. Load level σ_x 317 MPa is not simulated because too much static damage occurs in the first cycle, which can not be simulated by ViFaSS because of the absence of a ply failure criterion. The corresponding number of cycles to failure is obtained by fitting experimental values from the Optidat database [36]. The fitted formulation is given in figure 4.5. The corresponding cycles to failure are; $6.28E + 04$ and $1.12E + 06$ for σ_x 252 MPa and σ_x 186 MPa respectively.

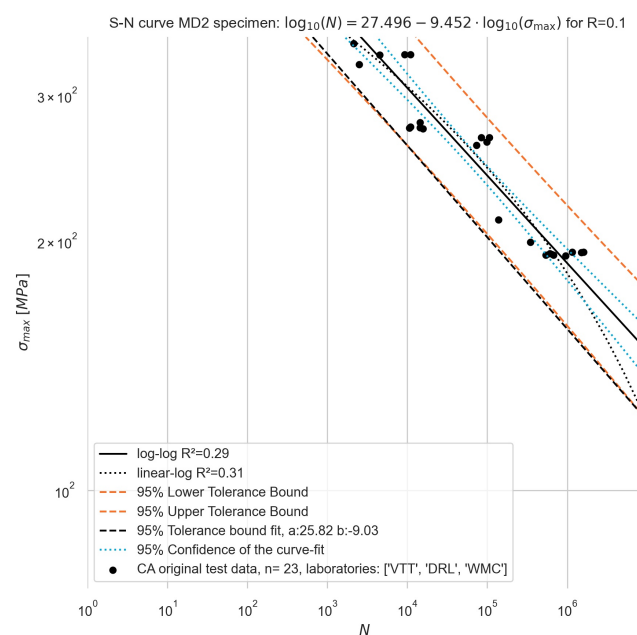


Figure 4.5: S-N formulation MD2 specimen

As also concluded by Eliopoulos and Philippidis [10] the experimental stiffness degradation shown in figure 4.2 represents the three-staged stiffness decrease as described in 2.2. ViFaSS results for σ_x 186 MPa and σ_x 252 MPa are given in figure 4.6a and 4.7a. In these figures three different analyses are presented.

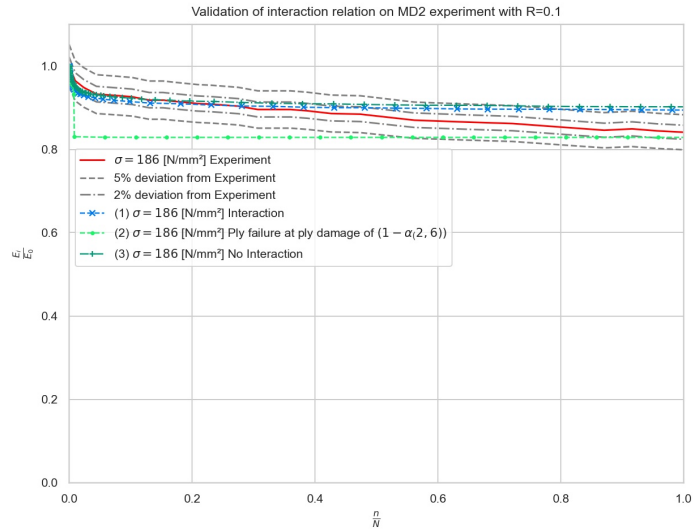
1. including the proposed interaction relation
2. including ply failure when the individual ply damage exceeds $(1 - \alpha_{2,6})$
3. no interaction

From figure 4.6a it can be observed that the model is capable of simulating the initial region and intermediate region of the typical three-staged stiffness decrease.

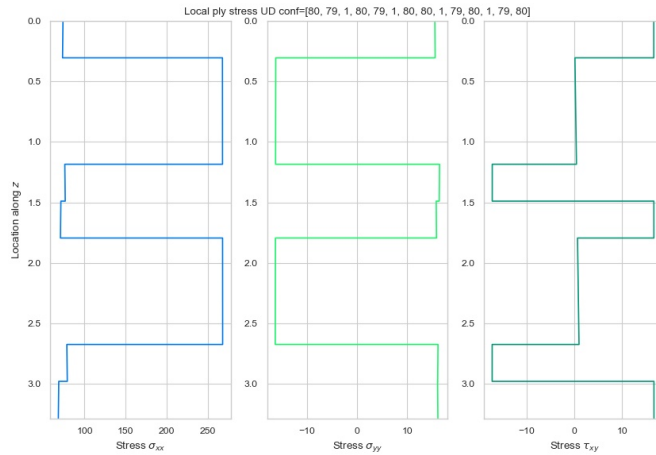
Simulation (2) results, where ply failure is included, show a drastic decrease in stiffness at the first 1-3% of the lifetime. This drastic reduction is not observed in the experiments, see figure 4.6a The expectation is that the stiffness decrease at failure measured in UD experiments is less compared to

the stiffness decrease of a heavily damaged confined UD plies within a MD laminate. The expectation is that the damaged layer will keep some effective stiffness due to the interaction with the 0° layers. This effective residual stiffness and interaction is described by Tao et al. [58] for 90° layers confined by 0° layers and is around 40 to 60% at a crack spacing of $2 \cdot t_{ply}$ in the 90° ply. Tao et al. [58] presented in their work that the effective stiffness is dependent on the angle between the cracked and stabilising plies. So a transverse and shear stiffness reduction of 90% at the UD failure damage is not realistic. Due to the above-described effect, it is chosen to apply the stiffness degradation relation without including the ply failure in the following analyses. Excluding the ply, failure results in optimistic results in the second half of the intermediate region. However, the first part of the intermediate region is better predicted. The degradation of the damaged layers will eventually stabilise due to the decrease in ply stress. The model output data shows that for the ±45° layers, a stiffness reduction of around 50-60% is present. This reduction is in the range Tao et al. found. Therefore it is assumed that this will represent the effective stiffness of the heavily damaged ply within the laminate. For the physical correctness of the degradation model, it is necessary to investigate this effect in more detail. By investigating this more thoroughly, more realistic stiffness reduction parameters: α and β , as described in section 3.3.4 can be determined for confined plies. Also, including the effect of the 1-2% stiffness reduction of the 0° plies in ViFaSS should be investigated. Due to limited time, it is assumed that reducing the stiffness in local ply directions will partially capture this effect.

Simulation (1) and (3) show similar behaviour with experimental results in the initial region and a comparable magnitude of stiffness reduction in the intermediate region. However, the simulation for σ_x 186 MPa is optimistic in the second half of its lifetime. A possible explanation can be found in potentially longitudinal cracks along the 0° fibres, influencing the residual stiffness of the damaged layers, which the model does not describe. This explanation is also in line with what Gamstedt and Sjögren [15] observed within their experiments, that in low loading fatigue, delamination occurs earlier compared to high loading fatigue.



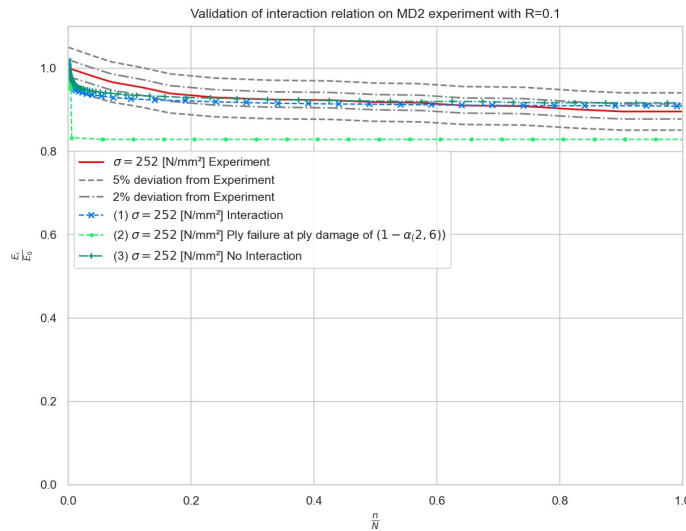
(a) Validation of stiffness degradation simulation $[(\pm 45, 0)_4, \pm 45]$ at σ_x 186 MPa, experimental values from [10]



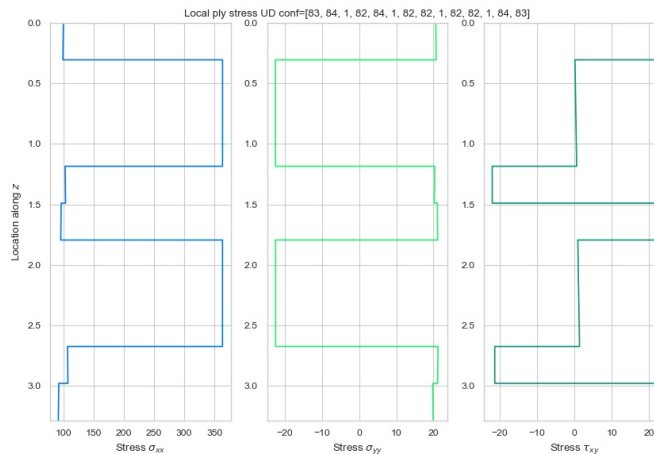
(b) Stress distribution at failure life time for $[(\pm 45, 0)_4, \pm 45]$ at σ_x 186 MPa

Figure 4.6: Stiffness degradation simulations (a) and stress distribution at $n/N=1$ (b)

With the numerical simulation, the stress redistribution is calculated. See figure 4.6b. For the applied stress of σ_x 186 MPa, stress parallel to the fibre direction in the 0° layers is increased by 3-4%. The transverse and shear stress in the $\pm 45^\circ$ layers is reduced by approximately 50% and 56%, respectively.



(a) Validation of stiffness degradation simulation $[(\pm 45, 0)_4, \pm 45]$ at σ_x 252 MPa, experimental values from [10]



(b) Stress distribution at failure life time for $[(\pm 45, 0)_4, \pm 45]$ at σ_x 252 MPa

Figure 4.7: Stiffness degradation simulations (a) and stress distribution at $n/N=1$ (b)

With the numerical simulation, the stress redistribution is calculated. See figure 4.7b. For the applied stress of σ_x 252 MPa, stress parallel to the fibre direction in the 0° layers is increased by 5-6%. The transverse and shear stress in the $\pm 45^\circ$ layers is reduced by approximately 56% and 60%, respectively.

A different representation of the results is used to visualise the difference to validate the proposed interaction relation. The stiffness decrease versus the \log_{10} of the number of cycles is plotted in figure 4.8. It can be seen that when the interaction effect is included, the stiffness reduction starts earlier and that the final reduction is ca 1% larger. From these results, it can be concluded that the interaction relation does not influence the shape of the degradation but does influence the magnitude of the total stiffness degradation. As far as can be concluded from these simulations, the proposed interaction relation gives an expected outcome. However, a better validation could be obtained by a two-staged loading experiment where the load direction changes from, e.g. shear loading to transverse loading to measure the influence on the transverse stiffness of the shear stress damaged laminate .

When comparing the simulations (1) and (3) with experimental results in figure 4.9a and 4.9b it is seen that including the interaction does not influence the results significantly. Therefore, no clear

conclusions can be drawn for now.

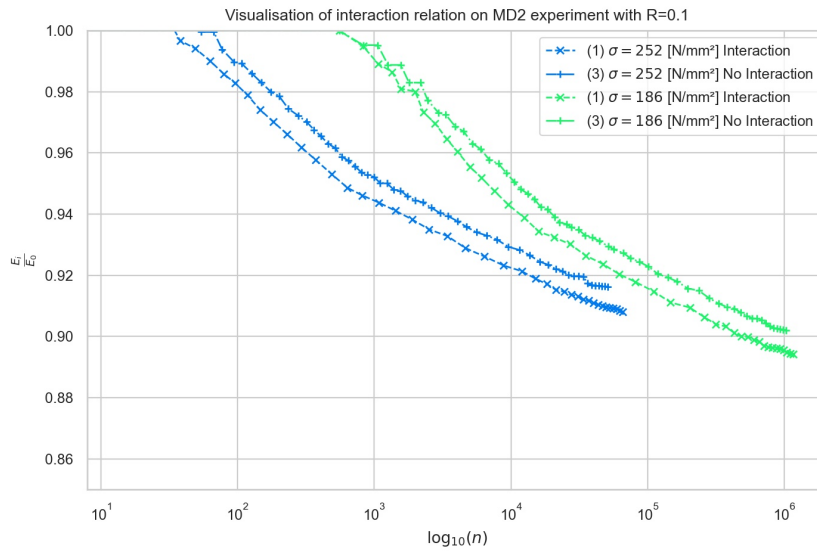
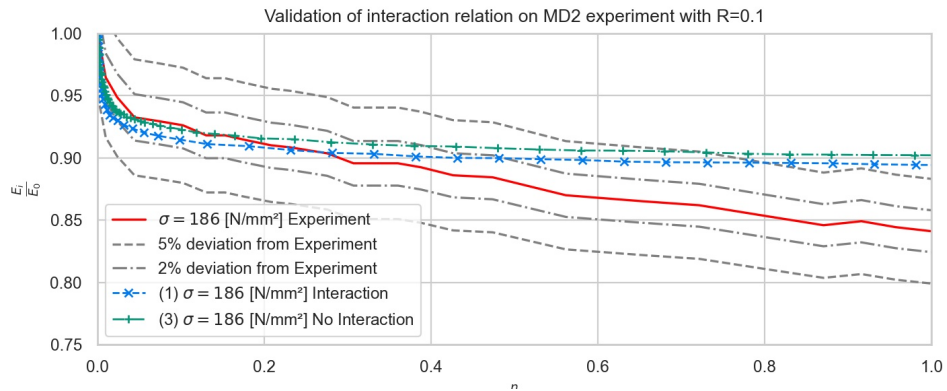
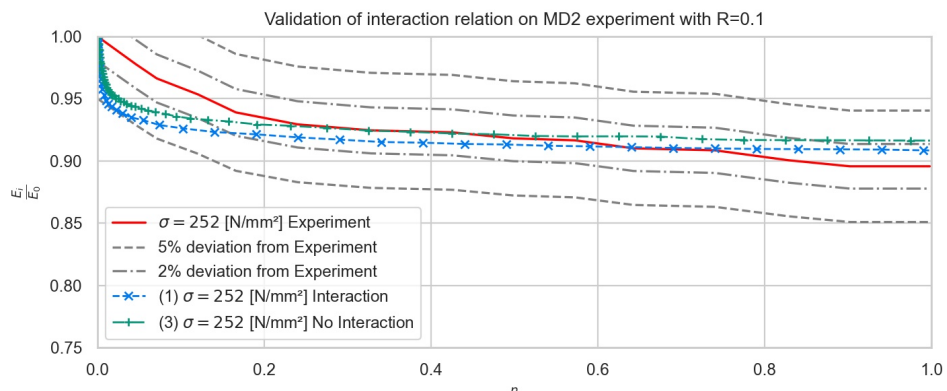


Figure 4.8: Visualisation of damage interaction relation, stiffness reduction versus \log_{10} of the number of cycles.



(a) Validation of damage interaction relation $[(\pm 45, 0)_4, \pm 45]$ at σ_x 186 MPa, experimental values from [10]



(b) Validation of damage interaction relation $[(\pm 45, 0)_4, \pm 45]$ at σ_x 252 MPa, experimental values from [10]

Sequence effect simulation

In section 3.3.4 it is indicated that the used stiffness degradation relation on UD ply level does not include a sequence effect in principle ply modulus degradation, see figure 3.13 and 3.14. The description

of the sequence effect given in the literature review in subsection 2.1.4, suggests that the damage interaction and stress redistribution within the layers cause the sequence effect in the fatigue performance of a laminate. To see if ViFaSS can simulate the sequence effect on a laminate scale the MD $[(\pm 45/0)_4/\pm 45]_T$ laminate is simulated with a high-low and low-high load sequence. The block loading is applied in two different manners; two large load blocks and six smaller load blocks. The results of this simulation are given in figure 4.10. From the figure, it can be seen that the stiffness degradation development does differ and that there is a slight difference in the total damage due to the order of loading. There is no difference in damage observed for the different load block types, i.e. two large blocks or six small blocks.

In ViFaSS, the effect of the different damage mechanisms in the ply are lumped to one stiffness decrease. Therefore, the contribution of the different damage mechanisms is lost. The loss of this information can potentially be one of the reasons there is no difference in damage between the simulation of two large or multiple smaller load blocks. Another reason could be that the interaction between damage mechanisms is not accounted for in the model.

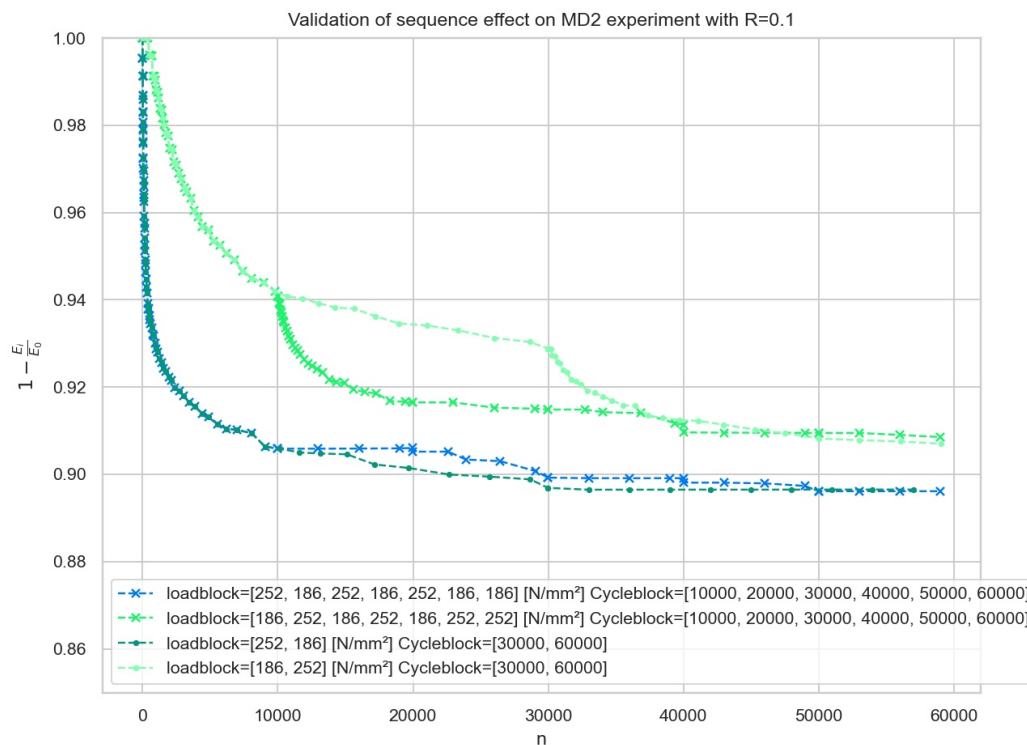


Figure 4.10: Simulation of block loading

4.1.5. Conclusion

An anisotropic linear material constitutive relation with a progressive stiffness damage model, fully characterised by **unidirectional (UD)** mechanical and fatigue ply properties, is validated with experimental results of a **multidirectional (MD)** $[(\pm 45, 0)_4, \pm 45]$ laminate. Three different simulations were performed: (1) including damage interaction between shear and transverse stiffness, (2) including ply failure when the individual ply damage exceeds $(1 - \alpha_{2,6})$ and (3) excluding damage interaction between shear and transverse stiffness. The validation did concern two aspects: first, the ability to predict the stiffness reduction of the **MD** laminate and second, the influence of the proposed damage interaction relation.

Regarding the stiffness degradation prediction of the **MD** $[(\pm 45, 0)_4, \pm 45]$ laminate, the following can be concluded:

- The model can simulate the initial and intermediate region of the typical three-staged stiffness decrease.
- Reducing the stiffness of a failed ply to 10%, as is done in simulation (2), is not realistic due to the effective ply stiffness that is still present, caused by the interaction with the 0° layers.
- The damage in the failed plies stabilises due to the stress redistribution between the layers.
- **Virtual Fatigue Stiffness Simulation (ViFaSS)** predicts that the stress in 0° layers increase with ca 3-4% and ca 5-6% for respectively σ_x 186 MPa and σ_x 252 MPa fatigue **Tension-Tension (T-T)** loading.
- **ViFaSS** predicts the transverse and shear stress to decrease with 50% and 56%, respectively for fatigue **T-T** loading at a stress level of σ_x 186 MPa
- **ViFaSS** predicts the transverse and shear stress to decrease with 56% and 60%, respectively for fatigue **T-T** loading at a stress level of σ_x 252 MPa
- In the second half of the intermediate region, the prediction is slightly optimistic, potentially caused by longitudinal cracks along the 0° plies, non included in **ViFaSS**, which reduces the effective stiffness of the damaged layers.
- **ViFaSS** can simulate a difference in damage for high-low load series and low-high load series. It should be investigated how this difference relates to the actual sequence effects obtained in experiments.
- When simulating different load block sizes, no difference is observed in the total stiffness degradation between high-low or low-high loading.

Regarding the proposed interaction relation, the following is observed from the simulations;

- When the interaction relation is included, degradation starts earlier.
- The stable damage is ca 1% larger than the analysis, which does not include the interaction.
- The interaction relation does not influence the shape of the degradation.
- A better validation of the proposed interaction relation can be obtained by a two-staged loading experiment where the quantification can be made of how much the shear damage influences the transverse stiffness.

The predicted stiffness reduction by the progressive damage model is satisfactory when compared with available experimental results.

4.2. Model validation on MD laminate $[\pm 45]_8$ under bending fatigue

To validate the predictions by ViFaSS regarding bending fatigue, experimental results are needed where a MD laminate is loaded under bending fatigue. The ply material properties used in the MD laminate need to correspond with the material input used in ViFaSS, i.e. UD experiments from the Optidat database [36], so that the fatigue material response is similar. An experiment that is close with fulfilling the above requirements is performed by Van Paepegem and Degrieck [62], fatigue test of $[\pm 45]_8$ laminate under T-T bending loading. A more detailed description of the experiment is given under 4.2.1.

4.2.1. Introduction

Various aspects of the experiment are addressed in this subsection regarding the geometry, loading, mechanical model and material.

Laminate and test setup The lay-up of the multi-directional laminate consists of 8 layers woven fabric under 45° with the load direction. The laminate is fabricated with epoxy resin by vacuum-assisted resin transfer moulding and has a fibre volume content of 48%. Figure 4.11 represents the geometry of the coupon specimen.

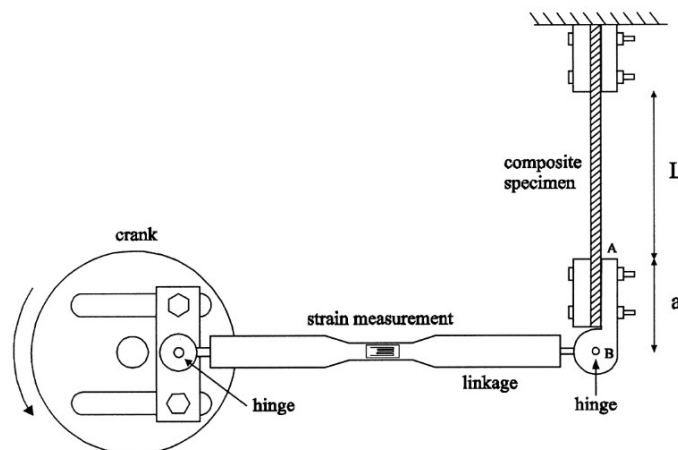


Figure 4.11: Geometrical representation of the coupon specimen, $L=54[\text{mm}]$ and a is assumed to be $48[\text{mm}]$ after calibration of the force.

The experiment is displacement controlled. See figure 4.12 which represents the force degradation.

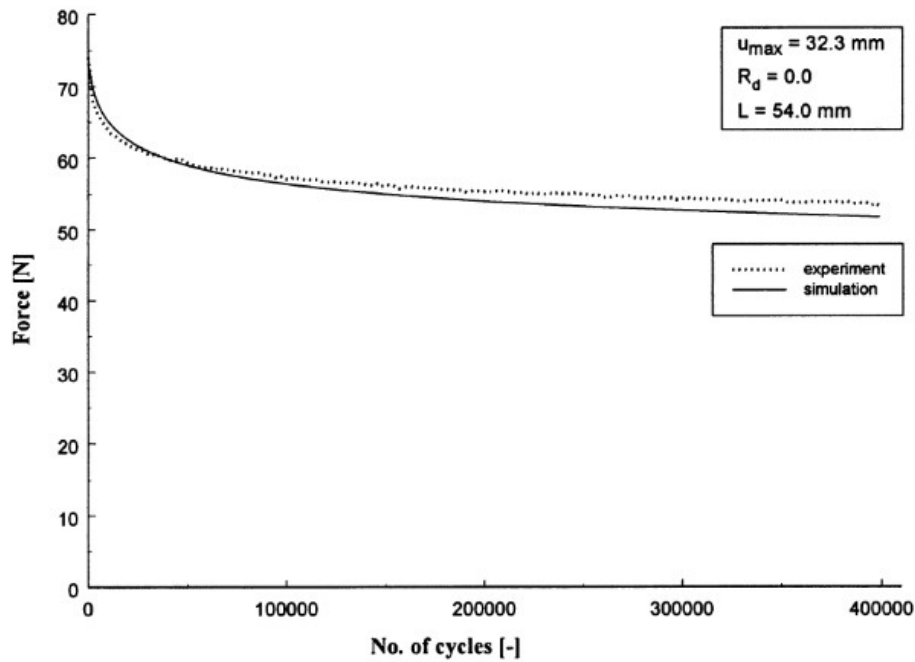


Figure 4.12: Force degradation measurements $[\pm 45]_8$ [62]

Mechanical and Finite Element (FE) model For a correct representation of the test conditions, the mechanical model given in figure 4.13 is used. For the clamped support, all directions are constrained except for the y-direction to prevent transverse stress concentrations. To represent the tabs at the end of the **Glas Fibre-Reinforced Polymer (GFRP)** the material is changed in steel with $E = 210000\text{MPa}$. It is assumed that this represents the mechanical behaviour of the composite laminate. Determining length, "a" in figure 4.12 the applied displacement is calibrated until the obtained force in the initial linear analysis corresponds to the experimentally applied force of 74.0 N [62].

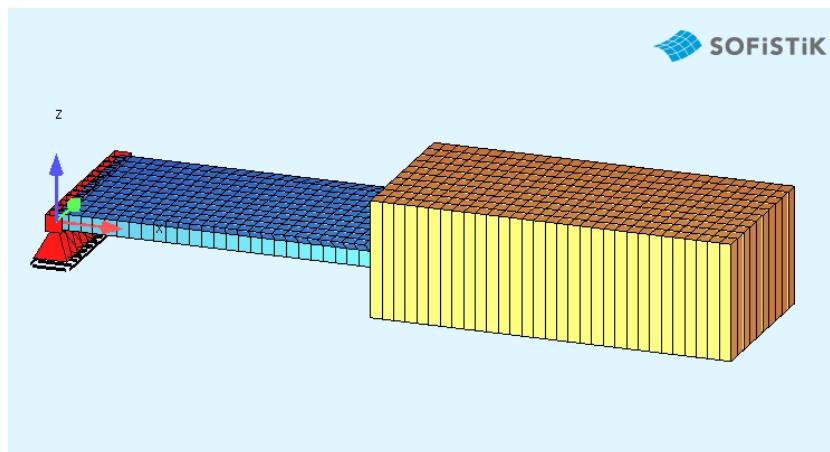


Figure 4.13: Mechanical model bending fatigue

Material The lay-up is given in table 4.3, where the $\pm 45^\circ$ layers are modelled separately with each half of the $\pm 45^\circ$ thickness. The measured material properties are given in [62]. Composing the laminate with the original **UD** material properties from the Optidat database [36], the results are slightly off. Therefore, the **UD** material is adjusted for the fibre volume content, and the shear modulus is increased to count for the woven behaviour. The adjusted material properties are provided in table 4.4 it shows the experimental results of the **UD** ply and of the **MD** laminate. At the last 3 rows, the analytical stiffnesses, obtained with the **Classical Laminate Theory (CLT)** method, and the experimental stiffnesses of the **MD**

laminate is shown. The CLT method shows a good comparison with the experimental results when the UD properties are adjusted for the V_f content. Therefore, it is expected that the stress distribution is determined correctly.

Table 4.3: Lay-up configuration

Lay-up nr.	Thickness [mm]	UD ply name	angle [°]	Layer title
301	0.17	Adjusted $V_f=48\%$	45	Woven 48%
301	0.17	Adjusted $V_f=48\%$	-45	Woven 48%
301	0.17	Adjusted $V_f=48\%$	45	Woven 48%
301	0.17	Adjusted $V_f=48\%$	-45	Woven 48%
301	0.17	Adjusted $V_f=48\%$	45	Woven 48%
301	0.17	Adjusted $V_f=48\%$	-45	Woven 48%
301	0.17	Adjusted $V_f=48\%$	45	Woven 48%
301	0.17	Adjusted $V_f=48\%$	-45	Woven 48%
301	0.17	Adjusted $V_f=48\%$	-45	Woven 48%
301	0.17	Adjusted $V_f=48\%$	-45	Woven 48%
301	0.17	Adjusted $V_f=48\%$	45	Woven 48%
301	0.17	Adjusted $V_f=48\%$	-45	Woven 48%
301	0.17	Adjusted $V_f=48\%$	45	Woven 48%
301	0.17	Adjusted $V_f=48\%$	-45	Woven 48%
301	0.17	Adjusted $V_f=48\%$	45	Woven 48%
301	0.17	Adjusted $V_f=48\%$	-45	Woven 48%
301	0.17	Adjusted $V_f=48\%$	45	Woven 48%

Table 4.4: Material properties UD and MD glass-epoxy laminate with V_f 48% (adjusted) and 52% (original)

Properties		Unit	Adjusted $V_f=48\%$	Original Optidat GEV206 $V_f=52\%$	Measured $V_f=48\%$
parallel modulus UD ply	E_1	[MPa]	36800	37950	
Transverse modulus UD ply	E_2	[MPa]	11538	13880	
Shear modulus UD ply	G_{12}	[MPa]	4800	4000	
Poisson's ratio 12-direction	ν_{12}	[-]	0.31	0.36	
Poisson's ratio 21-direction	ν_{21}	[-]	0.10	0.13	
Laminate properties			CLT method	CLT method	Experimental results
Modulus of the laminate in x-direction	E_x	[MPa]	24473	26280	24570
Modulus of the laminate in y-direction	E_y	[MPa]	24473	26280	23940
Shear modulus of the laminate	G_{xy}	[MPa]	4800	4000	4830

The stiffness degradation is determined by the decrease in the total support force. The FE results are derived based on the use of layered shell elements.

4.2.2. Computational procedure

For the simulation of this coupon test, the cycle step is determined with the 5% percentile of a 3% damage increase per ply. Ply properties in the FE model are updated with a step size of 1% damage increase.

4.2.3. Verification of FE model

To verify the FE model, the stresses are plotted for an FE element in the centre at the support. These plots visualize the stress development in the specimen for the fatigue cycles. The stress distribution is shown below for the first load cycle.

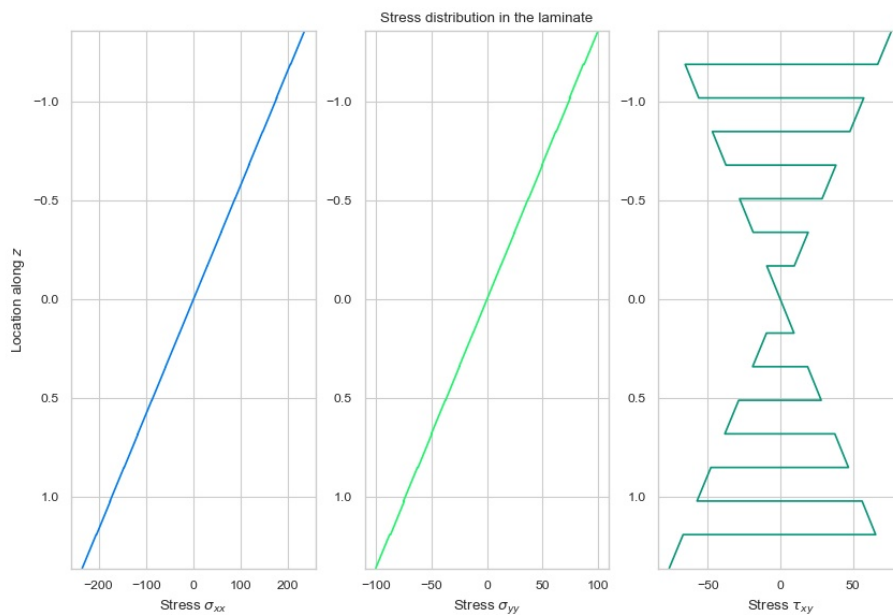


Figure 4.14: Stress distribution close at the support.

4.2.4. Results and discussion

The input UD properties from the Optidat [36] experiments are slightly modified to adjust for the difference in V_f and shear stiffness. This adjustment results in a more realistic stress distribution in the laminate. Adjustment for the lifetime estimation is not possible in the absence of a database. Therefore, the UD ply experimental results from the Optidat database [36] are used. It is assumed that the lifetime for the UD material in the Optidat program is applicable in the simulation due to the same manufacturing procedure and the 4% difference in V_f .

In figure 4.15 the experimental results and the simulation of ViFaSS are presented as well as the simulation by Van Paepegem and Degrieck [62]. It can be seen that the stiffness in the initial region degrades rapidly and that it stabilises in the intermediate region.

The simulation of the degradation is comparable to the experimental results. However, some differences occurs in the initial region where the simulation is conservative, potentially caused by an overestimation of the transverse and shear stress in the ply due to excluding the non-linear material behaviour in the transverse and shear direction. Also, the interlaminar damage that occurs will influence the stiffness degradation of the laminate, which is not included in the model.

In bending, each ply experiences a different stress state, and to be able to visualise the global degradation on individual ply levels, the stress development in local ply coordinates is given in the figures below.

From the figures on the next page, it can be seen that only the transverse and shear stress decreases, which is expected due to excluding degradation of the parallel to fibre stiffness. When comparing the S-N curves given in appendix C figure C.4 and C.6 the lifetime for Compression-Compression (C-C) loading is much longer than T-T loading for the same σ_{max} . Also, the stiffness degradation in compression is much smaller as can be seen in figure 3.11 and 3.10. Therefore, it is expected that the transverse stiffness does degrade much faster in the tension zone compared to the compression zone. The prediction is in line with the expectation.

The shear stress does degrade more or less symmetrically due to the symmetrical layup and because the stiffness reduction is equal for positive and negative shear stress. There is some difference in shear stiffness between the top and bottom plies due to the damage interaction with the transverse damage.

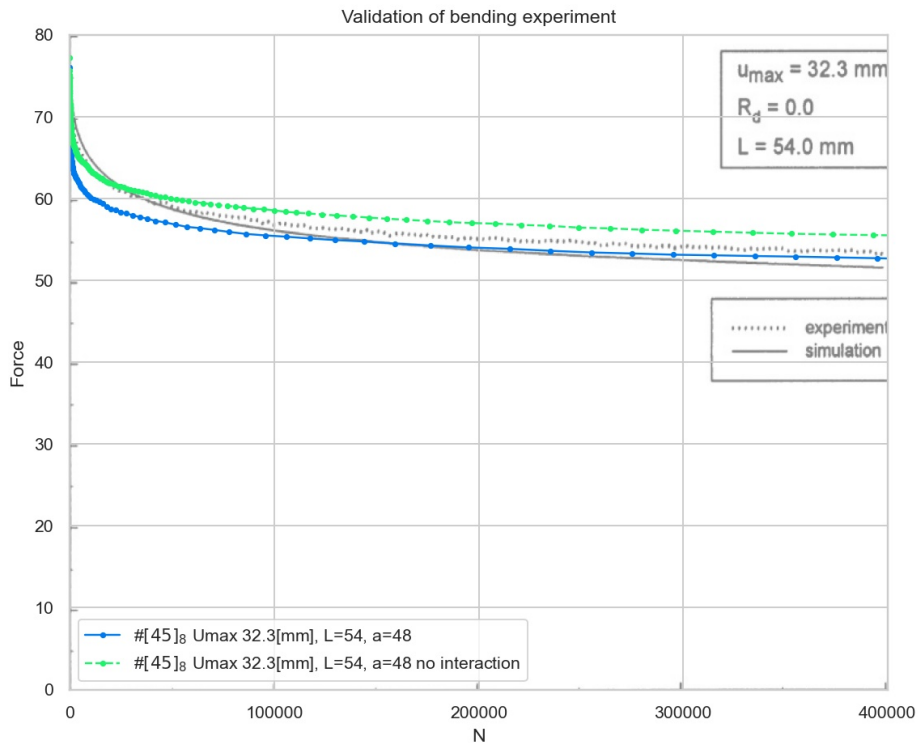


Figure 4.15: Validation of force degradation simulation $[\pm 45]_8$, underlay from [62]

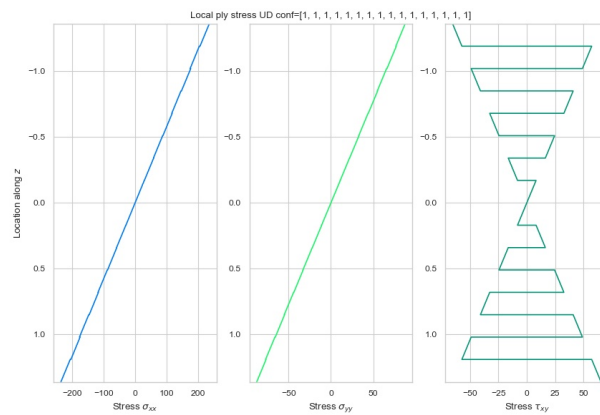


Figure 4.16: Stress distribution at the support after 1 cycle, in local ply coordinates.

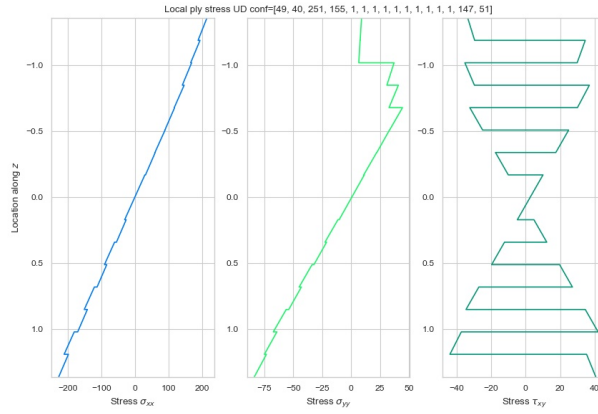


Figure 4.17: Stress distribution at the support after 100 cycle, in local ply coordinates.

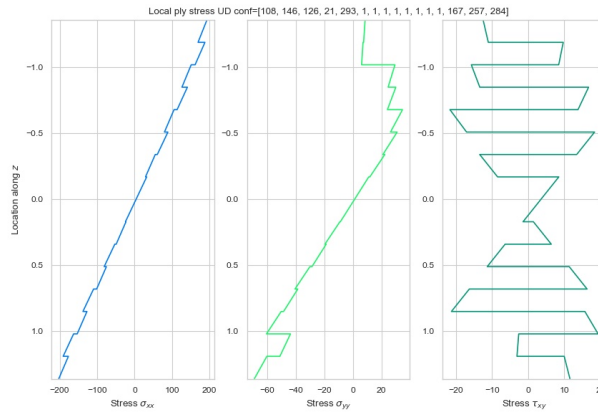


Figure 4.18: Stress distribution at the support after 1000 cycle, in local ply coordinates.

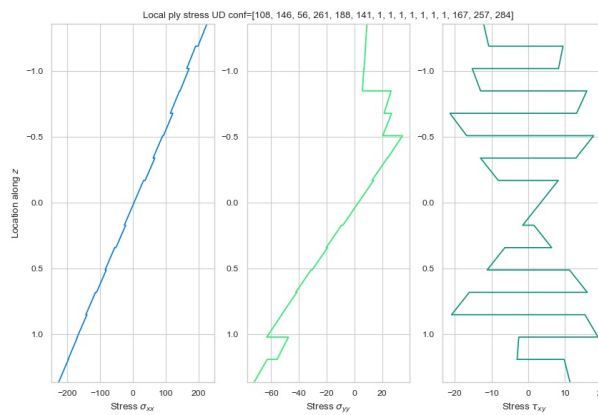


Figure 4.19: Stress distribution at the support after 10000 cycle, in local ply coordinates.

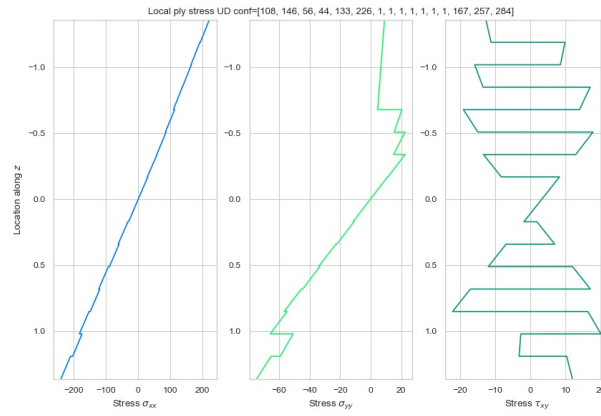


Figure 4.20: Stress distribution at the support after 100000 cycle, in local ply coordinates.

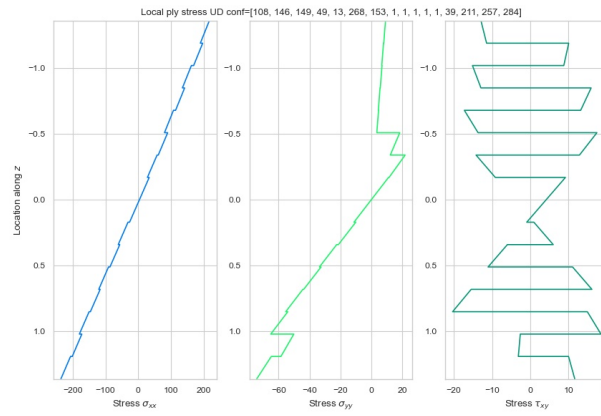


Figure 4.21: Stress distribution at the support after 400000 cycle, in local ply coordinates.

4.2.5. Conclusion

Virtual Fatigue Stiffness Simulation (ViFaSS) which use anisotropic linear material constitutive relations, and the fatigue material response fully characterised by **unidirectional (UD)** ply experimental results, is validated with experimental results of a $[\pm 45]_8$ woven laminate loaded in bending. The validation concerned two aspects; first, predicting the stiffness reduction under bending fatigue with R-ratio of 0.1 and second, the damage behaviour under **Compression-Compression (C-C)** loading in the bottom plies of the laminate.

Regarding the stiffness degradation prediction under bending, the following can be concluded;

- ViFaSS can simulate the initial and intermediate region of the typical three-staged stiffness decrease.
- Potentially, the initial non-linear material stress-strain behaviour plays an important role in the initial region of the degradation.
- The degradation of the tension side mostly causes the decrease in load.

Regarding the **C-C** fatigue behaviour, the following is observed;

- Damage under **C-C** loading is limited and not the dominating factor in bending fatigue.

The predicted stiffness reduction by the progressive damage model is satisfactory compared with available experimental results for bending fatigue.

4.3. Model limitations

Design decisions made during the development of the model lead to limitations regarding the model's applicability to multiple cases. To provide the reader with a clear overview of those limitations. This section highlights the limitations and their effect in a simulation.

The fatigue material response is fully characterised by **unidirectional (UD)** experimental results for in-plane stress states. Therefore, the fatigue prediction is limited to components and structures that can be modelled only characterised by the in-plane stress-strain material response. The out of plane fatigue material response is not included in the current version of the model. Interface stresses between plies are also not considered. Failure modes driven by out of plane stresses, e.g. delamination and crushing, can therefore not be predicted.

Both the stress-strain relation in the **Finite Element (FE)** model and the fatigue material response characterisation are assumed to have a linear stress-strain behaviour. This assumption holds for the ply response in fibre -and transverse direction. However, the shear stress in the ply determined by the **FE** model will be overestimated because the actual shear stress-strain response is highly non-linear. See figure 4.22. This overestimation of shear stress causes that the predicted shear stiffness degradation is also overestimated.

It is not possible to predict the actual failure of the component. The effect of the damage on the strength properties is not included. Within **Virtual Fatigue Stiffness Simulation (ViFaSS)**, only the effect of the damage on the stiffness reduction is included. In the above-described validations of **ViFaSS**, it is observed that there is a difference in the fatigue material response of a **UD** ply experiment and the response of a **UD** ply confined in a laminate. The damaged ply will not completely fail if it is confined and contributes some effective stiffness to the laminate. This effect is not yet correctly incorporated in the model because it depends on the interaction between the different layers.

To summarise, the current version of the model is only applicable to components where the response can be described by an in-plane (linear) stress-strain response and will give inside into the stiffness degradation and stress redistribution. Final failure and out of plane fatigue failure modes cannot be predicted.

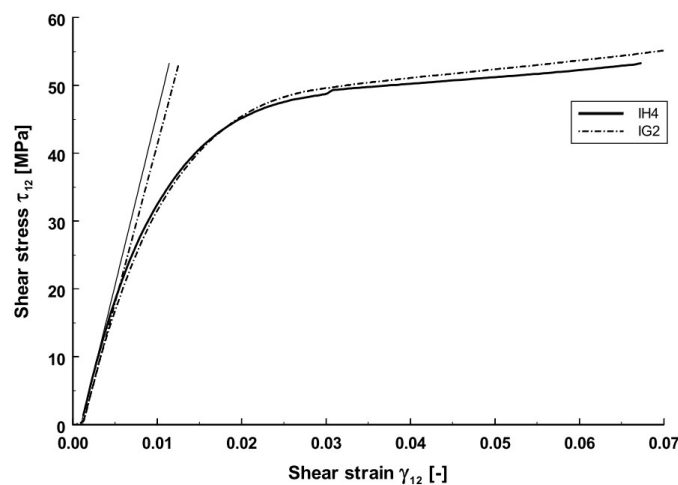


Figure 4.22: Shear stress-strain response of $[\pm 45^\circ]_s$ [63].

5

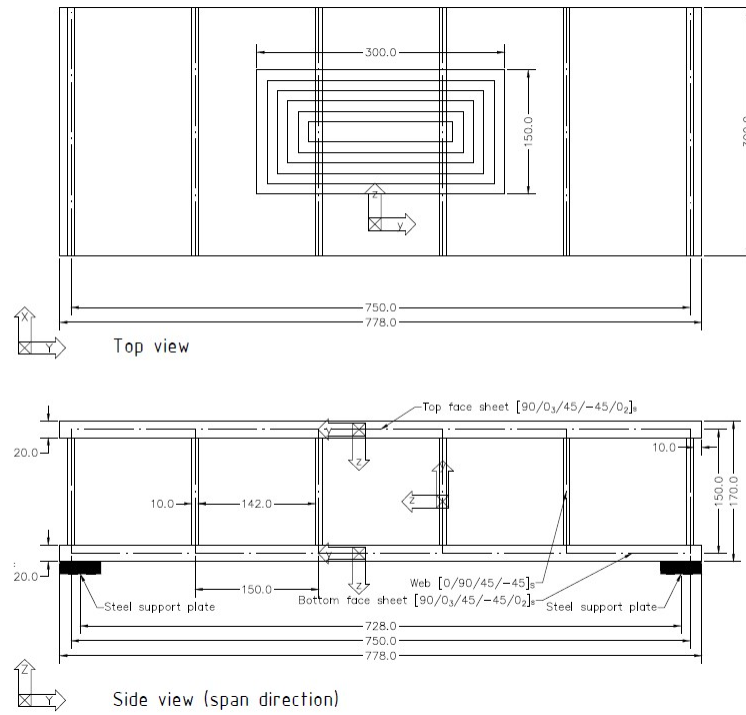
Virtual stiffness based fatigue degradation of a sandwich webcore panel

To demonstrate [Virtual Fatigue Stiffness Simulation \(ViFaSS\)](#)'s capabilities regarding the fatigue damage simulation of a sandwich webcore panel. Two types of configuration are considered: one panel loaded such that there is high local bending present, and second a panel is loaded equally to its design situation. The first analysis aims to see if the areas where high local bending occurs will also degrade the most. The second analysis will show the stiffness loss of a webcore panel, equivalent to a design situation. The webcore sandwich panel design is given in figure [5.1a](#) and figure [5.1b](#) for the first and second analysis respectively.

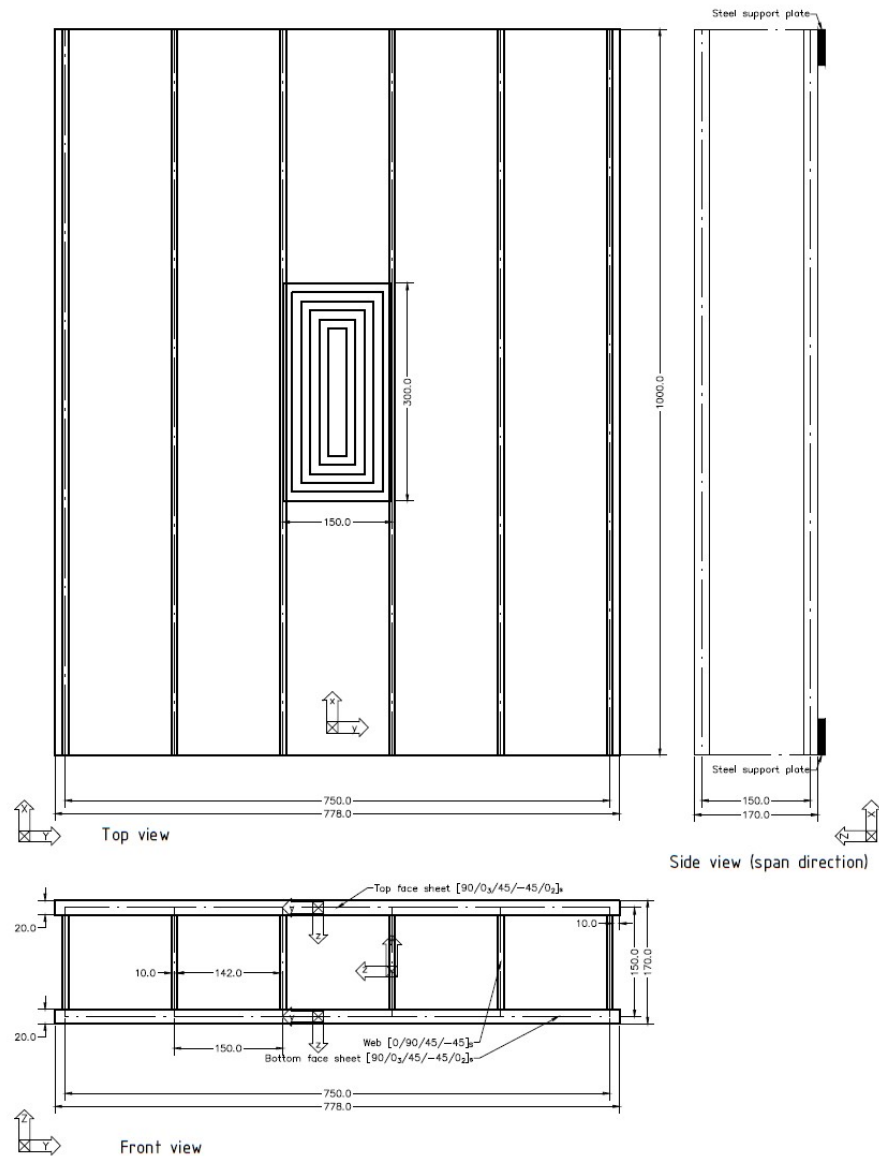
5.1. Introduction

The dimensions of the specimen are based on the preliminary design of samples for a PhD research at the Delft University of Technology into the fatigue behaviour of the connection between [Glas Fibre-Reinforced Polymer \(GFRP\)](#) webcore panels and the steel superstructure.

General The webcore panel specimens given in figure [5.1a](#) is a regular design with a face sheet thickness of 20 mm and a web thickness of 10 mm. The total height of the panel is 170 mm.



(a) Drawing of model 1, local bending.



(b) Drawing of model 2, design situation

Material The tested laminate is produced with the vacuum infusion process. It is built up from 600 g/m² uni-directional and 1200 g/m² bi-directional fabrics of E-glass fibre reinforcement embedded in an epoxy resin. For the face sheets, this results in a multidirectional, anisotropic laminate, with the composition: [0/62.5%, 90/12.5%, ±45/25%] and has approximately a V_f of 52%. For the webs, this results in a quasi-isotropic laminate with the composition; [0/25%, 90/25%, ±45/50%] and has approximately a V_f of 30%.

Below in table 5.1 and 5.2 are the lay-ups given of respectively the face sheets and webs.

However, in the model, the webs are assumed to have a V_f of 52% because the experimental data in the model is based on fatigue results of a V_f 52%.

Table 5.1: Lay-up configuration face sheets GFRP anisotropic laminate [90/0₃/45/ - 45/0₂]_s

NO	T	MNO	BETA	TITL
301	1.43	Optidat GEV206	90	Uni-directional
301	1.43	Optidat GEV206	0	Uni-directional
301	1.43	Optidat GEV206	0	Uni-directional
301	1.43	Optidat GEV206	0	Uni-directional
301	1.43	Optidat GEV206	45	Bi-directional
301	1.43	Optidat GEV206	-45	
301	1.43	Optidat GEV206	0	Uni-directional
301	1.43	Optidat GEV206	0	Uni-directional
301	1.43	Optidat GEV206	-45	Bi-directional
301	1.43	Optidat GEV206	45	
301	1.43	Optidat GEV206	0	Uni-directional
301	1.43	Optidat GEV206	0	Uni-directional
301	1.43	Optidat GEV206	0	Uni-directional
301	1.43	Optidat GEV206	90	Uni-directional

Table 5.2: Lay-up configuration webs GFRP quasi-isotropic laminate [0/90/45/ - 45]_s

NO	T	MNO	BETA	TITL
302	1.25	Optidat GEV206	0	Uni-directional
302	1.25	Optidat GEV206	90	Uni-directional
302	1.25	Optidat GEV206	45	Bi-directional
302	1.25	Optidat GEV206	-45	
302	1.25	Optidat GEV206	-45	Bi-directional
302	1.25	Optidat GEV206	45	
302	1.25	Optidat GEV206	90	Uni-directional
302	1.25	Optidat GEV206	0	Uni-directional

Loading From the literature, it is known that during testing, stress concentrations should be prevented when applying the tyre load on the specimen. Therefore, the load distribution applied in the **Finite Element (FE)** model should represent the correct pressure between tyre and deck as well [50]. In figure 5.2 the pressure distribution derived by Majumdar et al. [29] from experimental data is given. This distribution is normalised in three dimensions to a unit volume such that the wheel load can easily be scaled.

Figure 5.1a and 5.1b displays the location of the applied tyre loading in analyses one and two, respectively. At each square, a different load is applied. Summing up all the area loads, the total applied load is found. In table 5.3 an example of the determination of the area loads is given. The factor to adjust for the area load is determined by increasing the normalised values such that when applying a unit load, the total volume is also unity.

In the simulation of model 1, a wheel load of 40 kN is applied to the specimen under a constant amplitude. The load area is chosen such that there is sufficient space between the edge of the specimen

and the applied load. To induce damage relatively quick. The load magnitude is designed such that the transverse stress in the plies of the top face sheet is a factor 2 of the design resistance.

In the simulation of model 2, a wheel load of 144 kN is applied to the specimen under a constant amplitude. The load area is chosen such that there is maximum local bending of the top face sheet. The load is designed based on an actual design situation where a deck panel with a span of 2.4m is loaded by Fatigue Load Model 3 from eurocode 1991-2 [35]. The wheel load of FLM3 is 60kN. This load is scaled to have the same design bending moment in the 1-meter span model as the actual application with a 2.4m span.

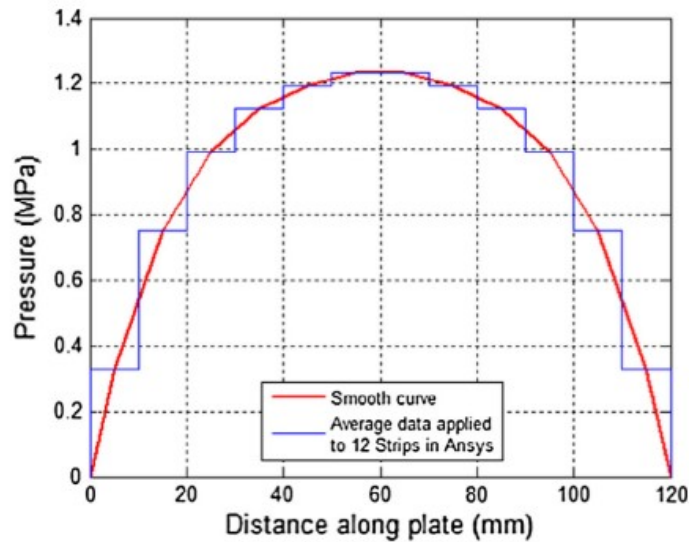


Figure 5.2: Tyre pressure distribution according to [29].

Table 5.3: Determination of load application

Loadplane	From paper	Normalized	Factor to adjust for area load [$1/M^2$]	Applied load [kN]	Area of loadplane [M^2]	Volume of load [kN]
1	0.3	0.286	9.46	40	0.045	17.02
2	0.3	0.286	9.46	40	0.034	13.01
3	0.2	0.190	6.30	40	0.025	6.30
4	0.1	0.095	3.15	40	0.017	2.13
5	0.1	0.095	3.15	40	0.010	1.26
6	0.05	0.048	1.58	40	0.004	0.28
Total	1.05	1.00				40

5.2. Computational procedure

For the simulation of these models, the cycle step is determined with the 5% percentile of a 1% damage increase per ply. Updating of ply properties in the **Finite Element (FE)** model happens with a step size of 1% damage increase. The simulation of model 1 at 10 million cycles took ca 10.5 hours, calculation of the uneven cycles, i.e. without the **Artificial Neural Network (ANN)** module took 13 minutes, calculation of the even cycles, i.e. with **ANN** took 9 minutes. The simulation of model 2 at 10 million cycles took 21 hours, calculation of the uneven cycles took 38 minutes, calculation of the even cycles took 25 minutes. On a HP ZBook Studio x360 G5 laptop with a Intel(R) Core(TM) i7-9750H CPU @ 2.60GHz 2.59 GHz processor and 16 GB RAM-memory.

5.3. Results and discussion

5.3.1. Results and discussion of virtual fatigue local bending analysis

Due to the geometry and loading, the face sheets will experience high normal stresses in the middle, and the outer webs will experience the largest local bending stresses. So it is expected that the material will degrade in those locations. A drawing of the structural model is given in appendix F.

This type of loading gives the ability to simulate the local bending of the face sheets and the webs under tyre loading and have both in-plane and out of plane loading. It is important to note that the span direction in the virtual experiment is different from the application's span direction in an actual structure. It would be desirable if this simulation could be validated with experimental observations to see which damage mechanisms occur and to what extent the model can simulate the fatigue behaviour under local bending.

Mechanical and FE model For a correct representation of a potential experiment, the supports are modelled over a wider contact area to prevent stress concentrations near the supports, as indicated in figure 5.1a. The model is build-up out of 4 noded layered shell elements, named QUAD elements in SOFiSTiK. With an element size of 15x15mm there are 10 elements over the height of the webs and 10 elements in the face sheets between the webs. The total number of shell elements for this model is ca 2940.

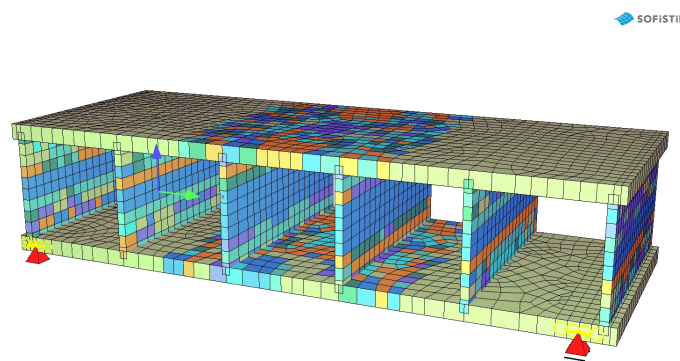
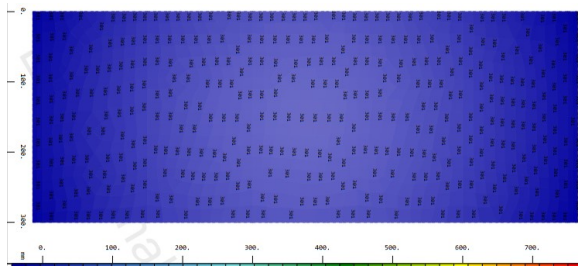


Figure 5.3: Finite element model local bending

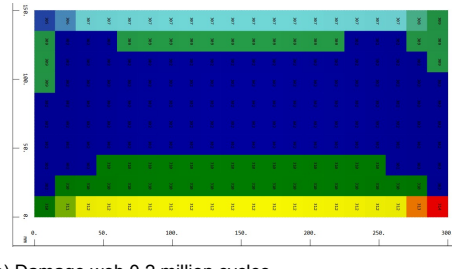
Damage development In figure 5.8 the damage development of the face sheet and the outermost web is given. It can be seen that below 0.2 million cycles, the damage in the face sheet is below the update threshold value of 1%, i.e. the minimum damage that is needed to update the shell elements in the FE model. From 0.7 million cycles, the damage in the face sheet starts to develop due to the local bending caused by the wheel load. At 1.2 million cycles, the stiffness degradation of the component enters the intermediate state, see figure 5.6. The damage in the face sheet gradually increases further.

In the outermost web, the damage starts before 0.2 million cycles. The component response, therefore, is entirely characterised by the degradation of the webs. From the figures, it can be seen that the damage starts in the areas with the most significant bending moment and grows towards the centre of the web.

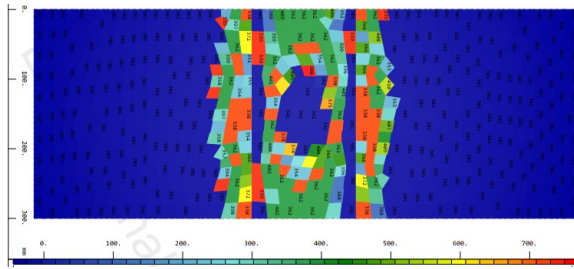
The outcome of ViFaSS is within the expectations related to the mechanical behaviour of the component. Damage starts in areas where high stresses occur and will grow from there.



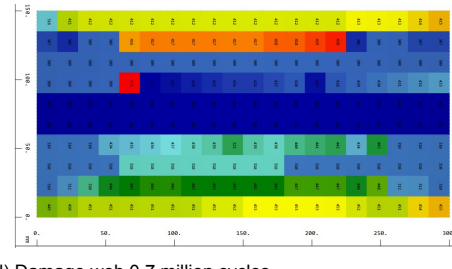
(a) Damage top face sheet 0.2 million cycles



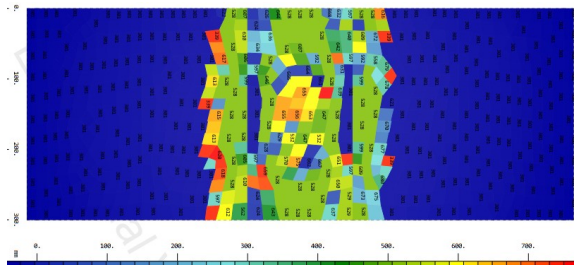
(b) Damage web 0.2 million cycles



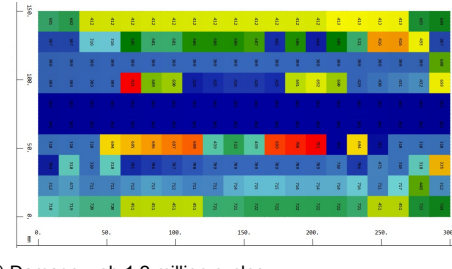
(c) Damage top face sheet 0.7 million cycles



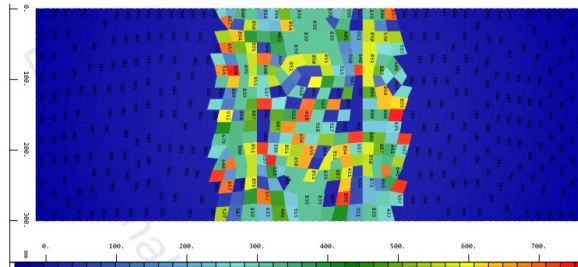
(d) Damage web 0.7 million cycles



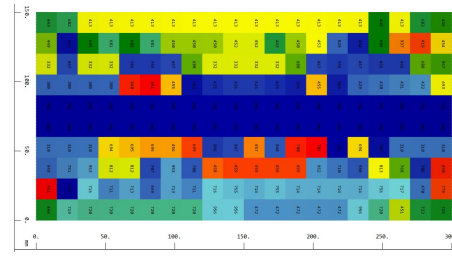
(e) Damage top face sheet 1.2 million cycles



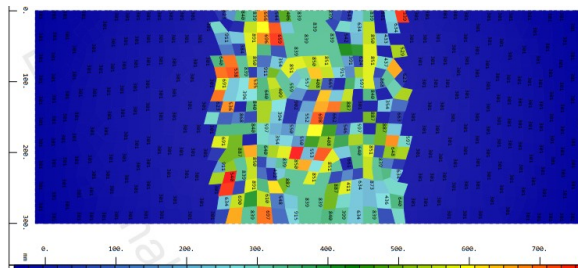
(f) Damage web 1.2 million cycles



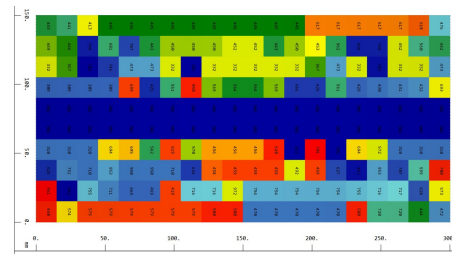
(g) Damage top face sheet 2.2 million cycles



(h) Damage web 2.2 million cycles



(i) Damage top face sheet 4.2 million cycles



(j) Damage web 4.2 million cycles

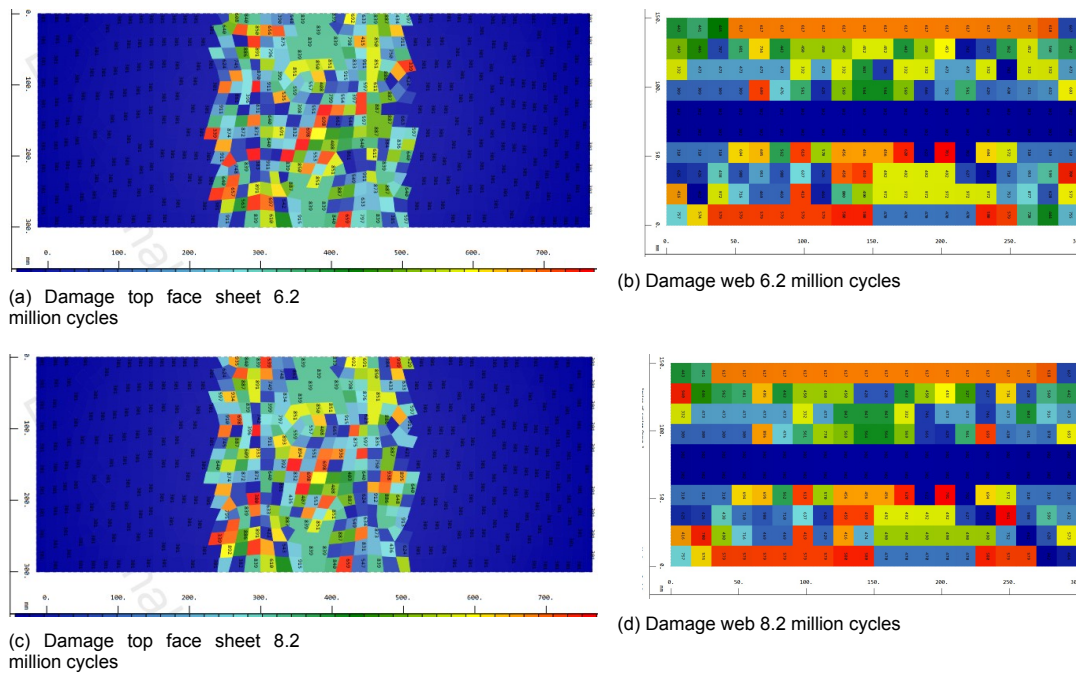


Figure 5.5: Damage development of bottom and top face sheet. Colours represent different material properties. There is no related colour scale.

Deflection The total deflection of the webcore panel does increase due to the localised stiffness degradation in the webs and face sheets. In figure 5.6 the midpoint deflection of the bottom face sheet is plotted for both the total discount, i.e. with a sudden drop in stiffness at the failure of a **unidirectional (UD)** ply and the gradual degradation, i.e. without a sudden drop in stiffness. A more detailed description is found in section 4.1.

There is a slight difference between the total and gradual discount methods. Areas with a relatively high damage state can cause this difference, such as the outermost webs. In the total discount method, the stiffness is degraded rapidly, and in the gradual method, those areas will degrade slower. Eventually, the damage in the plies will stabilise due to the stress redistribution.

Because of the absence of dominant 0° layers in stress direction, the redistribution of stresses between the individual layers will not stabilise. Therefore, no actual equilibrium state develops. This effect can be seen in the small slope in the intermediate region.

The total stiffness reduction of the component measured based on the midspan deflection of the bottom flange is 21%, which is not within the limit of the Eurocode proposal of a maximum stiffness reduction of 5%. However, the component span and load configuration are not comparable with a design situation.

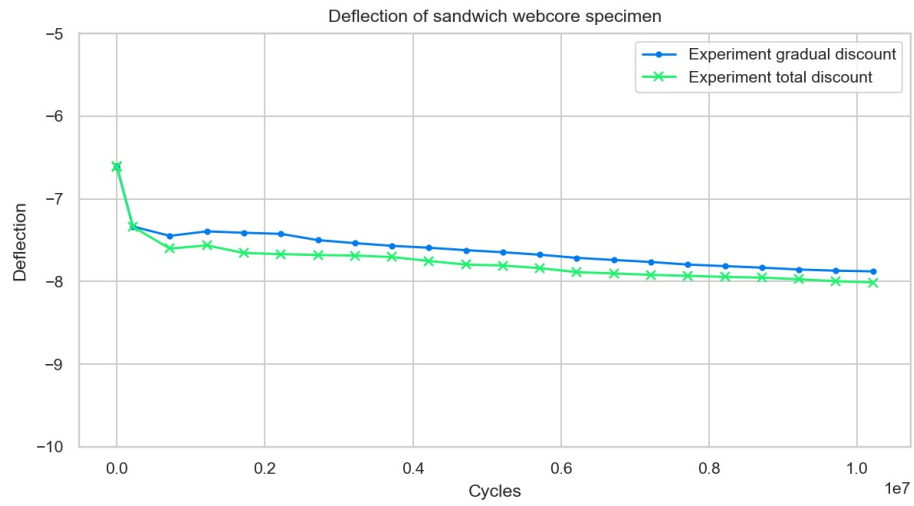


Figure 5.6: Deflection versus the number of cycles

5.3.2. Results and discussion of virtual fatigue equivalent design case analysis

Due to the geometry and loading, the face sheets will experience high local bending under the wheel print. The expectation is that the material will degrade in those locations. A drawing of the structural model is given in appendix F.

As described under paragraph "loading", the virtual model is comparable with a design situation. The simulation will give insight into the predicted fatigue behaviour of an actual webcore sandwich deck panel. In the simulation, partial and conversion factors are not taken into account.

Mechanical and FE model For a correct representation of a potential experiment, the supports are modelled over a wider contact area to prevent stress concentrations near the supports, as indicated in figure 5.1b. The model is build-up out of 4 noded layered shell elements, named QUAD elements in SOFiSTiK. With an element size of 25x25mm for the face sheets and 22x22mm for the webs, there are 7 elements over the height of the webs and 5 elements in the face sheets between the webs. The total number of shell elements for this model is ca 5940.

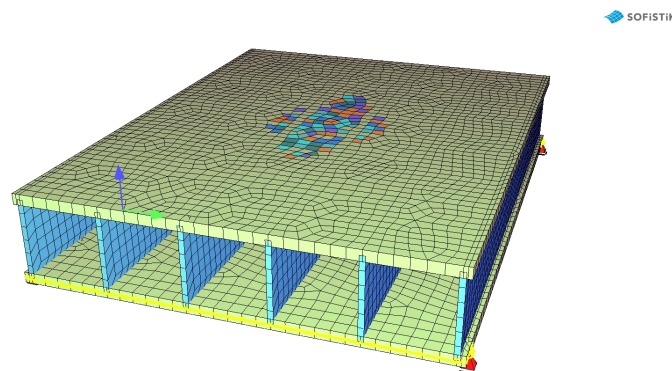


Figure 5.7: Finite element model parallel

Damage development In figure 5.8 the development of the stiffness degradation is shown for the bottom and top face sheet from 2 to 10 million cycles. ViFaSS predicts that the top face sheet under the wheel print will mostly be degraded, and at a small area at the bottom face sheet, the stiffness degrades. In the webs, almost no damage is predicted and therefore not shown.

The stiffness degradation of the component in the initial region is caused by the damage in the top face sheet. From 1 million cycles, the component stiffness response enters the intermediate stage, and the damage growth stabilises. The damaged areas increase slowly; however, the effect on the component response of this increase is limited, as can be seen in figure 5.9. That the global response is stable. That is probably due to the damage growth in span direction. The effective width of the cross-section with original properties stays stable.

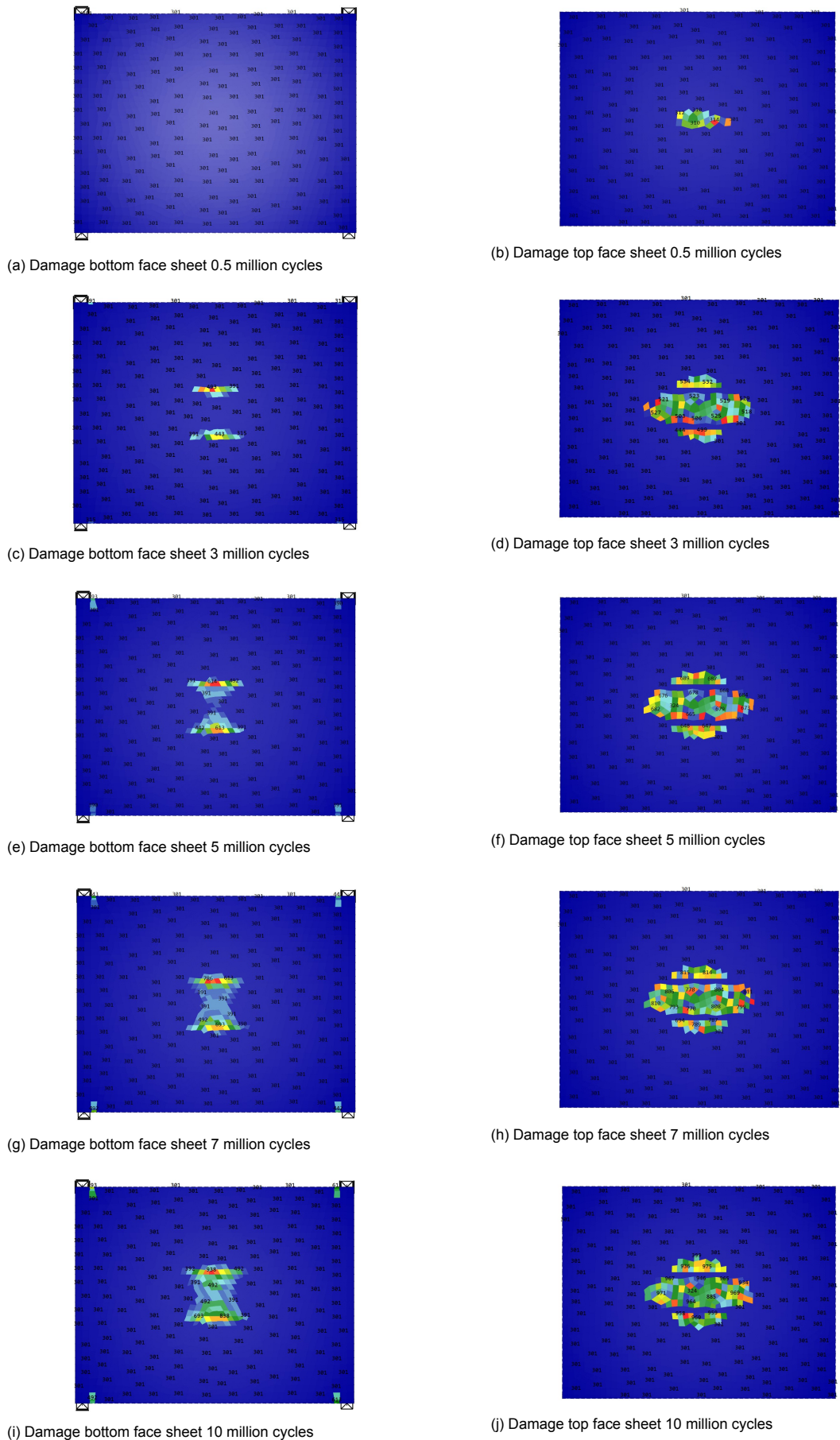


Figure 5.8: Damage development of bottom and top face sheet. Colours represent different material properties. There is no related colour scale.

Deflection The total deflection of the webcore panel does increase due to the localised stiffness degradation under de wheel print. In figure 5.9 the midpoint deflection of the bottom face sheet is plotted for both the total discount, i.e. with a sudden drop in stiffness at the failure of a UD ply and the gradual degradation, i.e. without a sudden drop in stiffness. A more detailed description is found in section 4.1.

There is almost no difference between the total and gradual discount methods from the two different plots. The redistribution of stresses between the individual layers of the top and bottom face sheet is limited due to the relatively low stress in the component. Therefore, an equilibrium state develops where the stiffness reduction of the damaged plies is below the stiffness reduction of failure.

The total stiffness reduction of the component measured based on the midspan deflection of the bottom flange is 6.5%, which is not within the limit of the Eurocode proposal of a maximum stiffness reduction of 5%. However, the area the wheel load is smaller than prescribed by Eurocode 1991-2 [35].

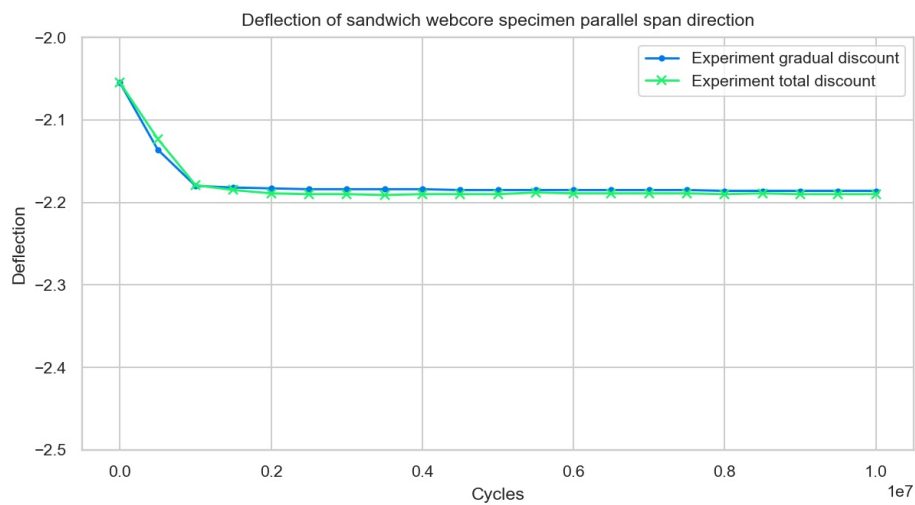


Figure 5.9: Deflection versus the number of cycles

5.4. Description of validation procedure

To validate the applicability of ViFaSS to sandwich webcore panels. The simulated results should be compared with experimental observations. Below is an overview is given of the experimental effort for this validation and how each experiment will contribute to the validation. First, the experiments needed for both simulations, local bending and design case, are given, followed by the experiments needed for each simulation separately.

In both simulations, the face sheets have a thickness of 25mm. The experimental results incorporated in ViFaSS are based on thinner laminates between 4-6mm. To exclude errors in the prediction due to a potential scale effect. It should be validated that the model simulation of a thick laminate, loaded with a constant amplitude under bending, Tension-Tension (T-T) and Compression-Compression (C-C) is comparable with experimental stiffness degradation results.

For the webs of the sandwich panel, a higher V_f is used in the model, due to the used Optidat database, then is achievable in reality. This difference can be solved in two ways. One could be to design a mould such that a V_f of 52% can be achieved in the webs. The second option is to extend the model with an additional database of UD results for V_f of the webs. The first option is most desirable because the simulations presented above can be used.

Simulation 1 Local bending To validate the applicability of ViFaSS to the local bending model and see to what extend the stiffness degradation can be predicted for such a component. There need to be performed a minimum of 3 experiments where the stiffness degradation of the component is measured. The way the tyre load is applied is of particular importance to prevent stress concentrations during the test. An ideal situation would be to use an actual tyre.

Simulation 2 design case To validate the applicability of ViFaSS to the design case model and see to what extend the stiffness degradation is limited to the local degradation as is simulated. There need to be performed a minimum of 3 experiments where the stiffness degradation of the component is measured, preferably local deflection of the face sheet and global deflection. The way the tyre load is applied is of particular importance to prevent stress concentrations during the test. An ideal situation would be to use an actual tyre.

6

Conclusions and Recommendations

6.1. Conclusions

This study aims to develop a numerical model based on existing knowledge and experiments and including relevant aspects of the **Glas Fibre-Reinforced Polymer (GFRP)**s fatigue behaviour, to predict the fatigue stiffness performance of in-plane stress dominated structures and components, to prevent the use of potential unconservative damage summation methods like Palmgren-Miner in design. In this report, **Virtual Fatigue Stiffness Simulation (ViFaSS)**, a numerical fatigue reduction model, is developed where the fatigue material response is fully characterised on a unidirectional ply level based on experimental results from the Optidat database [36]. The component response in the numerical simulations under constant amplitude **Tension-Tension (T-T)** and bending fatigue loading are in reasonable agreement with experimental results. First, the sub-questions are answered, which will help to answer the main research questions.

Subquestions

1. *How does damage due to cyclic fatigue loading influence **GFRP** stiffness properties?*

- The damage process within the matrix mainly causes the decrease in the laminate's stiffness in the initial and first part of the intermediate region. For a **multidirectional (MD)** laminate, the intralaminar damage in the transverse plies causes the transverse and shear stress to decrease. Which initiates a stress redistribution between layers, resulting in higher stresses in the on-axis (0°) plies. This phenomenon is more severe at higher stress levels and results in a lower stiffness of the original laminate.
- For an **MD** $[(\pm 45/0)_4/\pm 45]_T$ laminate, loaded between σ_x 186 MPa and σ_x 252 MPa, **ViFaSS** predicts the intralaminar damage in the transverse plies to cause the transverse and shear stress to decrease with 50-60%, resulting in 3-6% higher stresses in the 0° plies.
- These answers can be found in chapter 2 and chapter 4.

2. *What are relevant aspects for predicting damage initiation, damage growth in **GFRP** material dominated by in-plane stress caused by **constant amplitude (CA)** and **variable amplitude (VA)** fatigue loading and what are available prediction methods proposed in the literature?*

- Aspects governing the fatigue behaviour of in-plane stress dominated components are related to the damage development in the material for a wide variety of lay-up compositions and random load configurations. Therefore, progressive damage accumulation, damage development under multi-axial stress states, redistribution of stress between layers and stress redistribution in the component caused by damage must be considered in developing a numerical model.
- Existing approaches to describe fatigue behaviour of **GFRP** can be categorised into three categories. 1: Fatigue Life Modeling and Prediction, 2: Phenomenological and Empirical Modeling and 3: Progressive Damage Modeling. Progressive damage models should allow for the incorporation of the aspect as mentioned earlier regarding the fatigue behaviour of **GFRP**.

- These answers can be found in chapter 2.

3. *How can those relevant aspects be incorporated into a model such that engineers can incorporate those in the predesign?*

- The fatigue stiffness reduction in ViFaSS is programmed in Python, and the Finite Element (FE) analyses are performed with SOFiSTiK; widely used by engineering companies. It allows for fast linear elastic calculations of layered materials. By implementing ViFaSS in the existing design procedure, limited additional activities need to be carried out by the designer.
- This answer can be found in chapter 3.

4. *What are the minimum input requirements for such a model?*

- A complete set of unidirectional (UD) data is required, existing of static material properties of the UD ply as indicated in table 6.1 and fatigue properties on ply level in the form of S-N formulations. The minimum required S-N formulations needed are given below;
 - UD 90°R=0.1
 - UD 90°R=-1
 - UD 90°R=10
 - ±45°R=0.1
 - ±45°R=-1

Table 6.1: Required static material properties

Property	Abbreviation	Test standard
Tensile modulus 1-direction	$E_{1,t}$	EN-ISO 527
Tensile modulus 2-direction	$E_{2,t}$	EN-ISO 527
Compressive modulus 1-direction	$E_{1,c}$	EN-ISO 14126
Compressive modulus 2-direction	$E_{2,c}$	EN-ISO 14126
Poisson's ratio 12-direction	ν_{12}	
Poisson's ratio 21-direction	ν_{21}	

- These answers can be found in chapter 3 section 3.2.

5. *What does such a model predict when the local fatigue effects of wheel loading on a sandwich deck panel are simulated?*

- In the simulation of a webcore sandwich panel that experience high local bending stresses in the face sheets and webs, ViFaSS predicts that in areas with large stresses, the plies loaded in tension degrade the most. This stiffness loss in those plies causes the global response of the component.
- For a webcore sandwich panel loaded by a small local wheel load and a comparable stress state in the panel to a design situation, ViFaSS predicts only a stiffness reduction under the wheel print area in the top en bottom face sheet. The global response shows a deflection increase of 6.5%.
- These answers can be found in chapter 5.

Main question

How can the fatigue performance of in-plane stress dominated Glass Fibre-Reinforced Polymer components, with arbitrary lay-up compositions, be modelled based on existing knowledge and experiments, including the damage development under complex stress states and stress redistribution?

This study showed that ViFaSS, a non-linear fatigue stiffness reduction model, where at least the non-linear and damage dependent fatigue material response is characterised on a UD ply level.

Predicts a stiffness reduction for various MD laminates similar to experimental coupon results in the initial and first part of the intermediate region. For in-plane stress dominated structures and components, where out of plane fatigue damage mechanisms do not occur, ViFaSS is capable of simulating the initial and intermediate region of the typical three-staged stiffness decrease. ViFaSS can simulate the sequence effect to a certain extent. The sequence effect of individual ply damage caused by the fibre-matrix debonding is not incorporated. However, simulation of an MD $[(\pm 45, 0)_4, \pm 45]$ laminate, the prediction indicates that a high-low load series causes more damage than a low-high load block. Simulating two large or multiple small load blocks shows no difference in predicted damage. Because the stiffness reduction in the ply caused by the different damage mechanisms is lumped in one stiffness reduction, the contribution per damage mechanism is lost.

Within this study, it is shown that ViFaSS provides the designer with the ability to incorporate multiple relevant aspects of the GFRP's material behaviour in the predesign of in-plane stress dominated structures. Such as the damage accumulation dependency on damage history and damage development dependency on the load type, e.g. T-T or Compression-Compression (C-C) and stress redistribution under multi-axial stress states.

ViFaSS predicted that locally induced damage under a wheel print causes the global deflection of a web core sandwich panel to increase by 6.5%. That raises the question if it is relevant to incorporate a prescribed deflection or stiffness loss in the serviceability limit state verification of webcore sandwich panels?

6.2. Recommendations

In this section, recommendations will be proposed regarding two different aspects; first, recommendations regarding knowledge and experimental input, and second possible optimisations of the numerical model will be indicated.

Recommendations regarding knowledge and experimental input

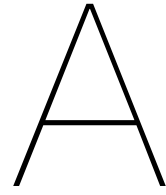
- The used stiffness damage relation, for **unidirectional (UD)** plies loaded in shear or 90 °off-axis, presented in section 3.3.4, does not allow for a sequence effect to exist. This stiffness damage relation indicates that the accumulation of damage is independent of the already induced damage in **UD** plies. Further experimental research could confirm or disprove this outcome. Verification can be done by doing four types of experiments; the first two where the stiffness degradation of the transverse modulus of a **UD** ply is measured during a sequence of two load blocks for a high-low and low-high sequence. The second two where the stiffness degradation of the shear modulus of a **UD** ply is measured during a sequence of two load blocks for a high-low and low-high sequence. Ideally, those experiments should be performed on a stress level comparable with actual design situations because the damage development depends on the load magnitude.
- It is concluded that applying full ply discount when the stiffness loss in the simulation is equal to the stiffness loss at the failure of the **UD** ply experiment is too conservative. The confinement of surrounding plies will result in an effective stiffness of the damaged plies. To include this physical effect in **Virtual Fatigue Stiffness Simulation (ViFaSS)**, it is desired to investigate this effect in more detail to propose a more realistic stiffness degradation relation for confined plies.
- Existing experimental results were insufficient to validate the proposed interaction relation between transverse and shear stiffness loss. Here a recommendation is made on how the relation can be validated. The importance is that shear damage is related to transverse stiffness decrease and the other way around. Two types of **UD** experiments can be used for this:
 1. The coupon is loaded under fatigue shear stress, where both the shear and transverse stiffness degradation are measured.
 2. The coupon is loaded transversely in fatigue, where again both stiffness degradations are measured.
- With the model, a high-low and low-high loading block is simulated. As expected from the literature, the high-low loading block results in a more significant stiffness decrease. However, to validate the total reduction in stiffness, future research should validate the simulated results in section 4.1 with experimental findings. This verification can be done by performing two **Tension-Tension (T-T)** experiment on the MD laminated described in section 4.1. The first experiment loaded by the following sequences: σ_x 186 MPa for 30000 cycles followed by σ_x 252 MPa for 30000 cycles. The second experiment should then be loaded by the inverse of the first, i.e. σ_x 252 MPa for 30000 cycles followed by σ_x 186 MPa for 30000 cycles. The number of cycles and stress levels can vary, the numbers given here are used in the sequence effect simulation from subsection 4.1.4.
- To validate the applicability of the model on a component scale, the simulation of the sandwich webcore panel given in chapter 5 should be validated. This validation can be done by performing multiple experiments. First, performing a series of experiments where the stiffness degradation of the face sheet material under bending is validated against model predictions to rule out any size effects caused by the increase in thickness. At least three full-scale experiments of the webcore specimen produced with an epoxy resin and where the foam insert is removed should be tested, where the displacements are compared with the model predictions.

Recommendations regarding possible optimisations of the numerical model

- Using SOFiSTiK as **Finite Element (FE)** software resulted in some limitations regarding material property adjustment due to the maximum allowable materials. However, implementing the proposed fatigue material response in a user-subroutine of, e.g. Ansys or Abaqus/Explicit, could increase the model's accuracy.

- By using linear material constitutive relations, the material behaviour can deviate from reality, primarily for matrix dominated behaviour. Using [FE](#) software where implementing non-linear material behaviour for layered materials is possible could give a more realistic stress distribution in the laminate.
- Extending the model by implementing strength degradation rules, also characterised on a unidirectional ply level. In combination with combined ply stress failure criterion, like Puck or Hashin, can give the ability to virtually test the strength degradation and residual static strength of the component as is required according to the technical specification.

This study and [ViFaSS](#) set a good starting point for the further development of numerical fatigue simulations to increase the predictability of the fatigue performance of in-plane stress dominated components. The numerical fatigue reduction model gives the advantage to research new applications for [Glas Fibre-Reinforced Polymer \(GFRP\)](#) components, e.g. application of sandwich webcore panels in the main road network, without the expenses of performing actual experiments.



Appendix CLT validation

A.1. Validation of the ABD matrix

Title:	Verification: Classical Laminate Theory: ABD-matrix
Version number:	2.0
Author:	Mathieu Koetsier
Approved by:	
Project name:	Virtual fatigue verification of Glass Fibre-Reinforced polymer components for civil engineering applications
Description of Verification subject:	The determination of the ABD-matrix by the algorithm is verified.
Start date:	2-2-2020
This document was updated on:	2-2-2020

Version	Date	Summary of Revision
1.0	2-2-2021	Verification of the ABD-matrix by TU Delft FRP tool (Unity WebGL Player FRPTool (tudelft.nl))
2.0	2-2-2021	Verification of the ABD-matrix with eLamX 2.6

1. Input data

1.1. Ply properties

E_0 [MPa]	E_{90} [MPa]	G_{12} [MPa]	M_0 [-]	M_{90} [-]	Name
37200	11400	3400	0.29	0.089	UD Ply

1.2. Layup configuration

Layer	Angle	Thickness	Material
1	0	0.625	UD Ply
2	90	0.625	UD Ply
3	45	0.625	UD Ply
4	-45	0.625	UD Ply
5	-45	0.625	UD Ply
6	45	0.625	UD Ply
7	90	0.625	UD Ply
8	0	0.625	UD Ply

2. Output data Algorithm

A in $10^5 \left[\frac{N}{mm} \right]$	1.06	0.35	0.00
	0.35	1.06	0.00
	0.00	0.00	0.35

B in [N]	0.00	0.00	0.00
	0.00	0.00	0.00
	0.00	0.00	0.00

D in 10^5 [Nmm]	2.89	0.45	0.06
	0.45	2.11	0.06
	0.06	0.06	0.45

3. Output data TU Delft FRP Tool

A	1.06	0.35	0.00	$\cdot 10^5 \text{ N/mm}$
	0.35	1.06	0.00	
	0.00	0.00	0.35	
B	0.00	0.00	0.00	N
	0.00	0.00	0.00	
	0.00	0.00	0.00	
D	2.89	0.45	0.06	$\cdot 10^5 \text{ Nmm}$
	0.45	2.11	0.06	
	0.06	0.06	0.45	

Figure 1 ABD matrix obtained with delftxtools FRP

4. Output data eLamx 2.6

106277.5	35404.0	-0.0	-0.0	-0.0	0.0
35404.0	106277.5	0.0	-0.0	-0.0	0.0
-0.0	0.0	35436.7	0.0	0.0	0.0
-0.0	-0.0	0.0	289011.6	44951.0	6465.5
-0.0	-0.0	0.0	44951.0	211426.0	6465.5
0.0	0.0	0.0	6465.5	6465.5	45019.1

Figure 2 ABD matrix obtained with eLamX 2.6

5. Conclusion

De result of the algorithm is the same as obtained with external tools. It can be concluded that the ABD matrix is calculated correctly by the algorithm.

A.2. Validation of the deformations

Title:	Verification: Classical Laminate Theory: Deformations
Version number:	1.0
Author:	Mathieu Koetsier
Approved by:	
Project name:	Virtual fatigue verification of Glass Fibre-Reinforced polymer components for civil engineering applications
Description of Verification subject:	The determination of the deformation vector by the algorithm is verified.
Start date:	2-2-2020
This document was updated on:	2-2-2020

Version	Date	Summary of Revision
1.0	2-2-2021	Verification of the deformation with eLamX 2.6

1. Input data

1.1. Ply properties

E_0 [MPa]	E_{90} [MPa]	G_{12} [MPa]	M_0 [-]	M_{90} [-]	Name
37200	11400	3400	0.29	0.089	UD Ply

1.2. Layup configuration

Layer	Angle	Thickness	Material
1	0	0.625	UD Ply
2	90	0.625	UD Ply
3	45	0.625	UD Ply
4	-45	0.625	UD Ply
5	-45	0.625	UD Ply
6	45	0.625	UD Ply
7	90	0.625	UD Ply
8	0	0.625	UD Ply

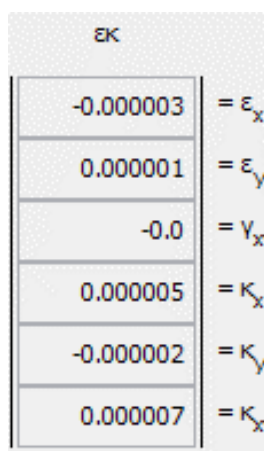
1.3. Load vector

Load type	Value	Unit
Nxx	-0.26758	[N/mm]
Nyy	-0.00212	[N/mm]
Nxy	-0.00494	[N/mm]
Mxx	1.481199	[N]
Myy	-0.19025	[N]
Mxy	0.314897	[N]

2. Output data Algorithm

Deformation	Value	Unit
ϵ_x	-0.000003	[-]
ϵ_y	0.000001	[-]
γ_{xy}	0.000000	[-]
κ_x	0.000005	[1/m]
κ_{xy}	-0.000002	[1/m]
κ_{xy}	0.000007	[1/m]

3. Output data eLamx 2.6



EK	
-0.000003	= ϵ_x
0.000001	= ϵ_y
-0.0	= γ_{xy}
0.000005	= κ_x
-0.000002	= κ_y
0.000007	= κ_{xy}

Figure 1 Deformations obtained with eLamX 2.6

4. Conclusion

De result of the algorithm is the same as obtained with external tools. It can be concluded that the deformation vector is calculated correctly by the algorithm.

A.3. Validation of the ply stresses

Title:	Verification: Classical Laminate Theory: Local ply stresses
Version number:	1.0
Author:	Mathieu Koetsier
Approved by:	
Project name:	Virtual fatigue verification of Glass Fibre-Reinforced polymer components for civil engineering applications
Description of Verification subject:	The determination of the local ply stresses by the algorithm is verified.
Start date:	2-2-2020
This document was updated on:	2-2-2020

Version	Date	Summary of Revision
1.0	2-2-2021	Verification of the local ply stress levels with eLamX 2.6

1. Input data

1.1. Ply properties

E_0 [MPa]	E_{90} [MPa]	G_{12} [MPa]	M_0 [-]	M_{90} [-]	Name
37200	11400	3400	0.29	0.089	UD Ply

1.2. Layup configuration

Layer	Angle	Thickness	Material
1	0	0.625	UD Ply
2	90	0.625	UD Ply
3	45	0.625	UD Ply
4	-45	0.625	UD Ply
5	-45	0.625	UD Ply
6	45	0.625	UD Ply
7	90	0.625	UD Ply
8	0	0.625	UD Ply

1.3. Load vector

Load type	Value	Unit
Nxx	-0.26758	[N/mm]
Nyy	-0.00212	[N/mm]
Nxy	-0.00494	[N/mm]
Mxx	1.481199	[N]
Myy	-0.19025	[N]
Mxy	0.314897	[N]

2. Additional information

2.1. Used coordination system

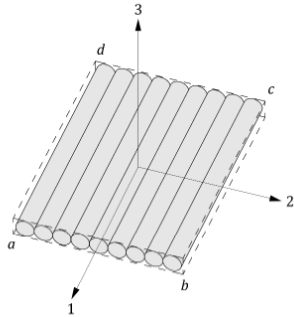


Figure 1 Reference axis for UD ply

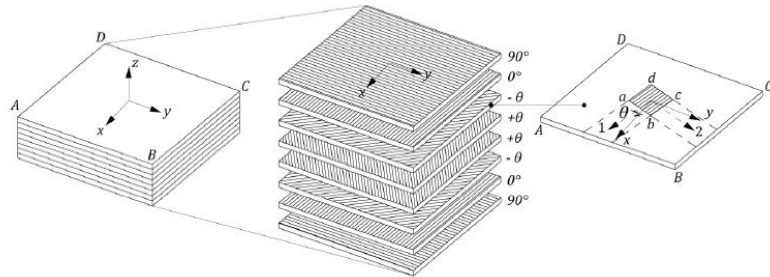


Figure 2 Reference axis for global laminate

3. Output data Algorithm

Table 1 Output results in local ply stress by the algorithm in table form

Layer	z [mm]	σ_{11} [MPa]	σ_{22} [MPa]	τ_{12} [MPa]
1	-2.5	-0.59418	0.02132	-0.05615
1	-1.875	-0.47182	0.01629	-0.04223
2	-1.875	0.15153	-0.13257	0.04223
2	-1.25	0.10955	-0.09836	0.02831
3	-1.25	-0.26482	-0.00896	0.04486
3	-0.625	-0.15341	-0.01137	0.02879
4	-0.625	-0.00612	-0.04655	-0.02879
4	0	-0.03714	-0.01495	-0.01273
5	0	-0.03714	-0.01495	-0.01273
5	0.625	-0.06817	0.01665	0.00333
6	0.625	0.06941	-0.01620	-0.00333
6	1.25	0.18082	-0.01862	-0.01939
7	1.25	-0.05838	0.03850	-0.02736
7	1.875	-0.10036	0.07272	-0.04128
8	1.875	0.26237	-0.01390	0.04128
8	2.5	0.38473	-0.01893	0.05520

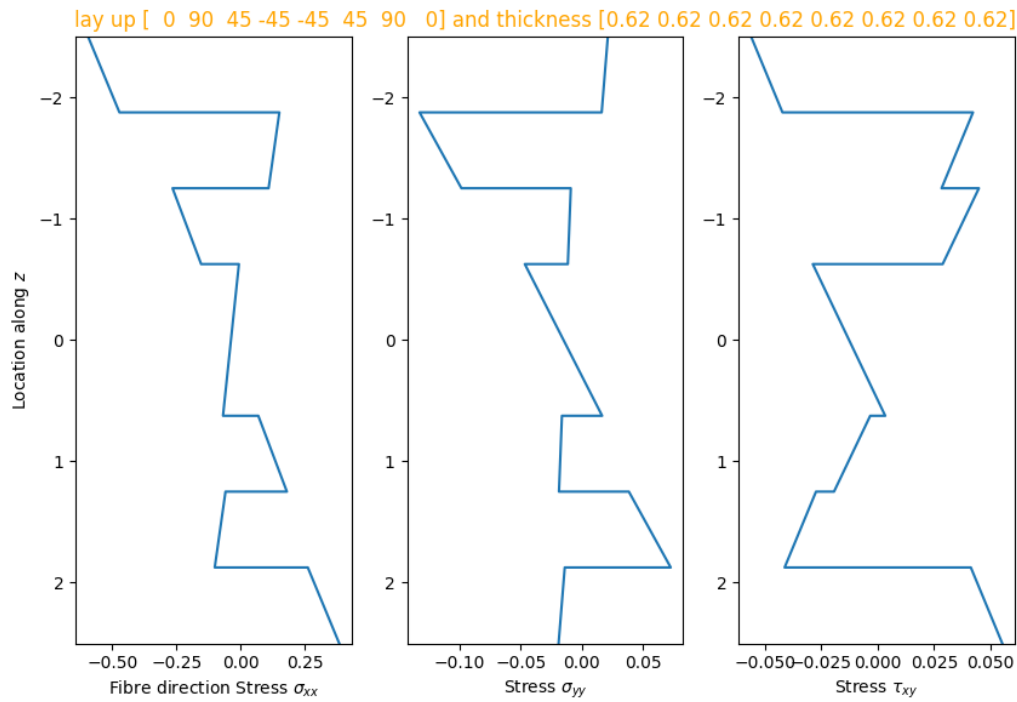


Figure 3 Output local ply stress by the algorithm as a plot

4. Output data eLamx 2.6

Layer	z [mm]	σ_{11} [MPa]	σ_{22} [MPa]	τ_{12} [MPa]
1	-2.5	-0.594	0.021	-0.056
1	-1.875	-0.472	0.016	-0.042
2	-1.875	0.152	-0.133	0.042
2	-1.25	0.11	-0.098	0.028
3	-1.25	-0.265	-0.009	0.045
3	-0.625	-0.153	-0.011	0.029
4	-0.625	-0.006	-0.047	-0.029
4	0	-0.037	-0.015	-0.013
5	0	-0.037	-0.015	-0.013
5	0.625	-0.068	0.017	0.003
6	0.625	0.069	-0.016	-0.003
6	1.25	0.181	-0.019	-0.019
7	1.25	-0.058	0.039	-0.027
7	1.875	-0.1	0.073	-0.041
8	1.875	0.262	-0.014	0.041
8	2.5	0.385	-0.019	0.055

Figure 4 Local ply stresses obtained with eLamX 2.6

5. Conclusion

The result of the algorithm is compared with eLamX 2.6 the difference in % is given in Table 2. It can be concluded that the differences are due to rounding of eLamX 2.6 results and that the algorithm obtains the correct stresses in the laminate.

Table 2 Result of comparison between algorithm and eLamX 2.6

Layer	z [mm]	$\Delta\sigma_{11}/\sigma_{11eLamX}$ [%]	$\Delta\sigma_{22}/\sigma_{22eLamX}$ [%]	$\Delta\tau_{12}/\tau_{12eLamX}$ [%]
1	-2.5	-0.03%	-1.52%	-0.27%
1	-1.875	0.04%	-1.80%	-0.56%
2	-1.875	0.31%	0.32%	-0.56%
2	-1.25	0.41%	-0.36%	-1.12%
3	-1.25	0.07%	0.49%	0.32%
3	-0.625	-0.27%	-3.38%	0.71%
4	-0.625	-1.94%	0.97%	0.71%
4	0	-0.39%	0.36%	2.04%
5	0	-0.39%	0.36%	2.04%
5	0.625	-0.25%	2.04%	-10.87%
6	0.625	-0.60%	-1.27%	-10.87%
6	1.25	0.10%	2.01%	-2.03%
7	1.25	-0.66%	1.27%	-1.35%
7	1.875	-0.36%	0.39%	-0.69%
8	1.875	-0.14%	0.70%	-0.69%
8	2.5	0.07%	0.35%	-0.37%

B

Appendix constant life surface validation

Title:	Validation of constant life surface
Version number:	1.0
Author:	Mathieu Koetsier
Approved by:	
Project name:	Virtual fatigue verification of Glass Fibre-Reinforced polymer components for civil engineering applications
Description of validation subject:	The lifetime prediction by a constant life surface is validated for known data.
Start date:	4-3-2020
This document was updated on:	2-2-2020

Version	Date	Summary of Revision
1.0	4-3-2021	The applicability of the developed lifetime prediction by a constant life surface is validated.

1. Input data

The OptiDAT database consists of several experiments; there are laminate types where fatigue experiments are done for multiple R values; 2, 10, -1, -0.4, 0.1, 0.5. Figure 1 gives a constant life diagram that is constructed for multi-directional laminate used in the OptiDAT experiments (Nijssen, 2007).

Constant Life Diagram for MD material

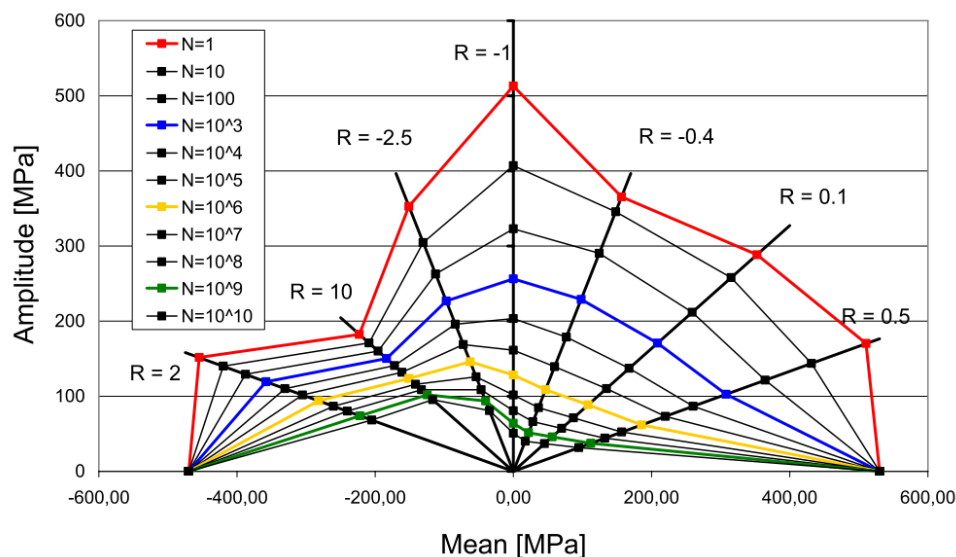
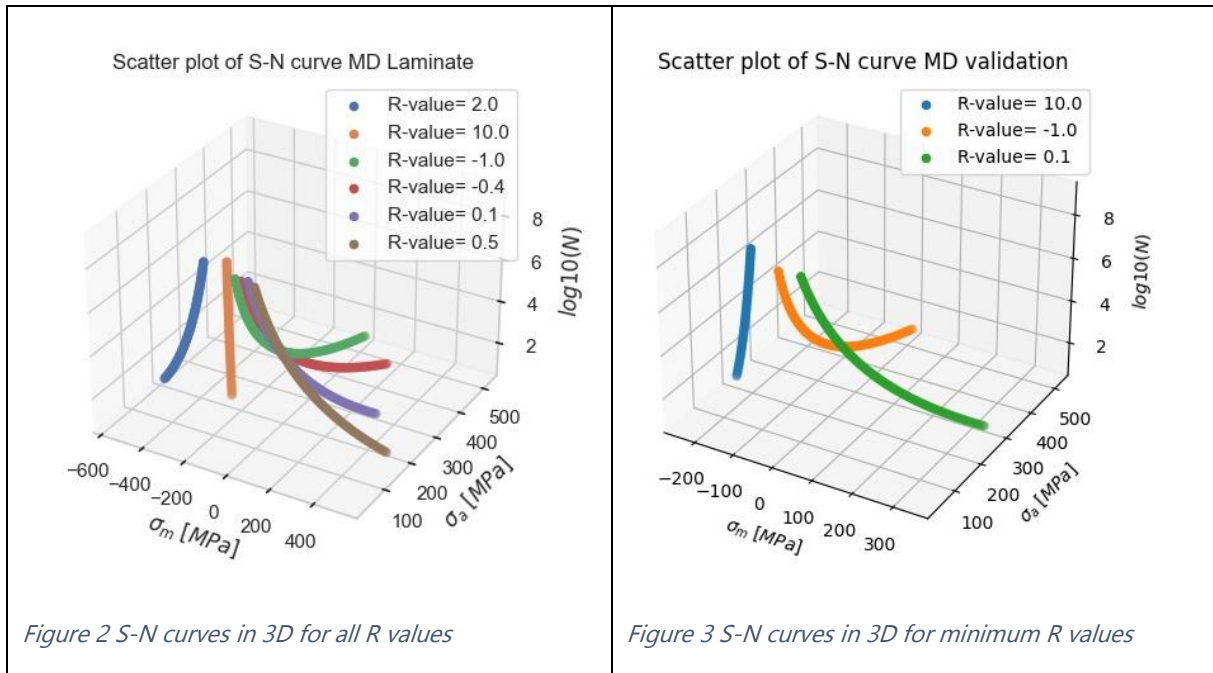
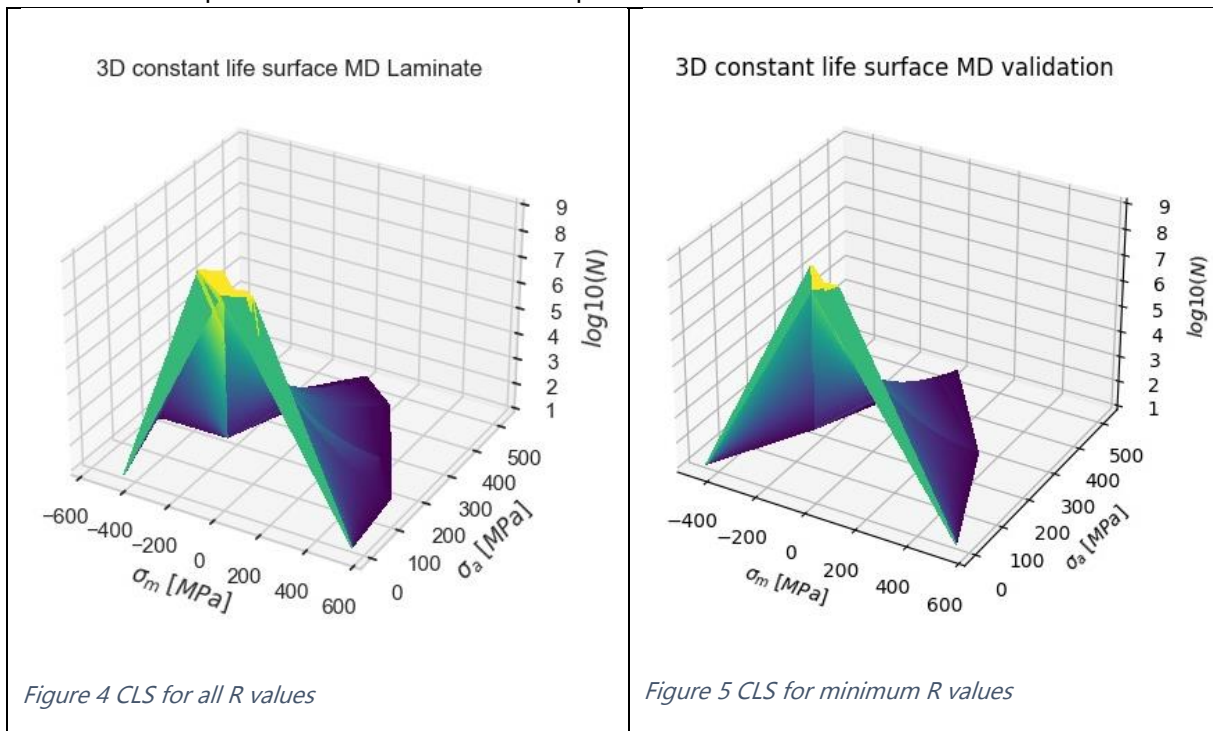


Figure 1 Constant life diagram from OptiDAT report (Janssen et al., 2006)

That multiple S-N formulations are known gives the ability to use R 10, -1 and 0.1 to predict S-N curves for R 2, -0.4 and 0.5. Translating this into a constant life surface, results are given in Figure 2 and Figure 3



From these 3D points, a surface can be interpolated, linear or cubic.



2. Output data Algorithm

Because the S-N formulations are fitted for R values 2, -0.4, and 0.5, the prediction and curves can be compared. The prediction is validated for all R values; Figure 6 til Figure 11 show the prediction by interpolating the linear and cubic surface.

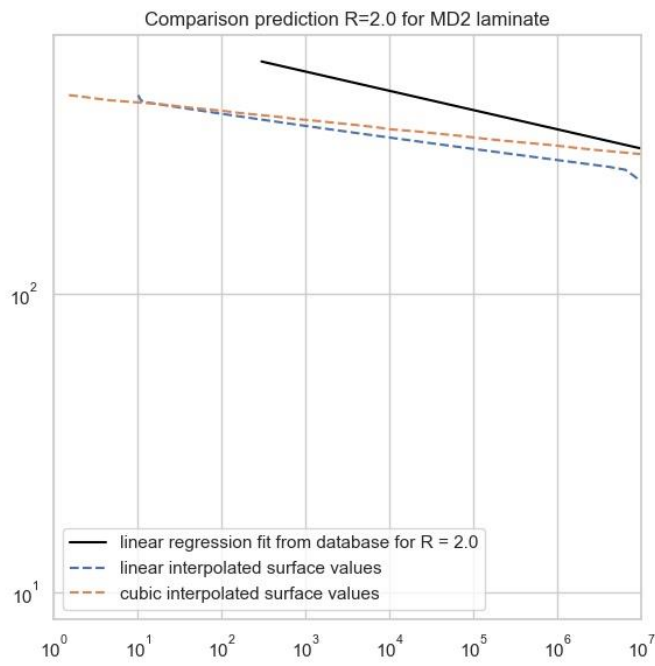


Figure 6 Prediction for R=2.0

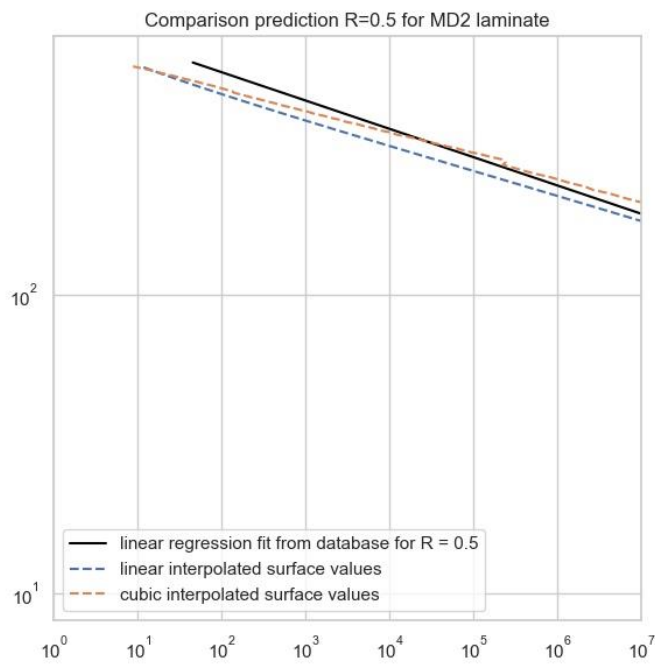


Figure 7 Prediction for R=2.0

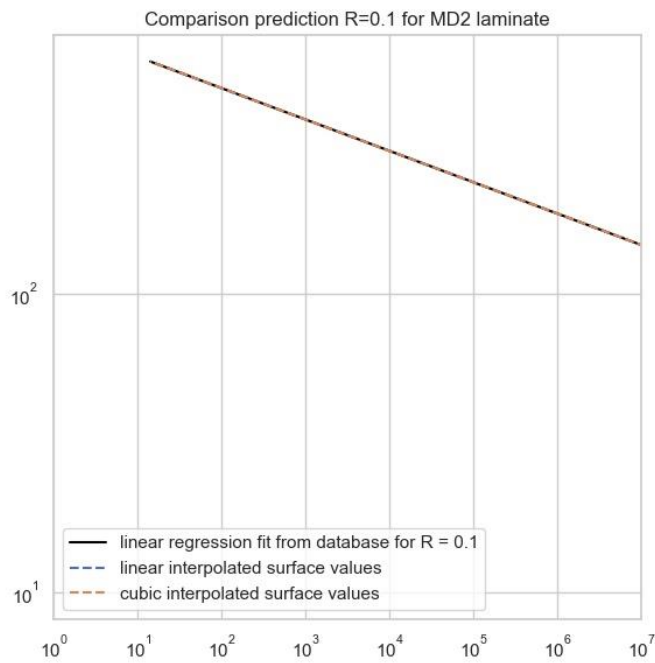


Figure 8 Prediction for R=0.1

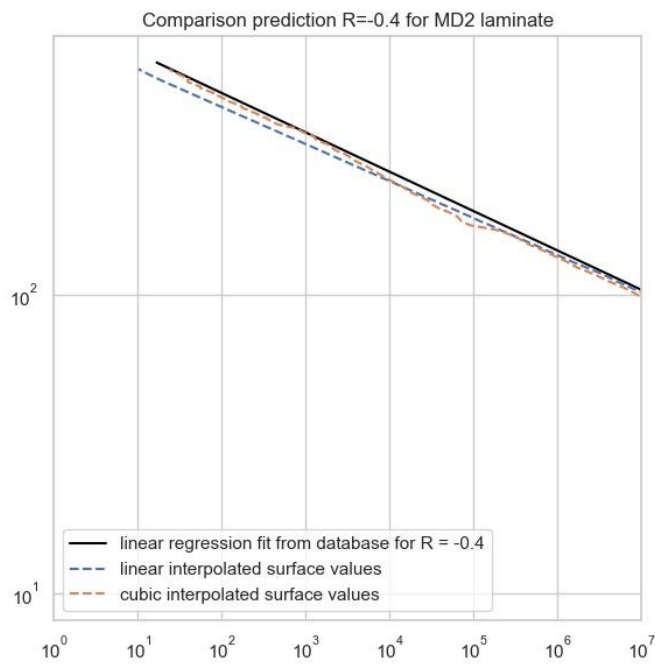


Figure 9 Prediction for R=-0.4

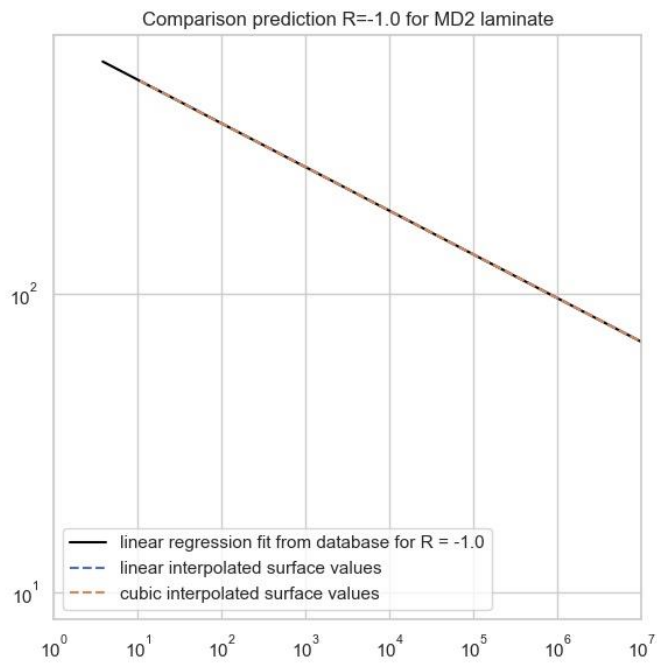


Figure 10 Prediction for R=-1.0

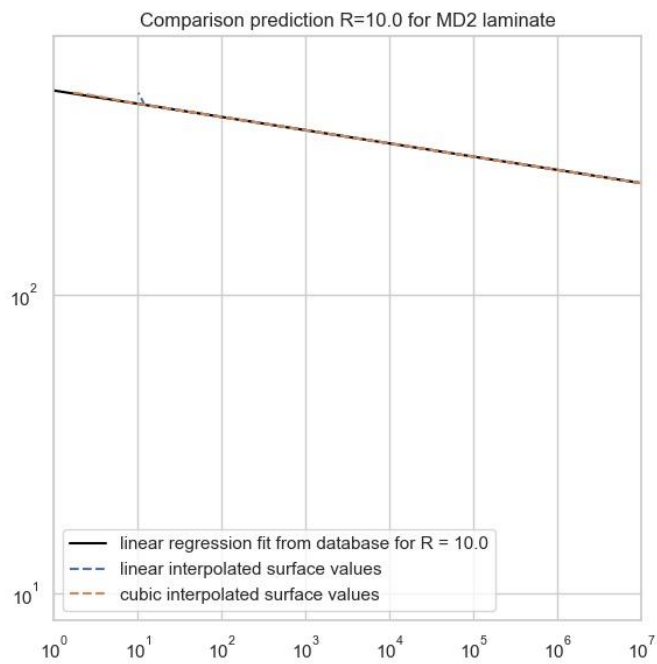


Figure 11 Prediction for R=10.0

3. Conclusion

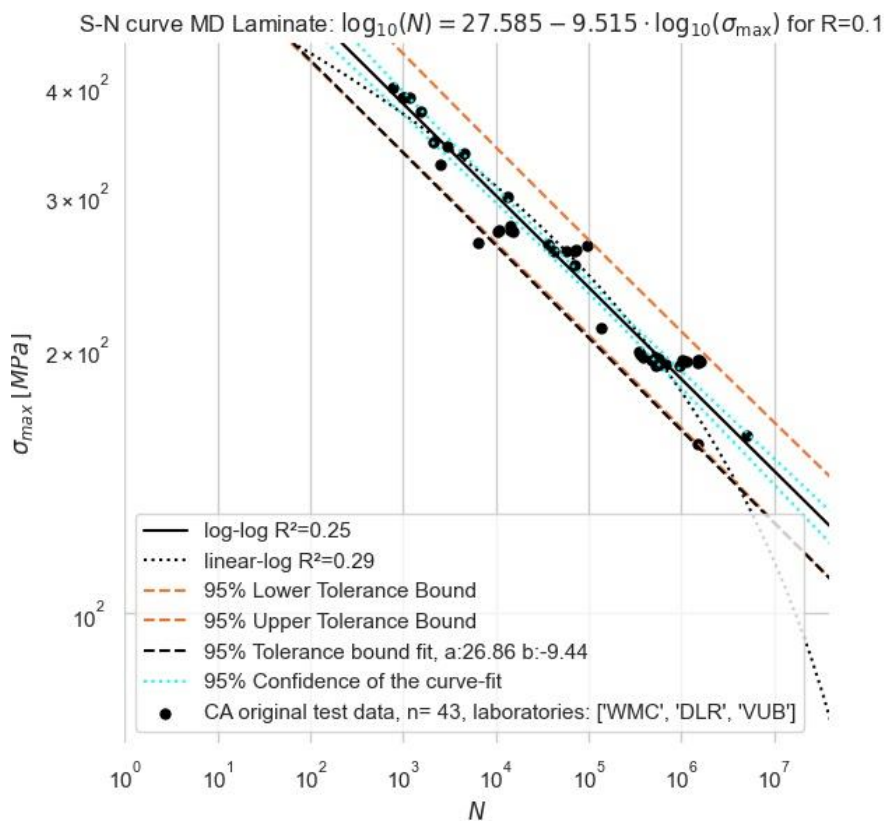
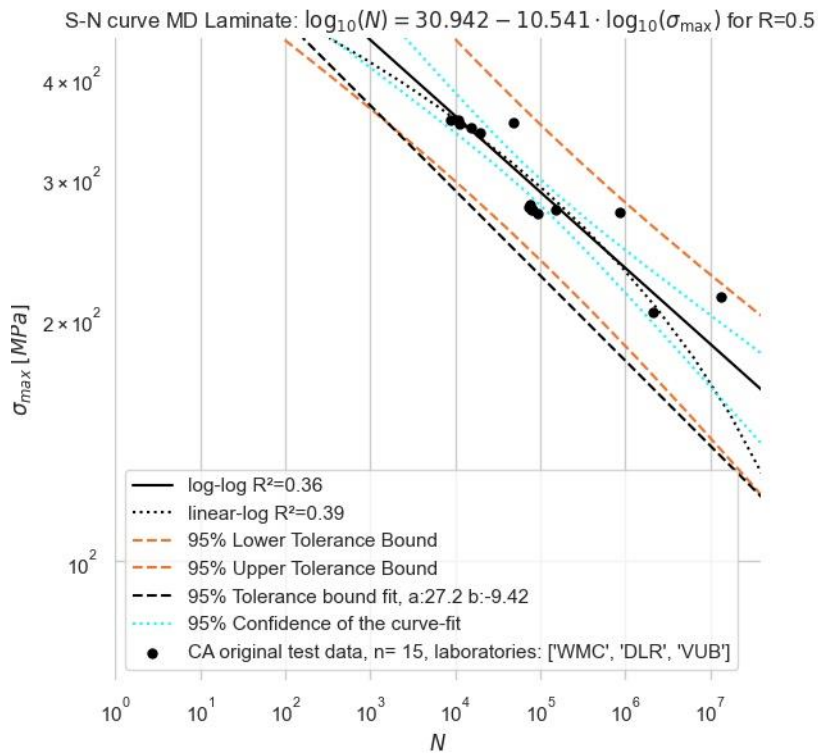
Figure 6, Figure 7 and Figure 9 present the S-N formulation's prediction by the surface in Figure 5. As can be seen, does the linear and cubic surface not differ much. All values are below the fitted S-N curves from experiments. It can therefore be concluded that linear and cubic interpolation of the surface gives conservative values. The OptiDAT program (Janssen et al., 2006) conclusion; that constant life diagrams must be constructed with at least an S-N curve for R values of 10, -1, 0.1 is valid.

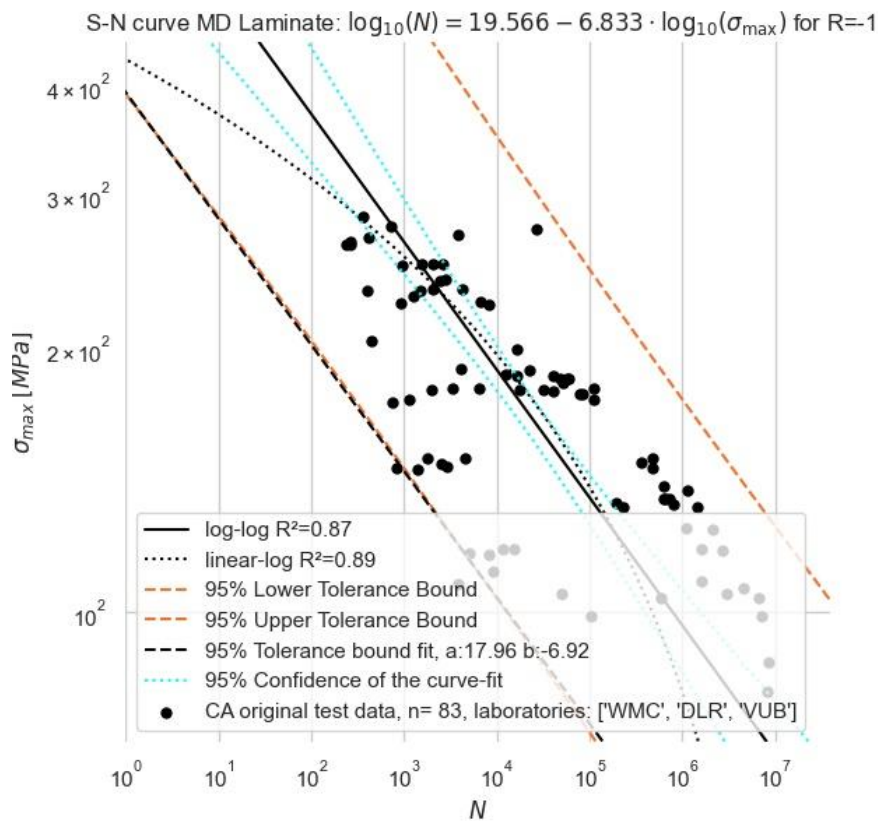
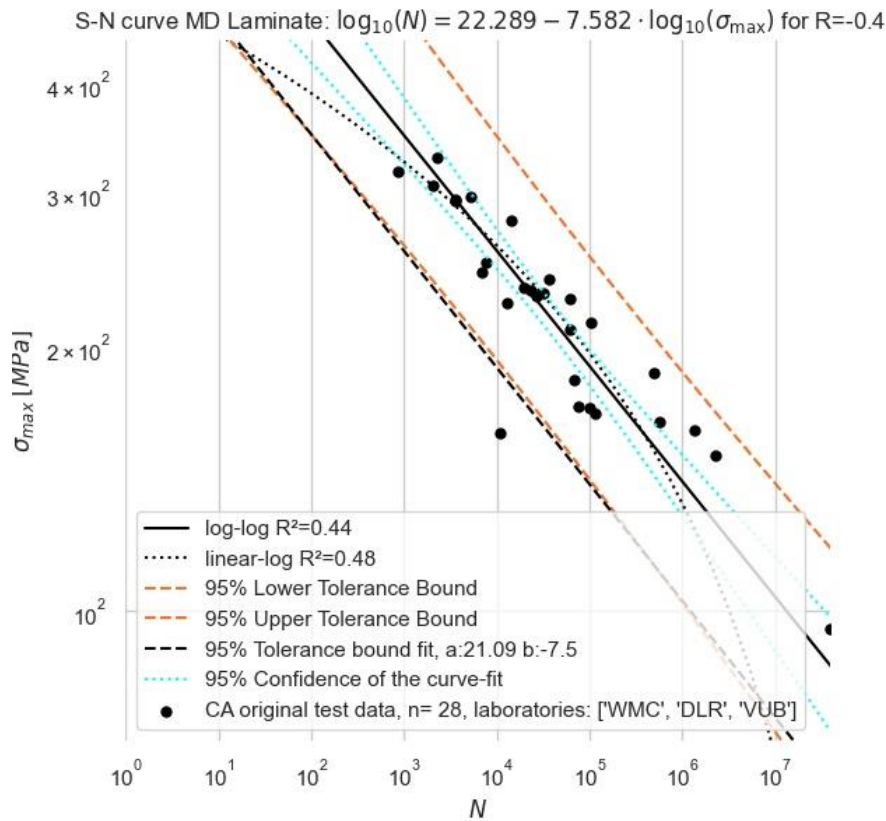
4. Bibliography

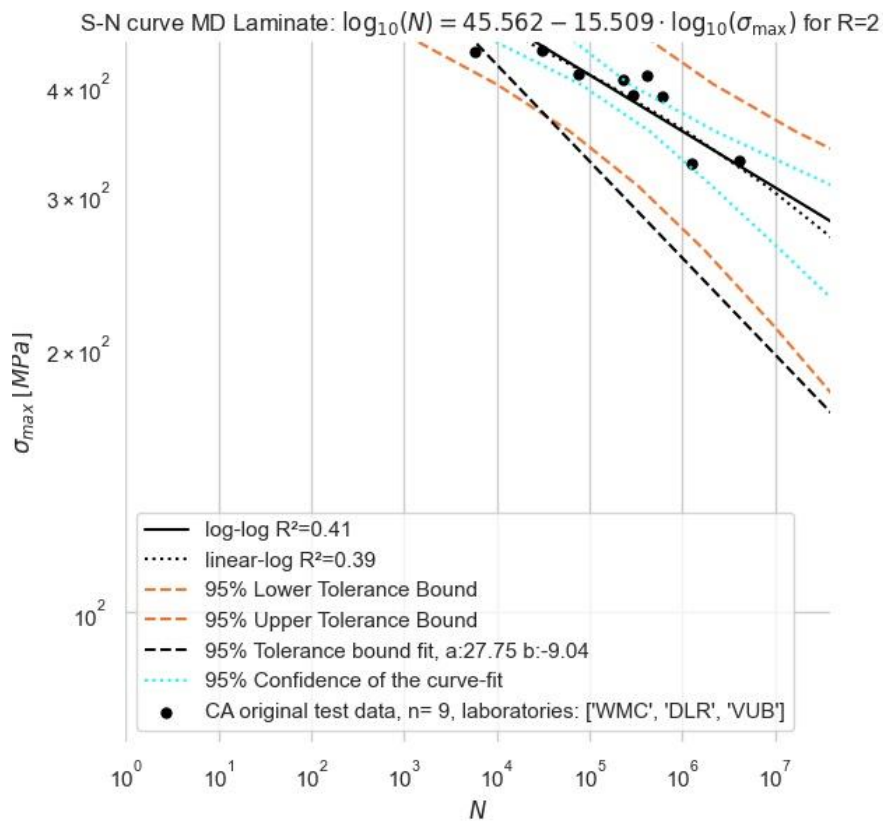
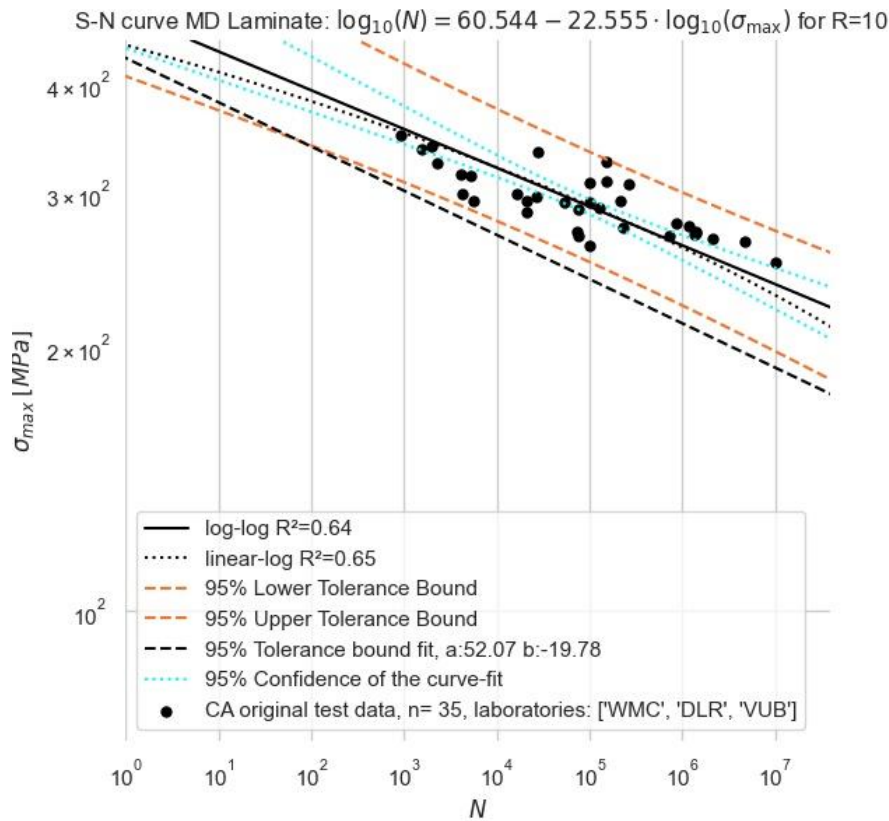
Janssen, L. G. J., Wingerde, A. M. van, Kensche, C. W., Philippidis, T. P., Brøndsted, P., Dutton, A. G., Nijssen, R. P. L., & Krause, O. (2006). *Reliable Optimal Use of Materials for Wind Turbine Rotor Blades* (Issue July).

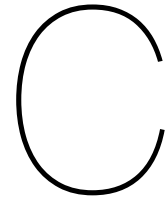
Nijssen, R. P. L. (2007). *OptiDAT – fatigue of wind turbine materials database*. www.kc-wmc.nl

Appendix S-N curve fits for MD3 laminate









Appendix S-N formulations

C.1. Parallel to fibres

The S-N curves parallel to the fibres are obtained from the OptiDAT database [36], the used experimental results are given in table C.1, C.2 and C.3.

The corresponding S-N formulations is given in figure C.1, C.2 and C.3.

Table C.1: Fatigue life test results parallel to fibres for R=0.1

optiDAT nr.	Name	smax, fatigue	Laminate
464	GEV206_R0300_0011	390.60	UD2
465	GEV206_R0300_0012	341.77	UD2
466	GEV206_R0300_0013	292.95	UD2
467	GEV206_R0300_0014	244.12	UD2
469	GEV206_R0300_0018	341.77	UD2
945	GEV206_R0300_0212	561.49	UD2
948	GEV206_R0300_0428	570.66	UD2
949	GEV206_R0300_0429	556.62	UD2
950	GEV206_R0300_0430	567.04	UD2
951	GEV206_R0300_0431	375.19	UD2
1107	GEV206_R0300_0432	369.74	UD2
2717	GEV206_R0300_0433	270.04	UD2
1108	GEV206_R0300_0434	271.53	UD2
952	GEV206_R0300_0435	369.68	UD2
1109	GEV206_R0300_0436	562.82	UD2
953	GEV206_R0300_0438	368.26	UD2
1110	GEV206_R0300_0440	266.19	UD2
954	GEV206_R0300_0441	372.66	UD2
1111	GEV206_R0300_0443	271.18	UD2
1112	GEV206_R0300_0445	263.48	UD2
956	GEV206_R0300_0446	366.17	UD2
2716	GEV206_R0300_0447	267.52	UD2
957	GEV206_R0300_0496	558.85	UD2
958	GEV206_R0300_0498	653.87	UD2
3201	GEV206_R0300_0810	229.89	UD2
3064	GEV206_R0300_0831	286.83	UD2
3056	GEV206_R0300_0882	289.46	UD2
3054	GEV206_R0300_0891	298.90	UD2
3053	GEV206_R0300_0894	289.46	UD2
3052	GEV206_R0300_0906	289.46	UD2
3051	GEV206_R0300_0929	290.27	UD2

Table C.2: Fatigue life test results parallel to fibres for R=-1.0

optiDAT nr.	Name	smax, fatigue	Laminate
461	GEV206_R0300_0008	263.16	UD2
462	GEV206_R0300_0009	153.85	UD2
463	GEV206_R0300_0010	190.29	UD2
647	GEV206_R0300_0015	263.16	UD2
468	GEV206_R0300_0017	210.53	UD2
649	GEV206_R0300_0019	188.72	UD2
650	GEV206_R0300_0020	210.53	UD2
651	GEV206_R0300_0021	209.69	UD2
653	GEV206_R0300_0023	263.16	UD2
654	GEV206_R0300_0024	189.47	UD2
659	GEV206_R0300_0133	304.52	UD2
660	GEV206_R0300_0134	181.24	UD2
661	GEV206_R0300_0135	256.89	UD2
662	GEV206_R0300_0136	253.77	UD2
665	GEV206_R0300_0139	181.98	UD2
668	GEV206_R0300_0142	351.01	UD2
669	GEV206_R0300_0143	246.09	UD2
670	GEV206_R0300_0144	328.26	UD2
673	GEV206_R0300_0147	198.70	UD2
677	GEV206_R0300_0151	296.51	UD2
683	GEV206_R0300_0158	177.19	UD2
686	GEV206_R0300_0161	159.17	UD2
1328	GEV206_R0300_0162	333.91	UD2
897	GEV206_R0300_0163	267.42	UD2
898	GEV206_R0300_0164	266.35	UD2
899	GEV206_R0300_0165	178.87	UD2
900	GEV206_R0300_0167	267.89	UD2
901	GEV206_R0300_0168	188.48	UD2
902	GEV206_R0300_0169	212.87	UD2
903	GEV206_R0300_0170	180.37	UD2
904	GEV206_R0300_0171	215.51	UD2
905	GEV206_R0300_0172	210.70	UD2
906	GEV206_R0300_0173	206.84	UD2
907	GEV206_R0300_0174	263.38	UD2
908	GEV206_R0300_0175	211.51	UD2
909	GEV206_R0300_0176	184.93	UD2
911	GEV206_R0300_0178	179.74	UD2
912	GEV206_R0300_0179	257.09	UD2
943	GEV206_R0300_0210	179.75	UD2
944	GEV206_R0300_0211	261.78	UD2
1187	GEV206_R0300_0348	268.72	UD2
1188	GEV206_R0300_0349	352.17	UD2
1189	GEV206_R0300_0350	350.92	UD2
1190	GEV206_R0300_0351	345.73	UD2
1191	GEV206_R0300_0352	347.23	UD2
2245	GEV206_R0300_0364	266.62	UD2
2213	GEV206_R0300_0367	257.92	UD2
2248	GEV206_R0300_0368	263.73	UD2
2218	GEV206_R0300_0369	176.27	UD2
2253	GEV206_R0300_0370	179.15	UD2
2244	GEV206_R0300_0371	184.05	UD2
2620	GEV206_R0300_0372	306.63	UD2

2247	GEV206_R0300_0373	429.53	UD2
2250	GEV206_R0300_0375	426.73	UD2
2252	GEV206_R0300_0377	180.41	UD2
2254	GEV206_R0300_0378	178.47	UD2
2215	GEV206_R0300_0382	256.75	UD2
1316	GEV206_R0300_0426	264.79	UD2
1330	GEV206_R0300_0442	175.97	UD2
955	GEV206_R0300_0444	175.38	UD2
1325	GEV206_R0300_0452	340.37	UD2
1326	GEV206_R0300_0497	335.68	UD2
2246	GEV206_R0300_0521	431.07	UD2
2216	GEV206_R0300_0523	417.21	UD2
2618	GEV206_R0300_0526	424.32	UD2
2217	GEV206_R0300_0531	255.26	UD2
2251	GEV206_R0300_0532	260.50	UD2
2214	GEV206_R0300_0533	178.04	UD2
2619	GEV206_R0300_0538	257.46	UD2
2243	GEV206_R0300_0551	436.10	UD2
2249	GEV206_R0300_0552	428.48	UD2
1369	GEV206_R0300_0625	175.53	UD2
1329	GEV206_R0300_0627	337.43	UD2
1327	GEV206_R0300_0628	344.64	UD2
2842	GEV206_R0300_0918	186.18	UD2

Table C.3: Fatigue life test results parallel to fibres for R=10.0

optiDAT nr.	Name	smax, fatigue	Laminate
893	GEV206_R0300_0093	397.90	UD2
894	GEV206_R0300_0094	461.01	UD2
895	GEV206_R0300_0095	421.40	UD2
896	GEV206_R0300_0096	440.78	UD2
1098	GEV206_R0300_0214	470.44	UD2
2617	GEV206_R0300_0347	460.96	UD2
3204	GEV206_R0300_0353	473.12	UD2
1099	GEV206_R0300_0420	470.46	UD2
1100	GEV206_R0300_0421	466.07	UD2
1091	GEV206_R0300_0422	469.48	UD2
1092	GEV206_R0300_0423	470.47	UD2
2718	GEV206_R0300_0427	440.27	UD2
1093	GEV206_R0300_0439	452.80	UD2
1094	GEV206_R0300_0449	452.77	UD2
1095	GEV206_R0300_0451	419.63	UD2
2715	GEV206_R0300_0454	440.28	UD2
2849	GEV206_R0300_0558	437.54	UD2
3202	GEV206_R0300_0564	473.12	UD2
2714	GEV206_R0300_0611	421.91	UD2
2713	GEV206_R0300_0612	419.05	UD2
2712	GEV206_R0300_0614	440.34	UD2
2711	GEV206_R0300_0616	419.07	UD2
2710	GEV206_R0300_0617	440.35	UD2
2708	GEV206_R0300_0622	440.34	UD2
2706	GEV206_R0300_0626	418.99	UD2
2848	GEV206_R0300_0851	483.23	UD2
2844	GEV206_R0300_0864	445.87	UD2
2775	GEV206_R0300_0871	361.98	UD2
2843	GEV206_R0300_0876	390.13	UD2
2600	GEV206_R0300_0879	389.52	UD2
3055	GEV206_R0300_0883	358.21	UD2
2599	GEV206_R0300_0885	473.10	UD2
3527	GEV206_R0300_0903	385.67	UD2
2763	GEV206_R0300_0905	328.41	UD2
2598	GEV206_R0300_0910	387.88	UD2
2597	GEV206_R0300_0930	392.40	UD2

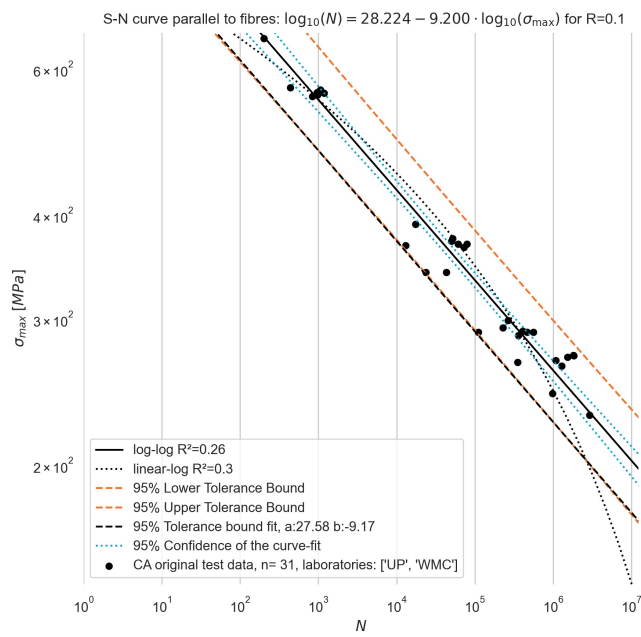


Figure C.1: S-N curve parallel to fibers for T-T

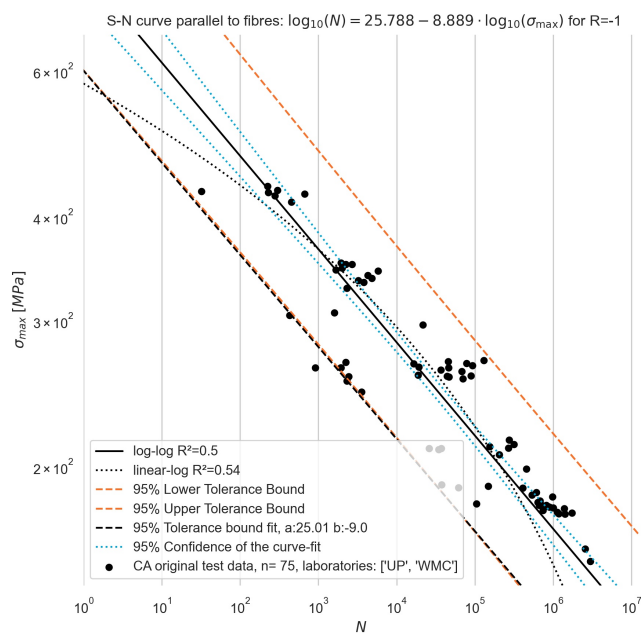


Figure C.2: S-N curve parallel to fibers for Tension-Compression (T-C)

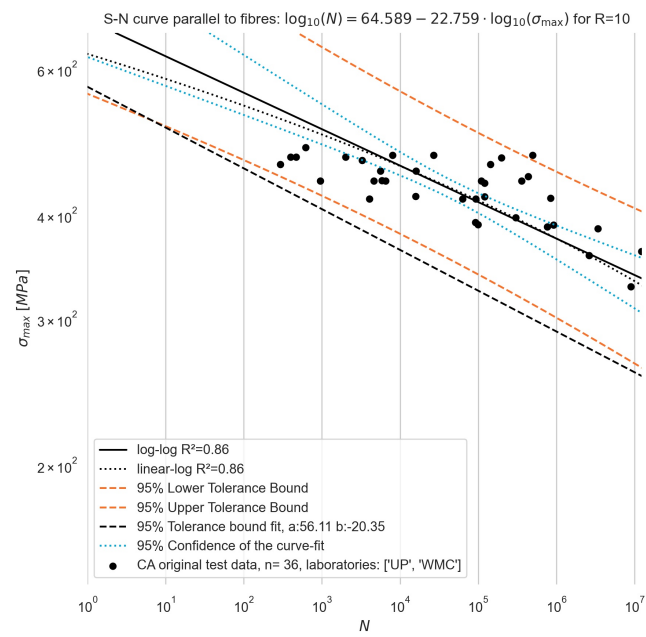


Figure C.3: S-N curve parallel to fibers for Compression-Compression (C-C)

C.2. Transverse to fibres

The S-N curves parallel to the fibres are obtained from the OptiDAT database [36], the used experimental results are given in table C.4, C.5 and C.6.

The corresponding S-N formulations is given in figure C.4, C.5 and C.6.

Table C.4: Fatigue life test results transverse to fibres for R=0.1

optiDAT nr.	Name	smax, fatigue	Laminate
1627	GEV213_R0390_0041	30.74	UD3
1802	GEV213_R0390_0044	31.10	UD3
1789	GEV213_R0390_0045	31.50	UD3
1923	GEV213_R0390_0048	40.67	UD3
1922	GEV213_R0390_0050	40.67	UD3
1924	GEV213_R0390_0051	40.67	UD3
1800	GEV213_R0390_0061	31.10	UD3
1801	GEV213_R0390_0082	31.12	UD3
1777	GEV213_R0390_0101	48.00	UD3
1776	GEV213_R0390_0102	48.00	UD3
1775	GEV213_R0390_0103	48.00	UD3
1774	GEV213_R0390_0104	48.00	UD3
1773	GEV213_R0390_0105	48.00	UD3
2679	GEV213_R0390_0237	20.00	UD3
1314	GEV213_R0390_0238	24.00	UD3
1313	GEV213_R0390_0262	38.00	UD3
1310	GEV213_R0390_0264	36.00	UD3
1312	GEV213_R0390_0265	26.99	UD3
1311	GEV213_R0390_0266	32.00	UD3
1396	GEV213_R0390_0294	30.00	UD3

Table C.5: Fatigue life test results transverse to fibres for R=-1.0

optiDAT nr.	Name	smax, fatigue	Laminate
1780	GEV213_R0390_0063	26.29	UD3
1772	GEV213_R0390_0107	17.69	UD3
1928	GEV213_R0390_0111	35.65	UD3
1927	GEV213_R0390_0112	35.65	UD3
1926	GEV213_R0390_0113	35.65	UD3
1318	GEV213_R0390_0241	26.76	UD3
1319	GEV213_R0390_0242	26.82	UD3
1308	GEV213_R0390_0244	25.00	UD3
1320	GEV213_R0390_0248	26.63	UD3
1309	GEV213_R0390_0254	17.83	UD3
1304	GEV213_R0390_0257	20.02	UD3
1322	GEV213_R0390_0259	26.95	UD3
1302	GEV213_R0390_0260	15.00	UD3
1307	GEV213_R0390_0263	34.99	UD3
1323	GEV213_R0390_0267	46.93	UD3
1306	GEV213_R0390_0269	39.88	UD3
1303	GEV213_R0390_0270	32.00	UD3
1383	GEV213_R0390_0274	26.95	UD3
1382	GEV213_R0390_0280	46.92	UD3
1379	GEV213_R0390_0290	26.95	UD3
1397	GEV213_R0390_0291	46.93	UD3
1395	GEV213_R0390_0295	46.92	UD3

1378	GEV213_R0390_0302	46.92	UD3
1391	GEV213_R0390_0305	26.95	UD3
1389	GEV213_R0390_0314	46.93	UD3
1388	GEV213_R0390_0315	46.93	UD3
1376	GEV213_R0390_0319	26.95	UD3
1373	GEV213_R0390_0324	46.91	UD3
1371	GEV213_R0390_0348	26.95	UD3
1370	GEV213_R0390_0350	26.95	UD3

Table C.6: Fatigue life test results transverse to fibres for R=10.0

optiDAT nr.	Name	smax, fatigue	Laminate
1625	GEV213_R0390_0037	113.86	UD3
1626	GEV213_R0390_0047	113.86	UD3
1317	GEV213_R0390_0239	136.83	UD3
1295	GEV213_R0390_0246	112.71	UD3
1104	GEV213_R0390_0247	144.17	UD3
1299	GEV213_R0390_0250	119.74	UD3
1297	GEV213_R0390_0252	112.45	UD3
1105	GEV213_R0390_0255	156.47	UD3
1106	GEV213_R0390_0256	157.59	UD3
1324	GEV213_R0390_0268	133.09	UD3
1384	GEV213_R0390_0271	153.35	UD3
1381	GEV213_R0390_0282	149.61	UD3
1380	GEV213_R0390_0285	153.36	UD3
1393	GEV213_R0390_0300	136.84	UD3
1392	GEV213_R0390_0301	136.84	UD3
1390	GEV213_R0390_0310	114.05	UD3
1377	GEV213_R0390_0316	153.34	UD3
1375	GEV213_R0390_0321	153.35	UD3
1374	GEV213_R0390_0323	153.35	UD3
1387	GEV213_R0390_0325	115.01	UD3
1386	GEV213_R0390_0326	136.84	UD3
1385	GEV213_R0390_0329	136.84	UD3
1372	GEV213_R0390_0330	153.36	UD3

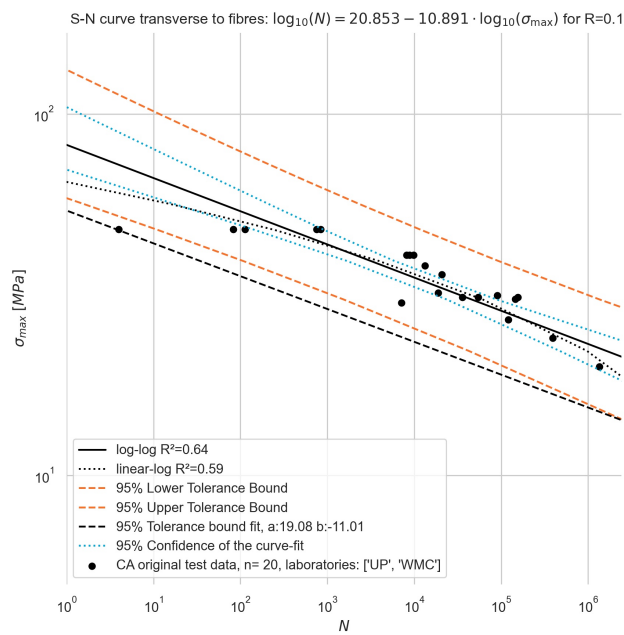


Figure C.4: S-N curve transverse to fibers for T-T

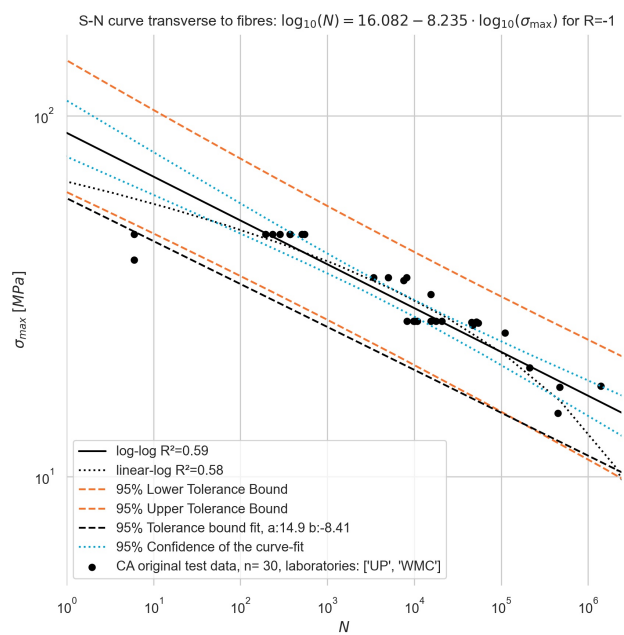


Figure C.5: S-N curve transverse to fibers for T-C

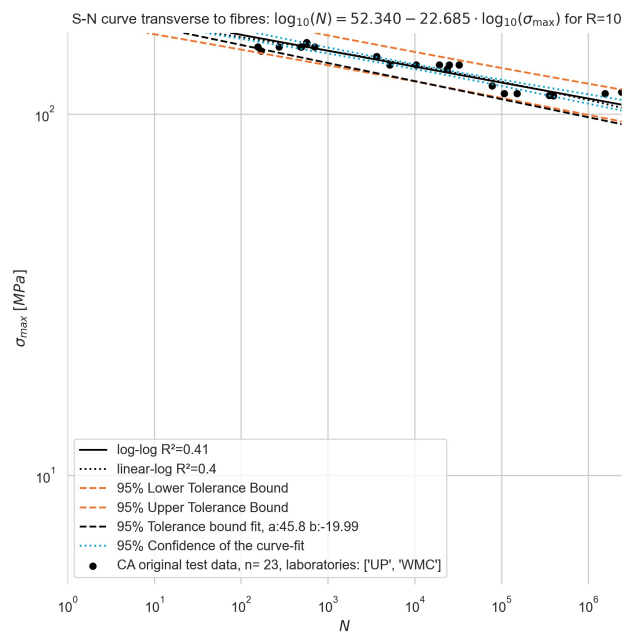


Figure C.6: S-N curve transverse to fibers for C-C

C.3. In-plane shear

The S-N curve for in-plane shear is obtained from the OptiDAT database [36], the used experimental results are given in table C.7.

The corresponding S-N formulations is given in figure C.7.

Table C.7: Fatigue life test results in-plane shear for R=0.1

optiDAT nr.	Name	smax, fatigue	Laminate
1622	GEV208_I1000_0026	24.200	MD3
1621	GEV208_I1000_0028	44.875	MD3
1620	GEV208_I1000_0029	44.880	MD3
1619	GEV208_I1000_0030	33.655	MD3
1618	GEV208_I1000_0031	25.765	MD3
1617	GEV208_I1000_0032	24.200	MD3
1616	GEV208_I1000_0033	33.660	MD3
1615	GEV208_I1000_0034	24.200	MD3
1614	GEV208_I1000_0037	25.500	MD3
1613	GEV208_I1000_0038	44.875	MD3
1612	GEV208_I1000_0040	33.655	MD3
1611	GEV208_I1000_0041	33.655	MD3
1610	GEV208_I1000_0042	24.200	MD3
1609	GEV208_I1000_0043	44.875	MD3
1608	GEV208_I1000_0044	33.655	MD3
1607	GEV208_I1000_0045	24.195	MD3
1606	GEV208_I1000_0046	44.875	MD3

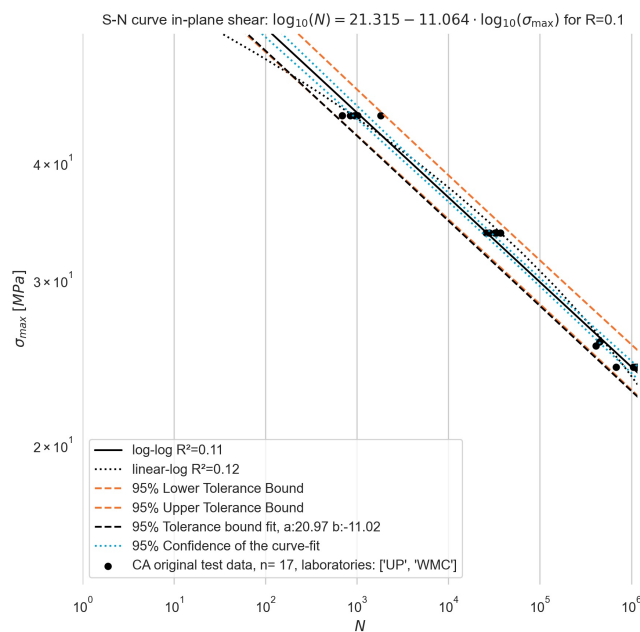
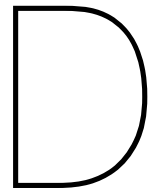


Figure C.7: S-N curve for in-plane shear R=0.1



Appendix Verification of primary stiffness degradation

Title:	Verification of modulus degradation
Version number:	1.0
Author:	Mathieu Koetsier
Aproofed by:	
Project name:	Virtual fatigue verification of Glass Fibre-Reinforced polymer components for civil engineering applications
Description of Verification subject:	Verification of unidirectional stiffness degradation relations of UD specimens.
Start date:	4-6-2021
This document was updated on:	4-6-2021

Version	Date	Summary of Revision
1.0	4-6-2021	Verification of UD modulus degradation simulation

1. Input data

The stiffness relations described in section 3.2.4 are implemented in the model. Therefore, these degradation curves should be reproducible with the model when performing the same type of virtual experiment.

1.1. Material properties

Table 1 UD material properties (Optidat plate GEV206)

E1	E2	G12	M12	M21
[MPa]	[MPa]	[MPa]	[-]	[-]
37950	13880	4000	0.36	0.13

2. Output data

2.1. Shear stiffness degradation

2.1.1. Introduction

In this section, the shear stiffness degradation simulation is validated against experimental results and the theoretical input in the model. The simulated experiments are obtained from the Optidat database [1], and the stiffness measurements are taken from [2].

The layout of the coupon specimen is given in Table 2.

Table 2 Layup configuration MD3 laminate

NO	T [mm]	MNO	BETA[°]	TITL
301	0.940000	GEV206	45	Original layup
301	0.940000	GEV206	-45	Original layup
301	0.940000	GEV206	-45	Original layup
301	0.940000	GEV206	45	Original layup

2.1.2. Results and discussion

In Figure 1, the experimental, simulation and analytical results are plotted. This verification aims to verify the model's advanced shear damage simulation procedure and compare this with the UD shear damage relation (orange line).

From the figure, it can be concluded that the shear modulus degradation is comparable with experimental results and the input relation. Therefore, the damage accumulation simulation in the model for the shear modulus works correctly.

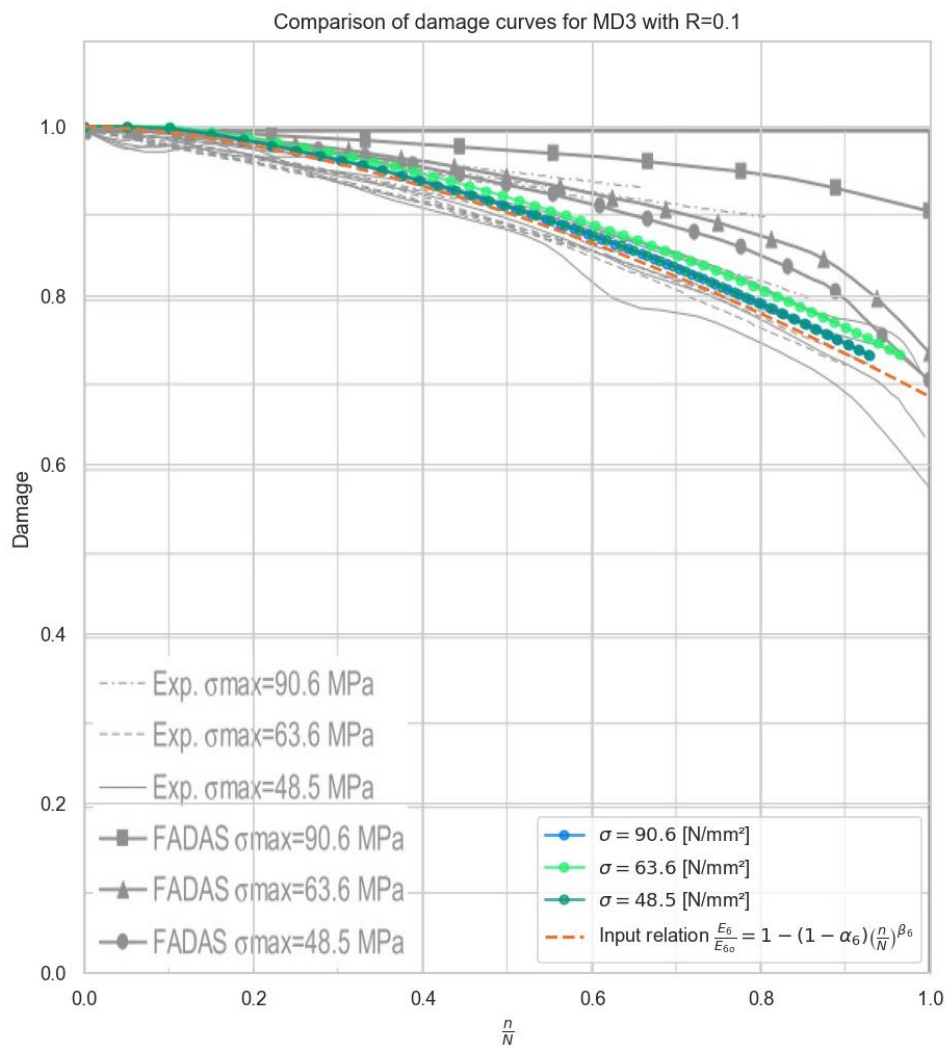


Figure 1 Test and simulation results underlay from [2]

2.2. Transverse stiffness degradation

2.2.1. Introduction

In this section, the transverse stiffness degradation is verified against the input relation. The model is used to virtually test in 90-degree ply orientation. The UD material properties are given in Table 1, and the layup is given in Table 3

Table 3 Layup configuration UD2 laminate

NO	T [mm]	MNO	BETA[°]	TITL
301	0.16425	GEV206	90	Original layup
301	0.16425	GEV206	90	Original layup
301	0.16425	GEV206	90	Original layup
301	0.16425	GEV206	90	Original layup

2.2.2. Results and discussion

Two input relations are verified in this verification, first for tension-tension loading and second for compression-compression loading. These verifications aim to verify the damage summation procedure for the modulus degradation.

In Figure 2, the results of the simulation and the input relation are given for T-T loading. As can be seen, is the simulation by the model compared with the input relation, and a good match is found. In Figure 3, the results are shown for C-C loading. Also, here, a good match is found. It can be concluded that both relations are simulated well by the model and that a relative course stepsize results in a limited error at failure.

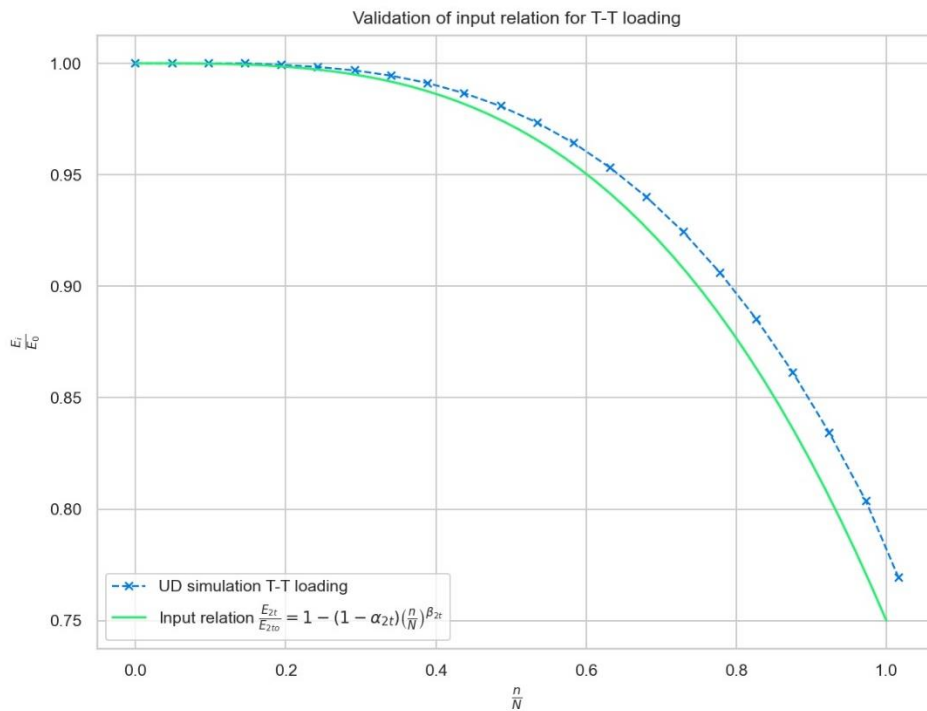


Figure 2 Input relation vs simulation for T-T loading

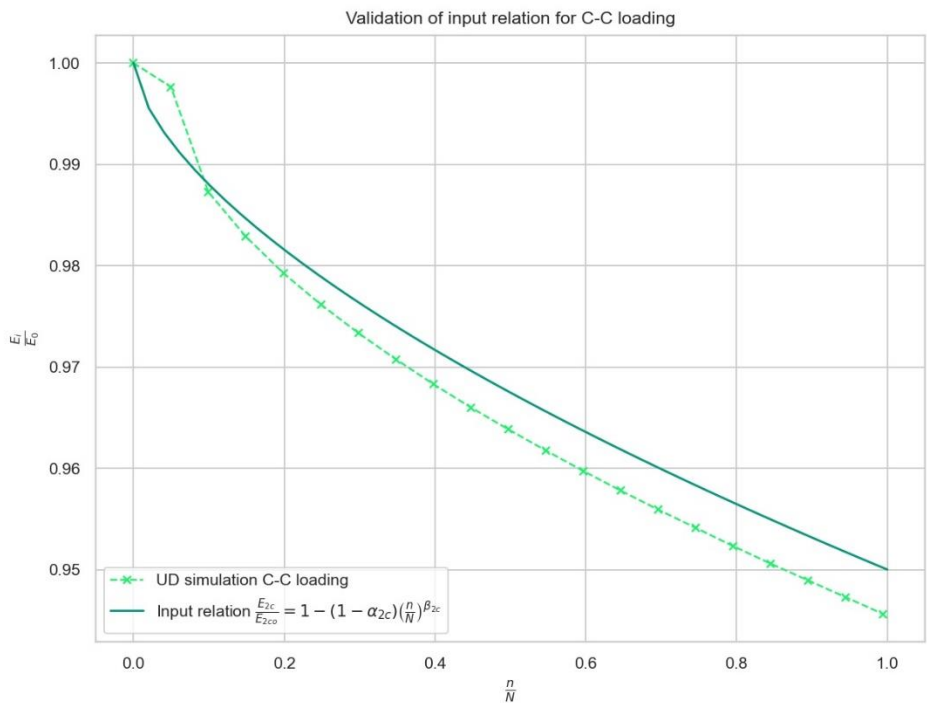


Figure 3 Input relation vs simulation for C-C loading

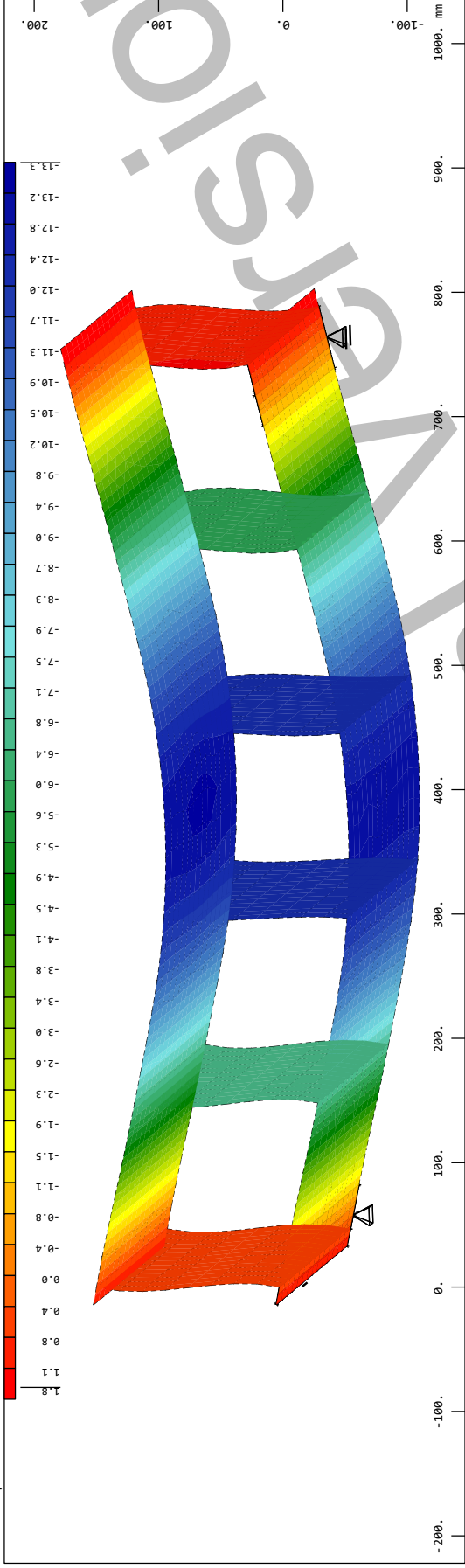
Bibliography

- [1] R. P. L. Nijssen, "OptiDAT – fatigue of wind turbine materials database," 2007. [Online]. Available: www.kc-wmc.nl.
- [2] E. N. Eliopoulos and T. P. Philippidis, "A progressive damage simulation algorithm for GFRP composites under cyclic loading. Part II: FE implementation and model validation," *Compos. Sci. Technol.*, vol. 71, no. 5, pp. 750–757, Mar. 2011, doi: 10.1016/j.compscitech.2011.01.025.

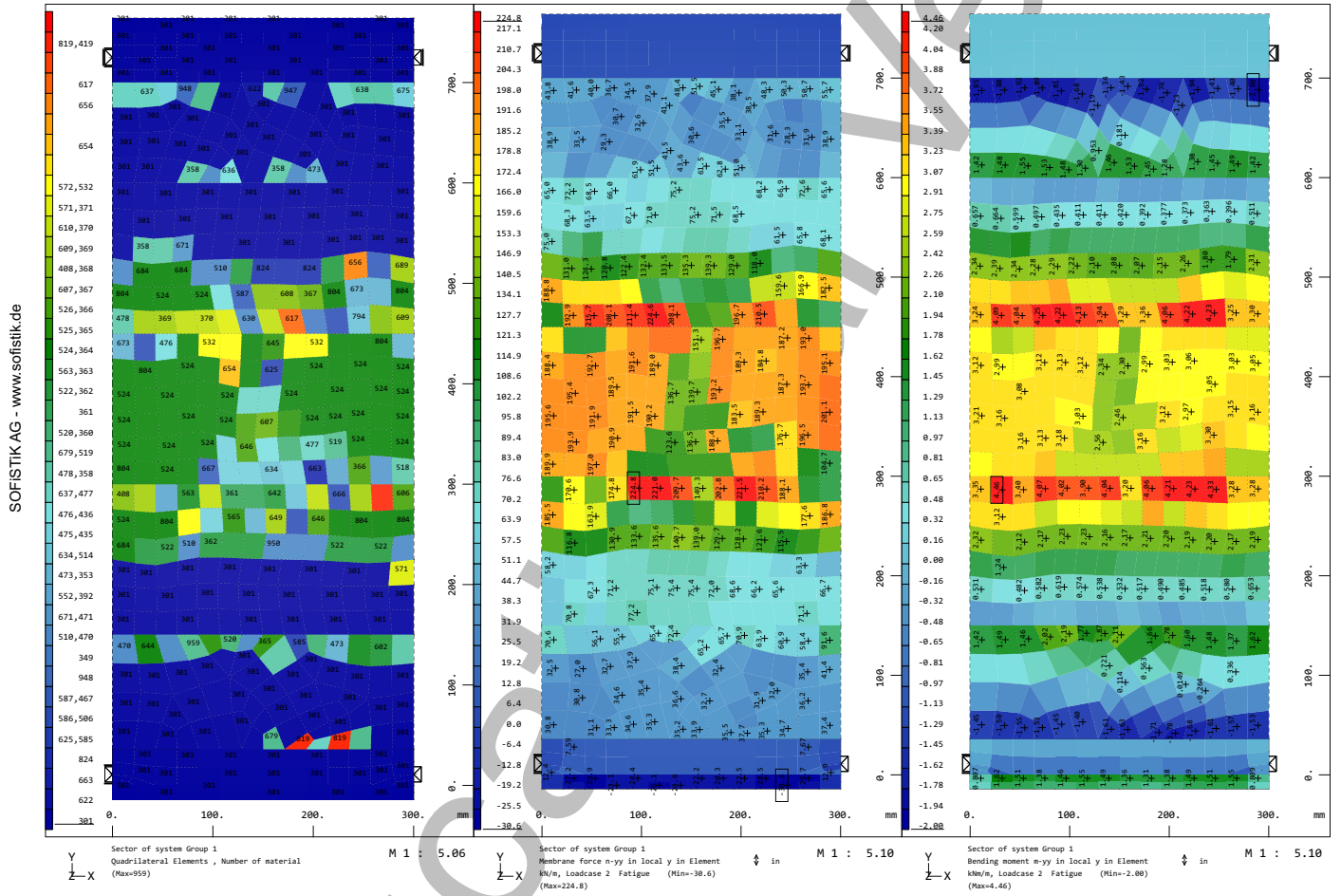
E

Appendix degradation report

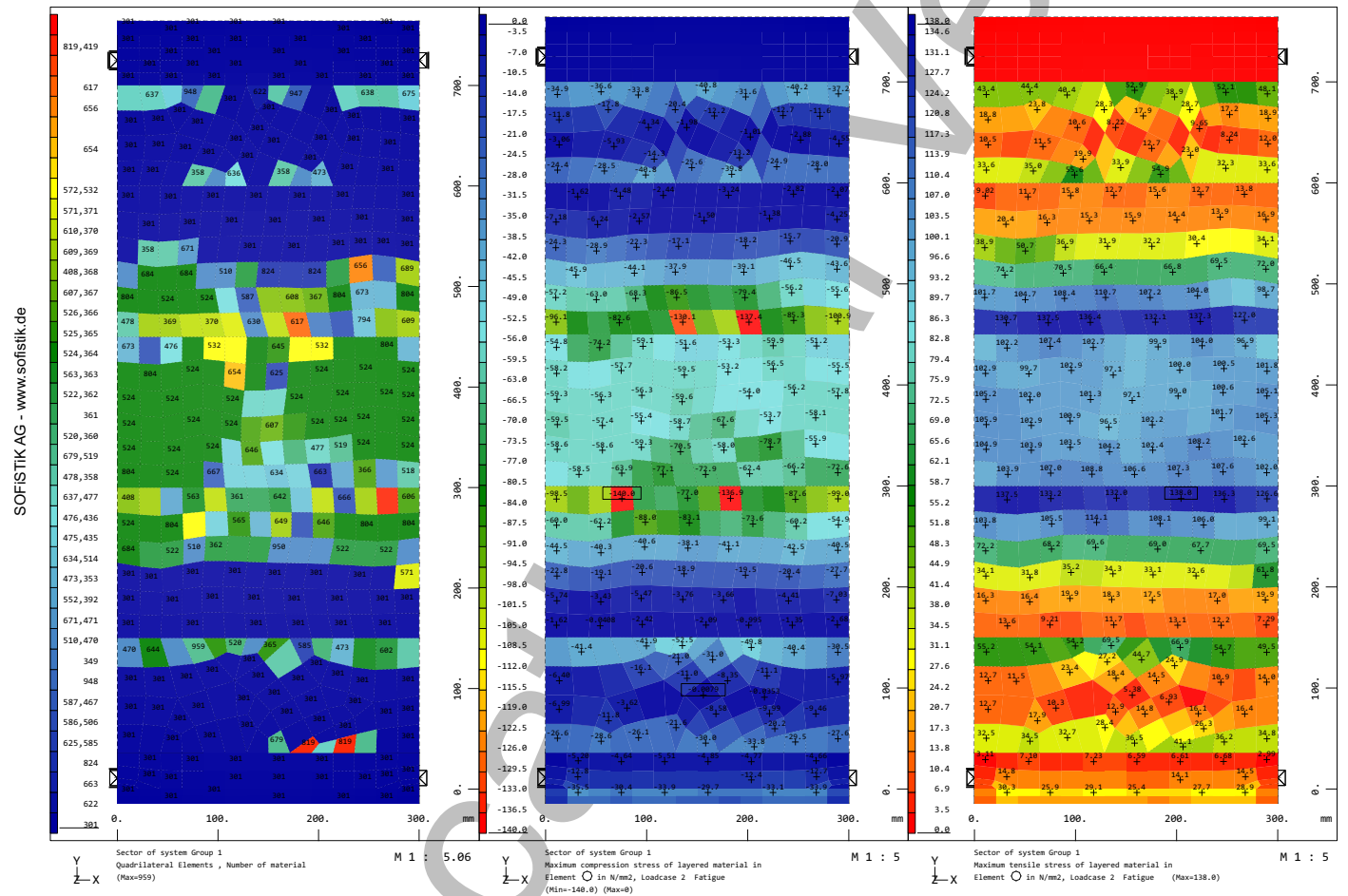
Sandwich_panel
 Interactive Graphics



Sandwich_panel
 Interactive Graphics

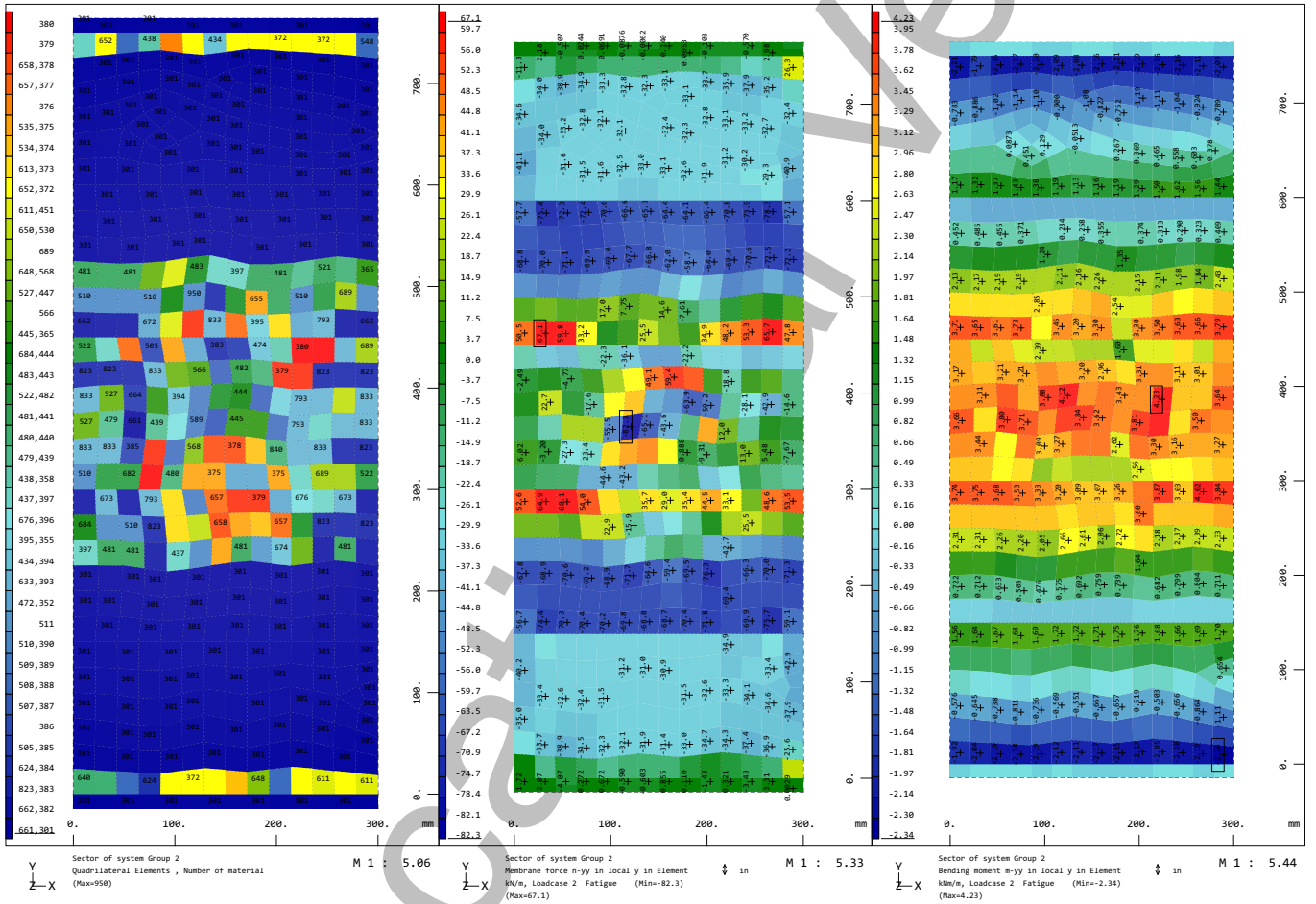


Sandwich_panel
 Interactive Graphics

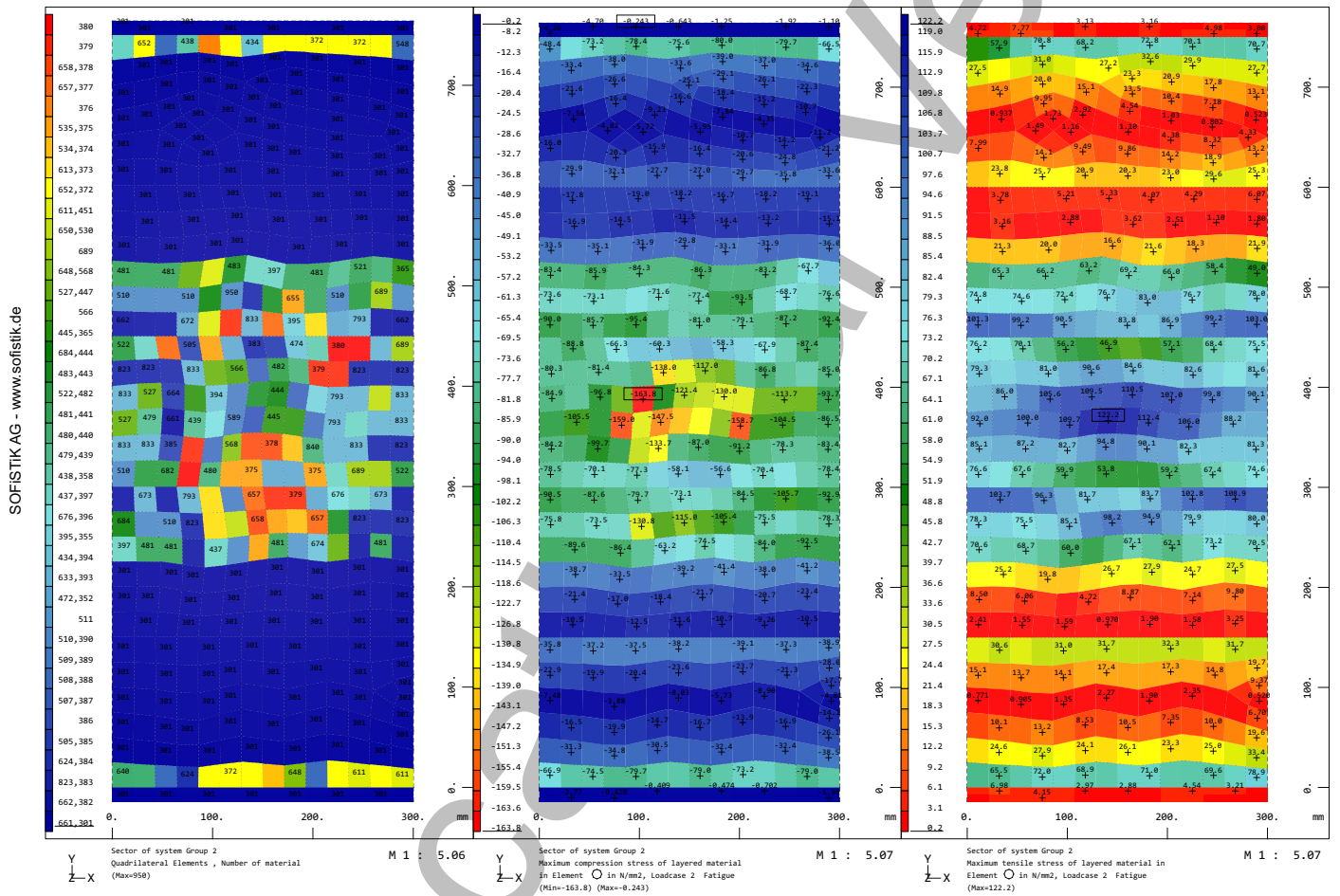


Sandwich_panel
 Interactive Graphics

SOFiSTiK AG - www.sofistik.de

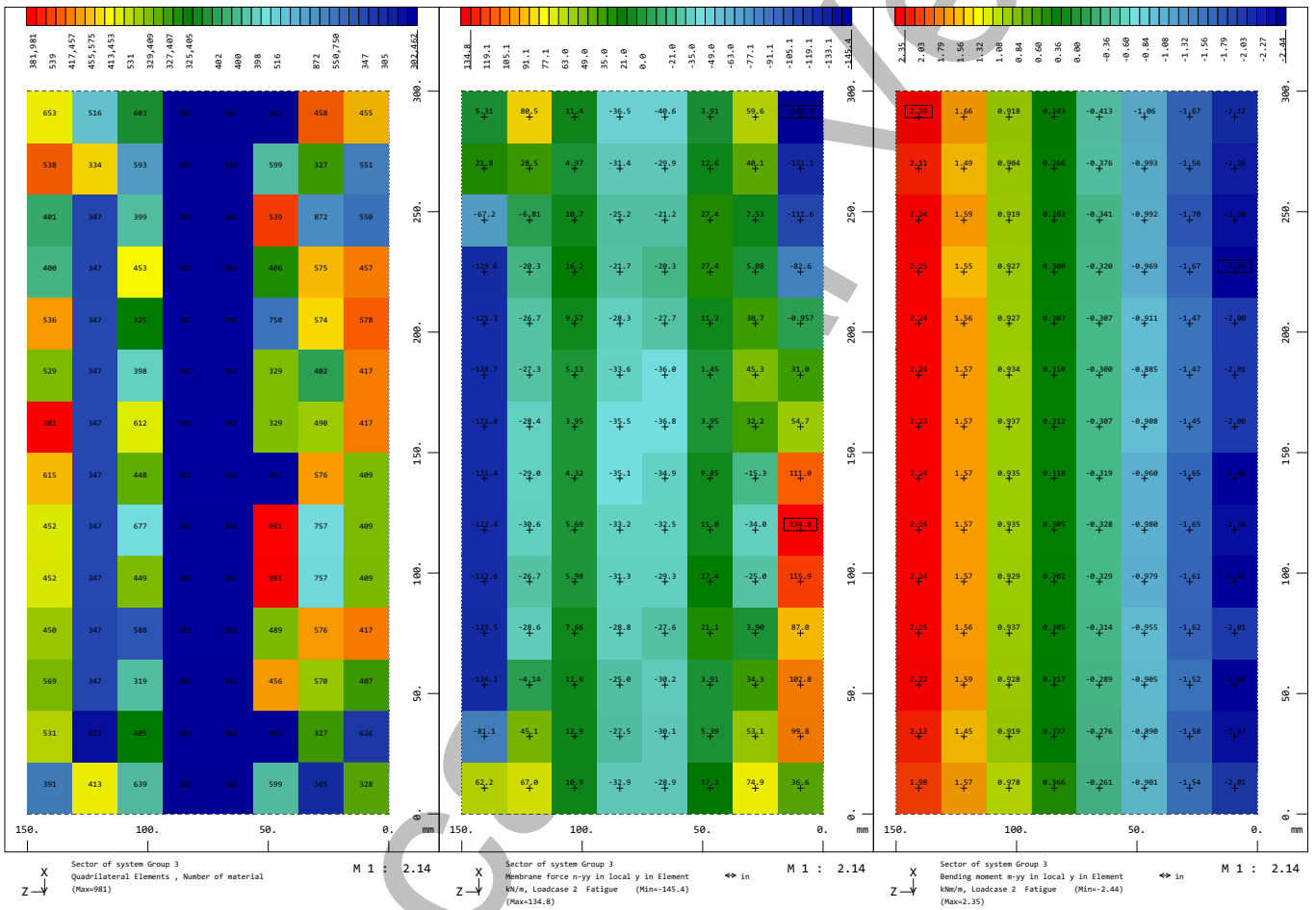


Sandwich_panel
 Interactive Graphics



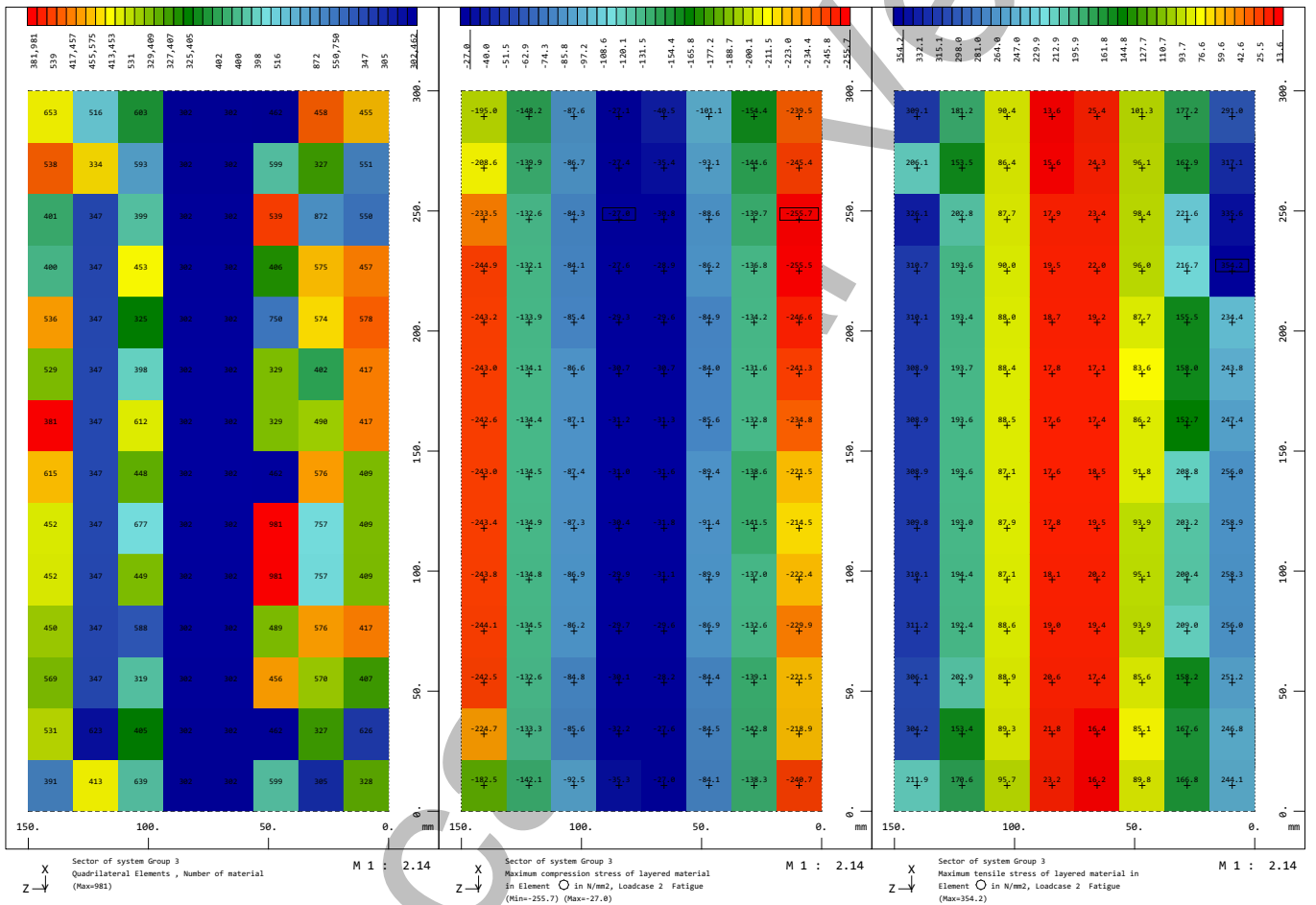
Sandwich_panel
 Interactive Graphics

SOFiSTiK AG - www.sofistik.de



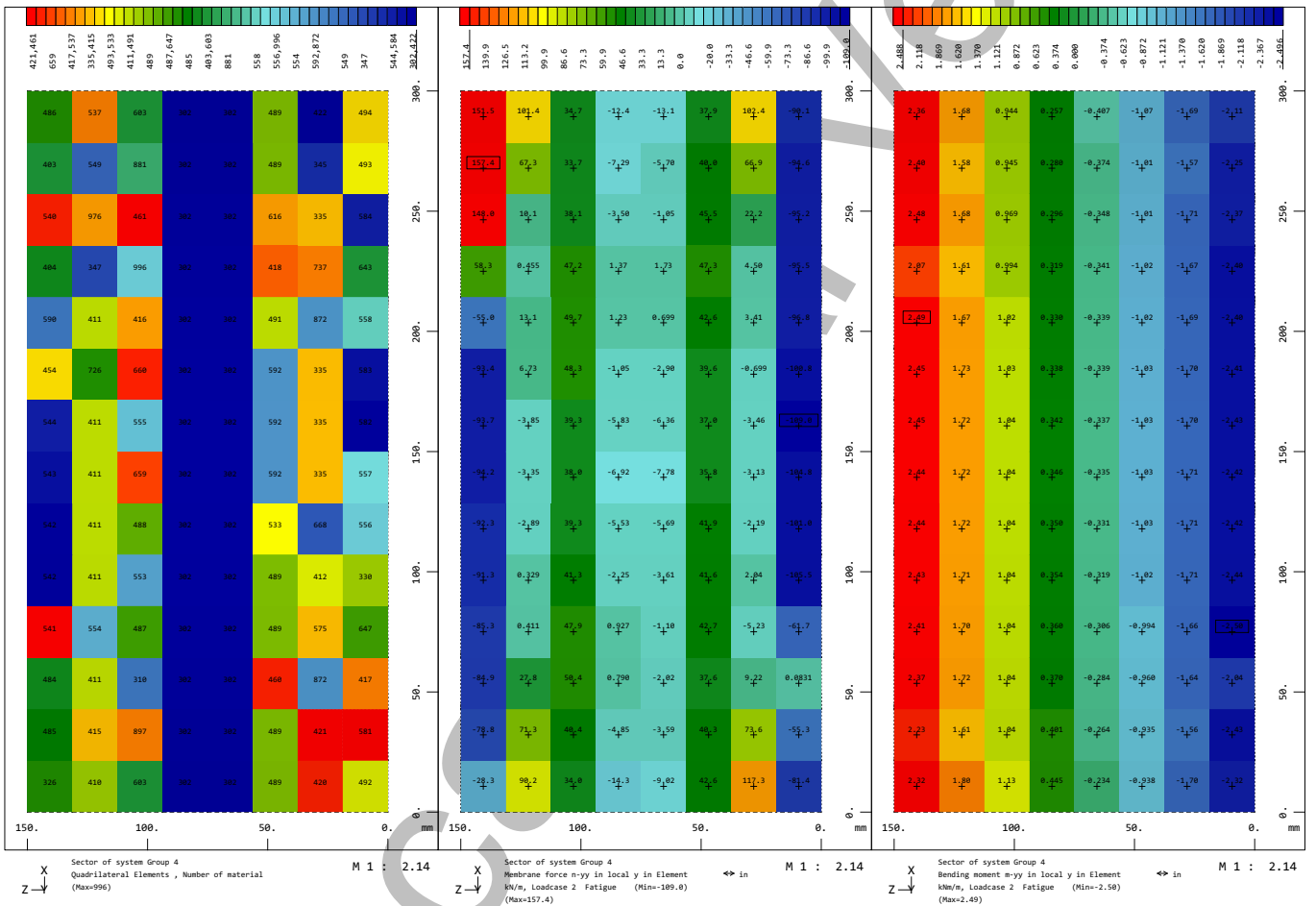
Sandwich_panel
 Interactive Graphics

SOFiSTiK AG - www.sofistik.de



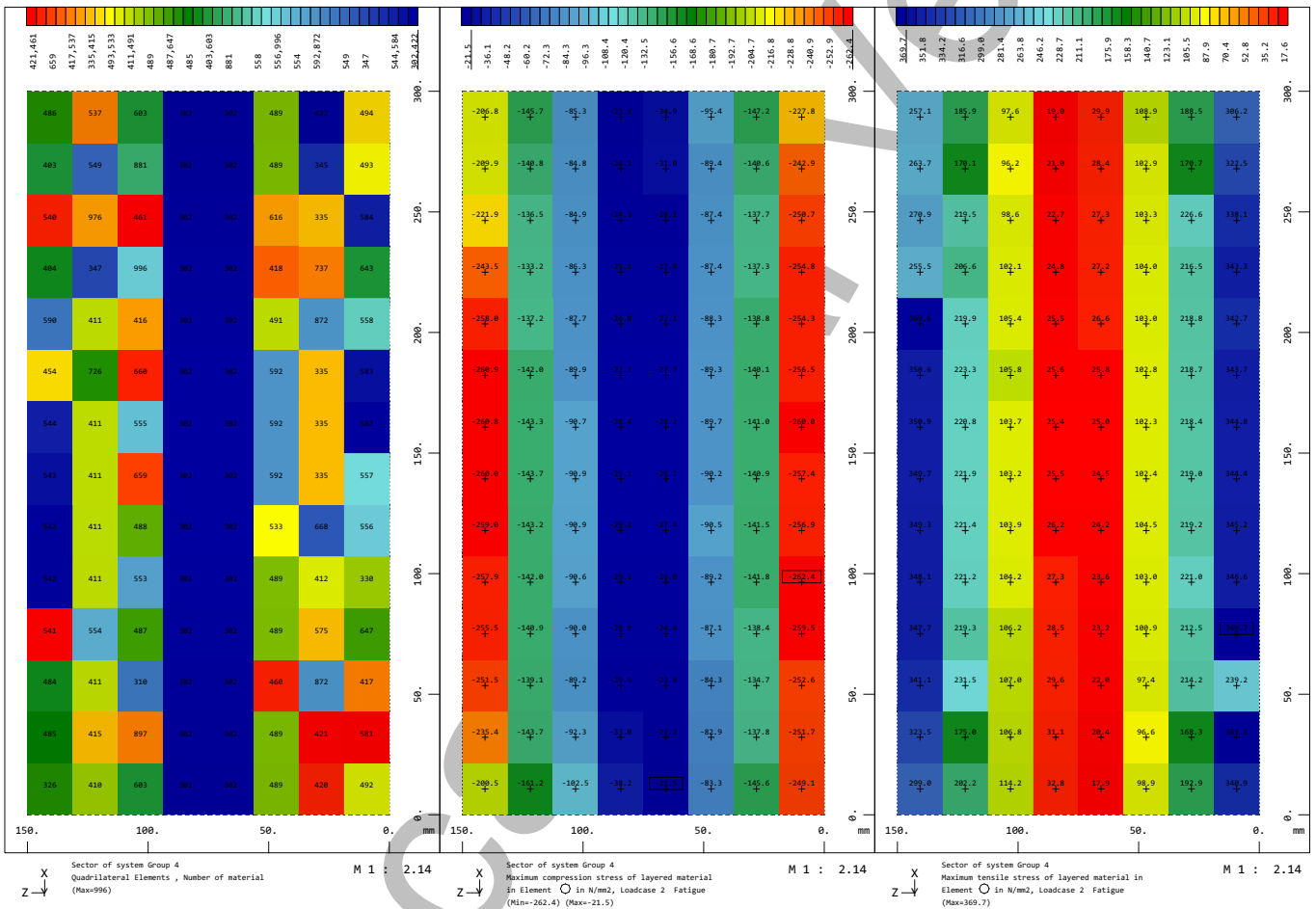
Sandwich_panel
 Interactive Graphics

SOFiSTiK AG - www.sofistik.de



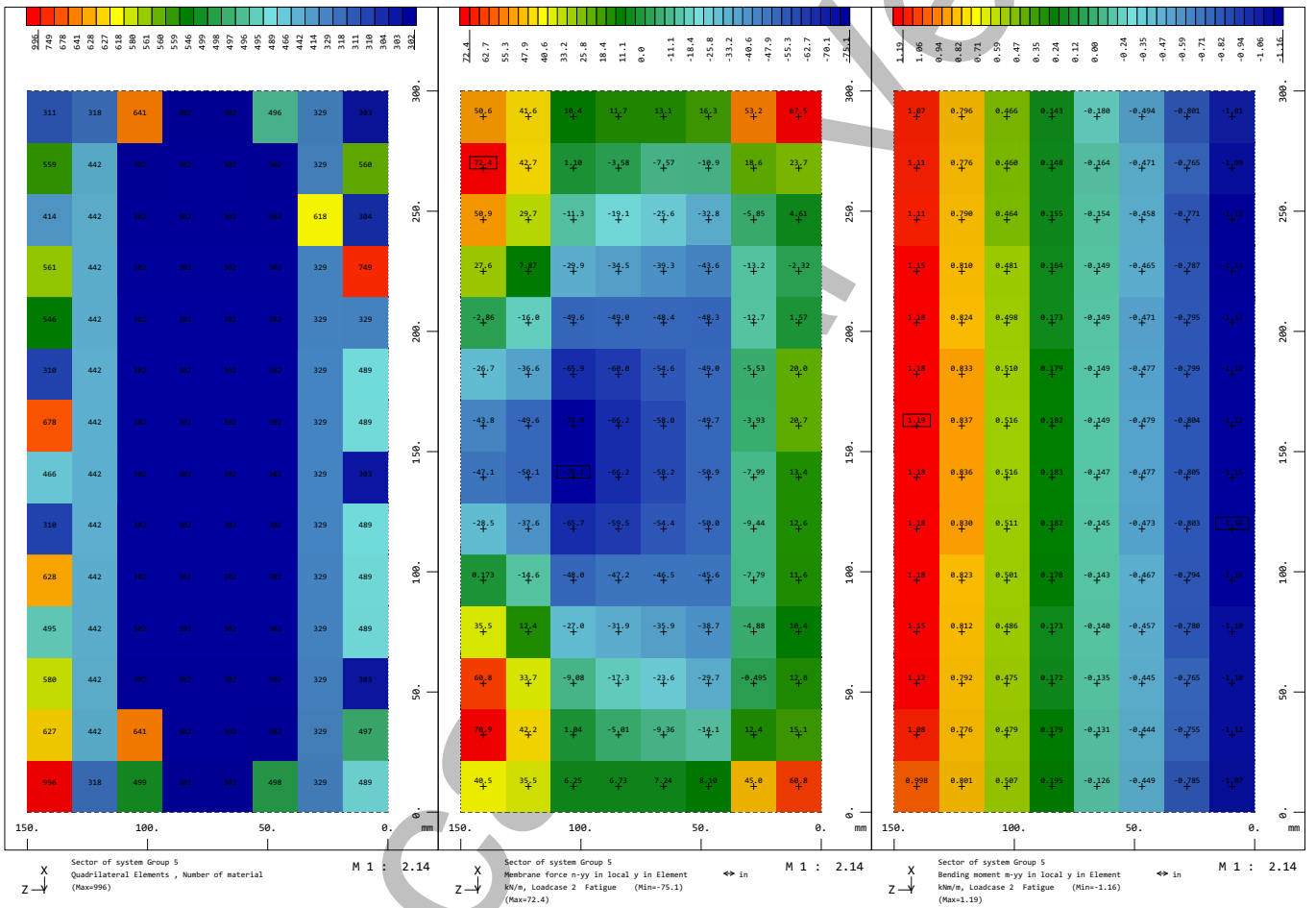
Sandwich_panel
 Interactive Graphics

SOFiSTiK AG - www.sofistik.de



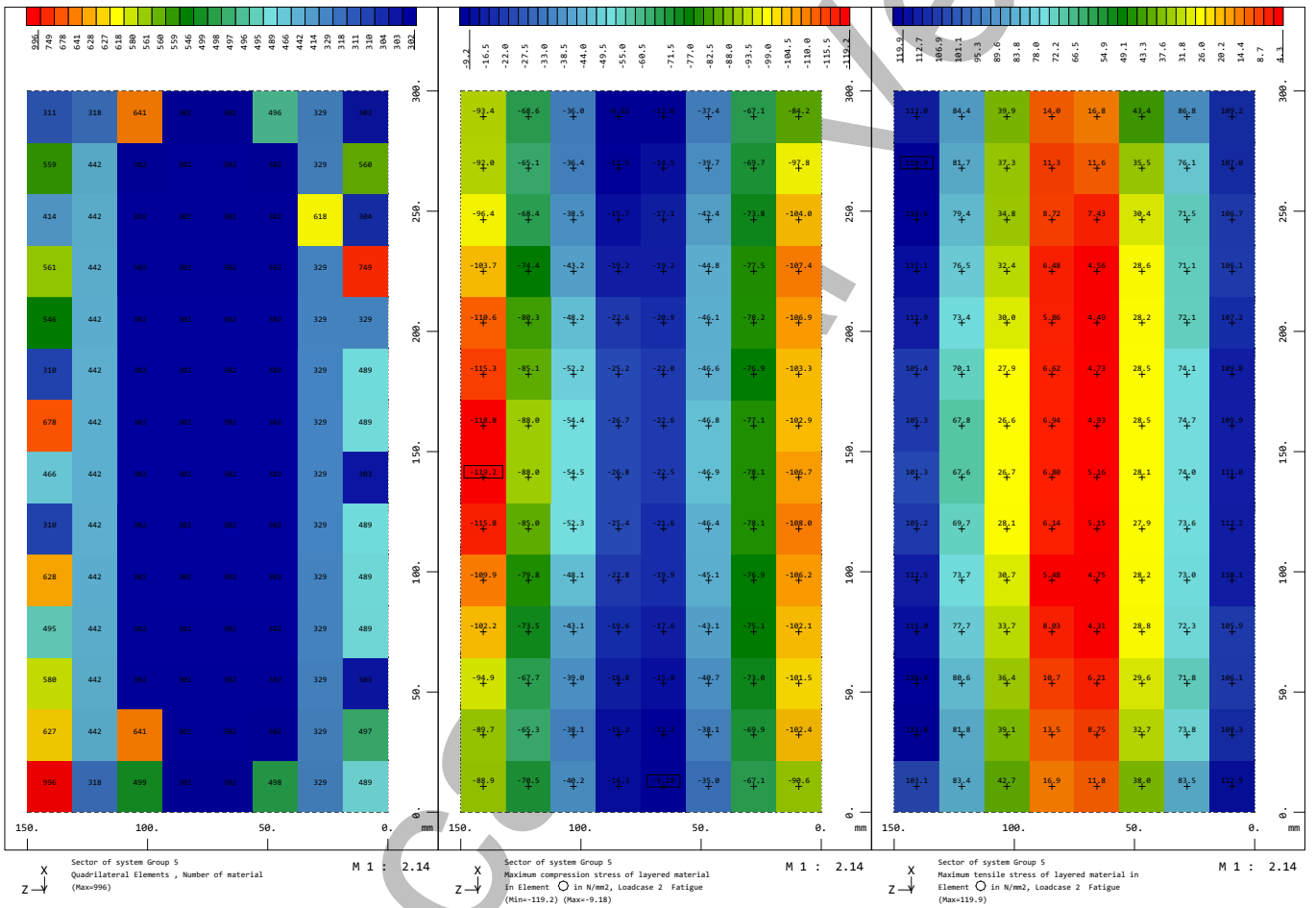
Sandwich_panel
 Interactive Graphics

SOFiSTiK AG - www.sofistik.de



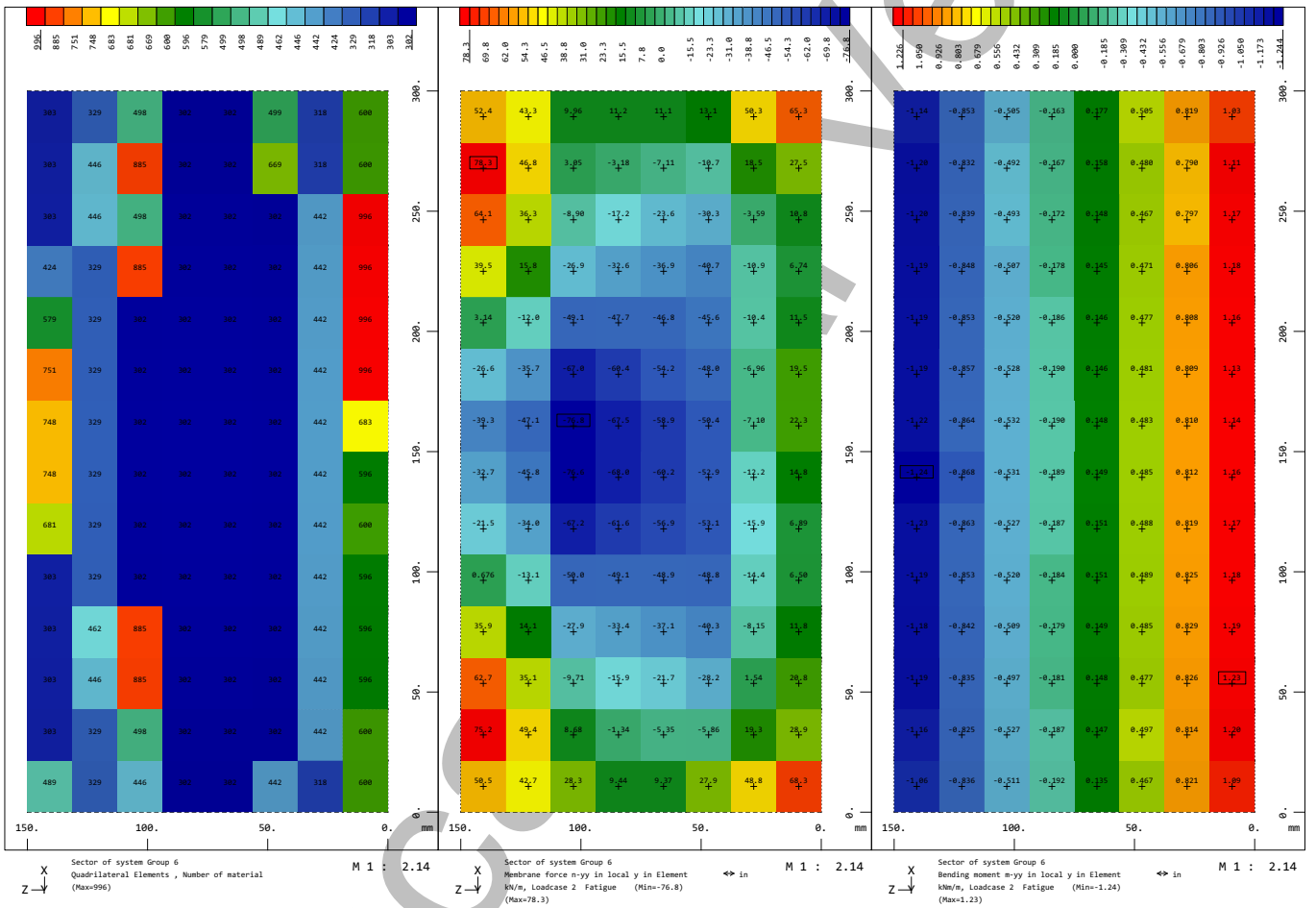
Sandwich_panel
 Interactive Graphics

SOFiSTiK AG - www.sofistik.de



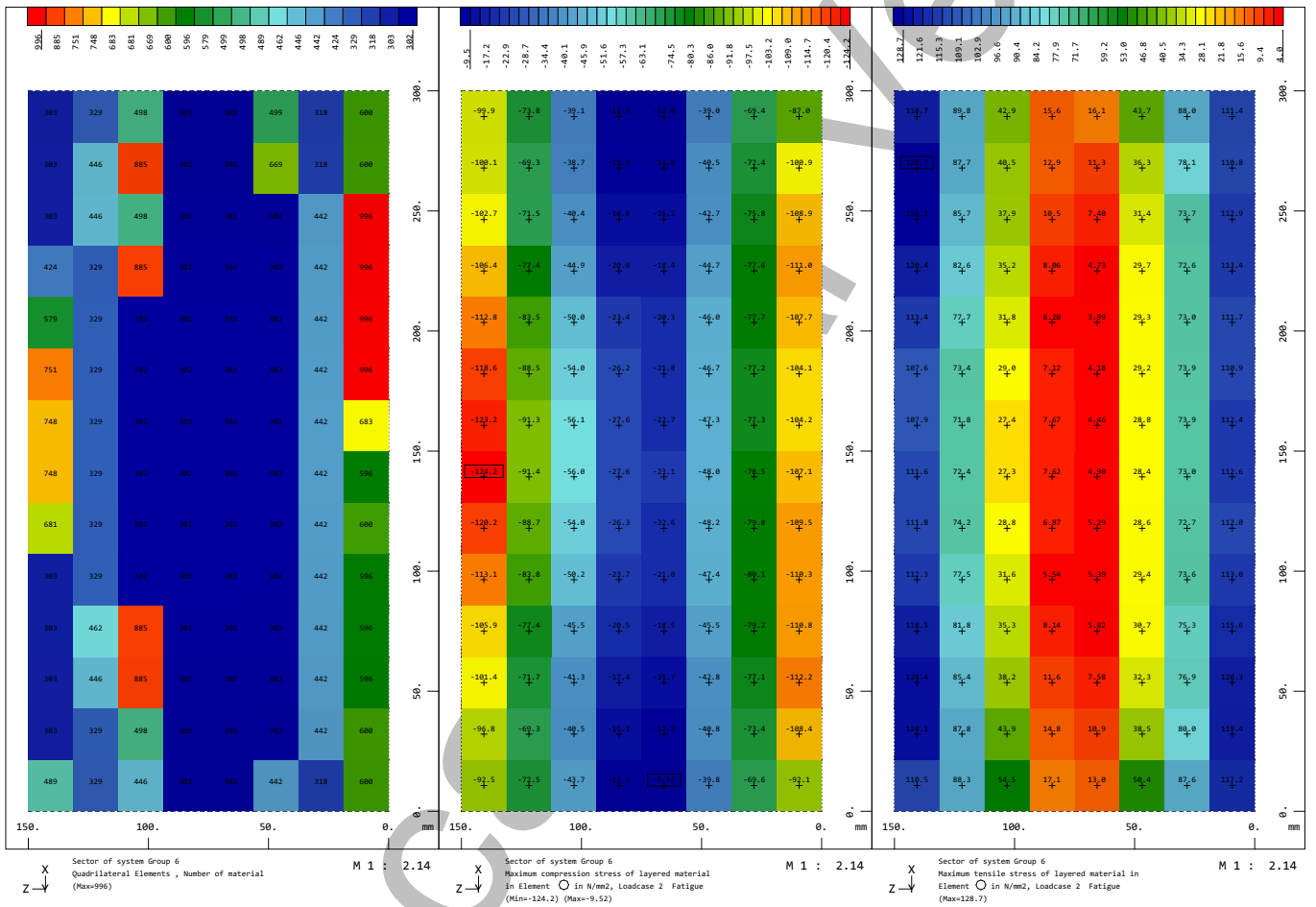
Sandwich_panel
 Interactive Graphics

SOFiSTiK AG - www.sofistik.de



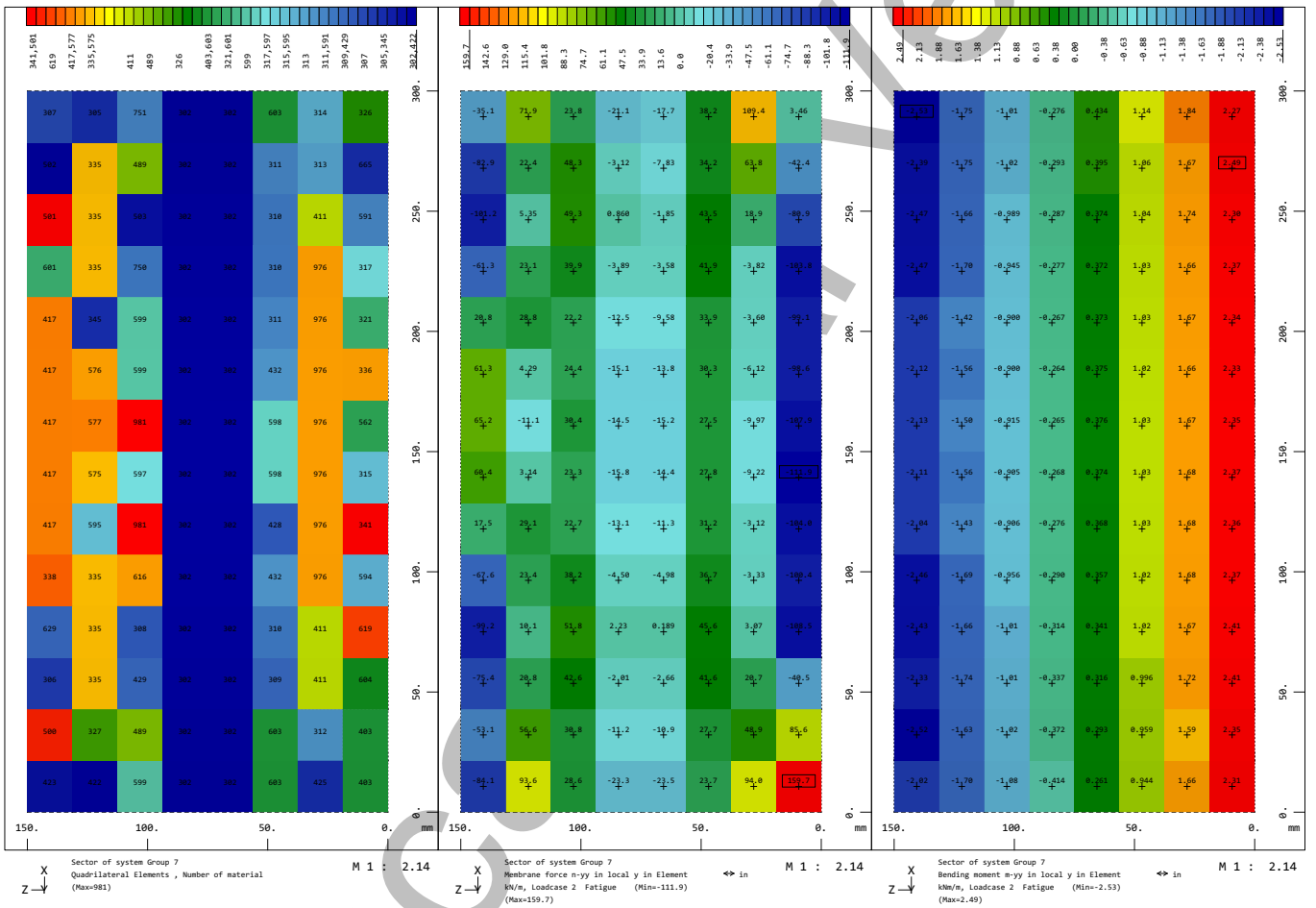
Sandwich_panel
 Interactive Graphics

SOFiSTiK AG - www.sofistik.de



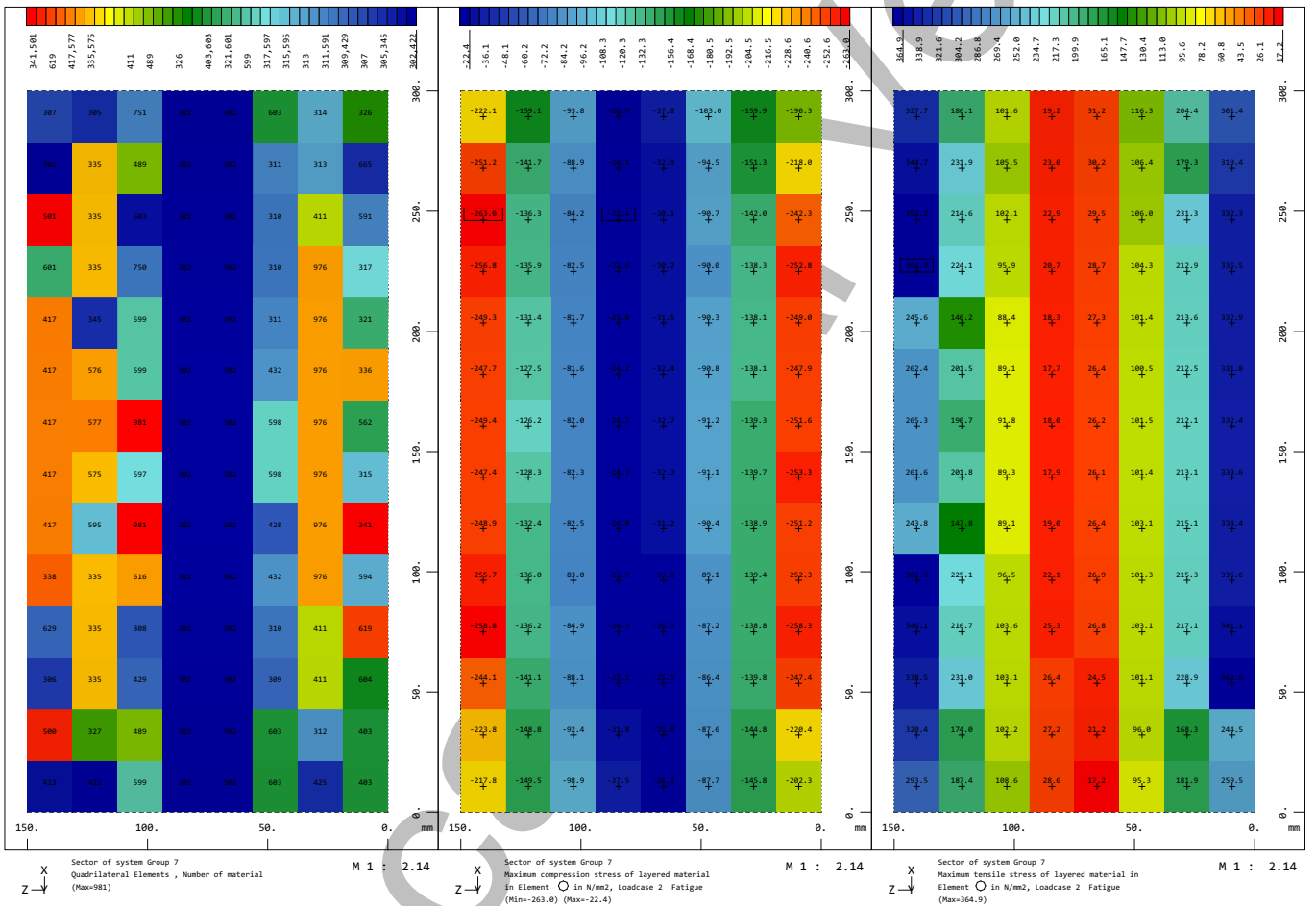
Sandwich_panel
 Interactive Graphics

SOFiSTiK AG - www.sofistik.de



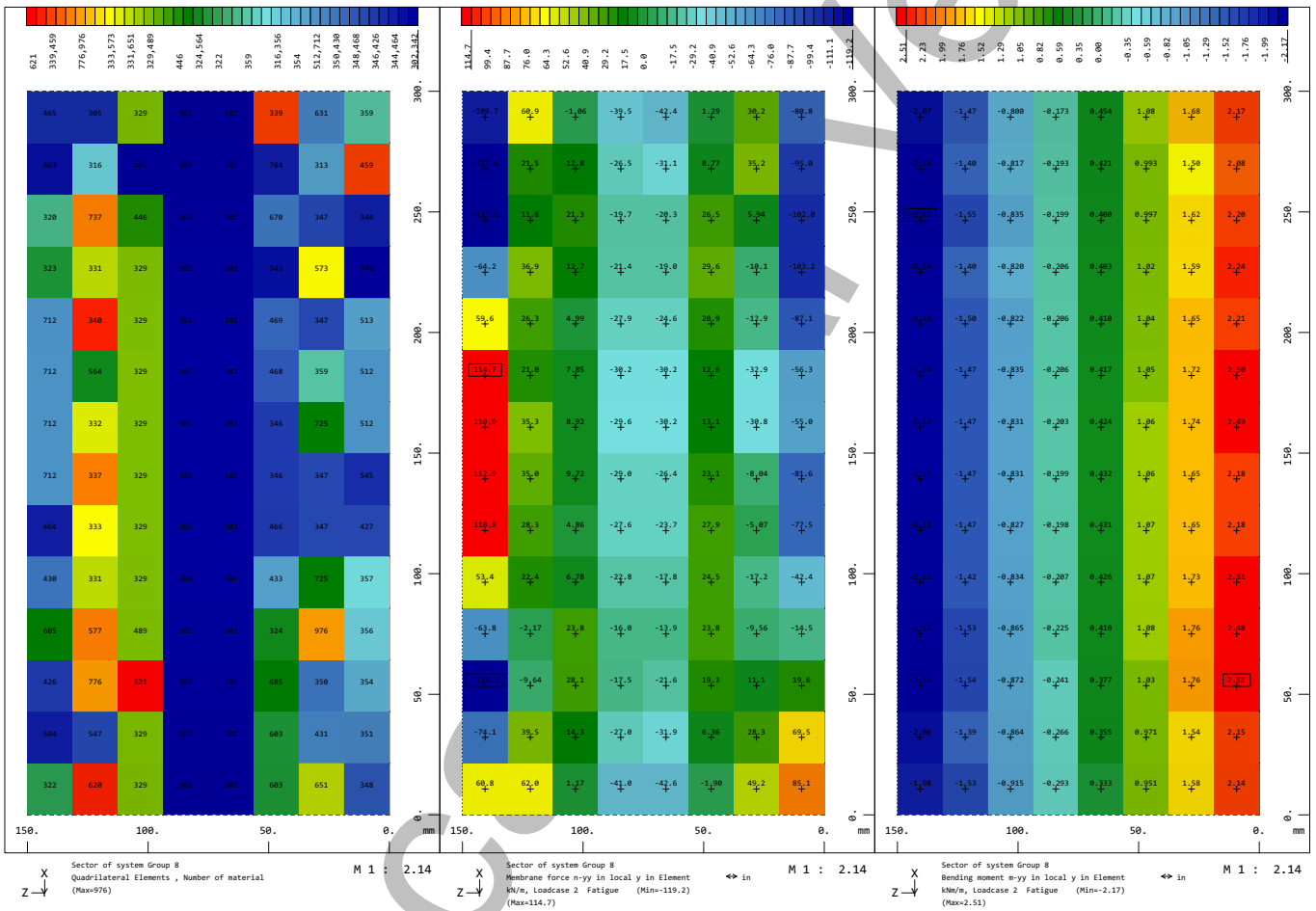
Sandwich_panel
 Interactive Graphics

SOFiSTiK AG - www.sofistik.de



Sandwich_panel
 Interactive Graphics

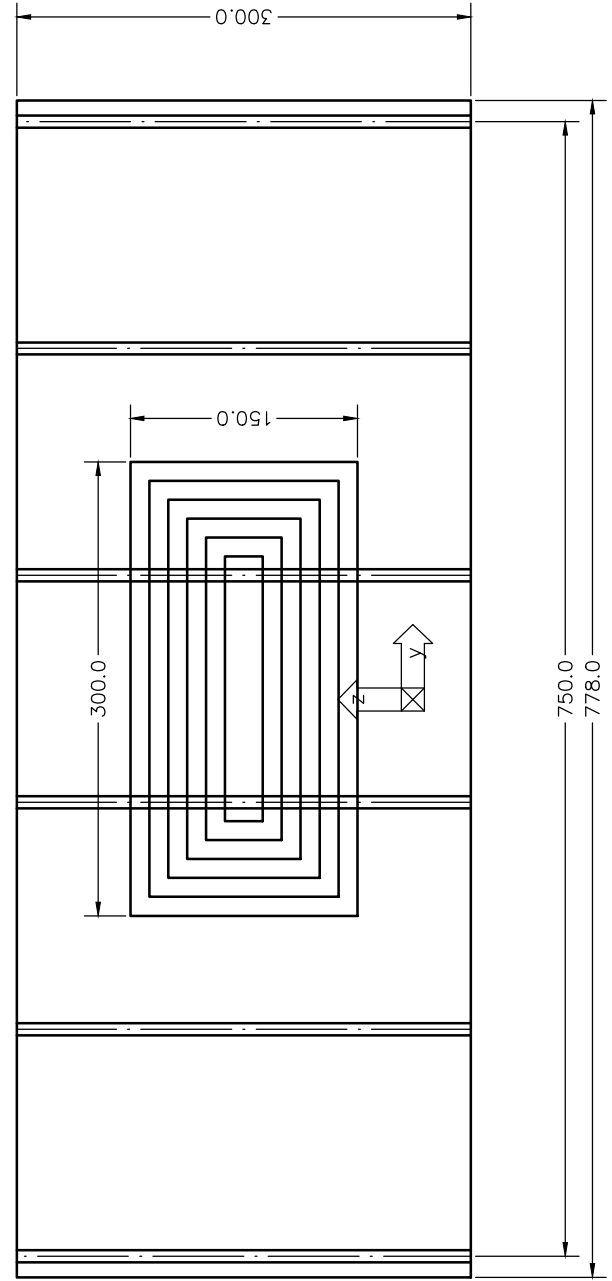
SOFiSTiK AG - www.sofistik.de



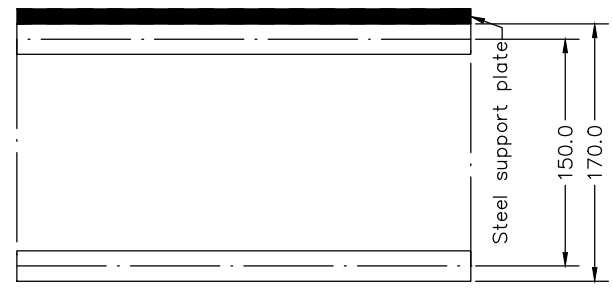
F

Appendix design webcore panel specimen

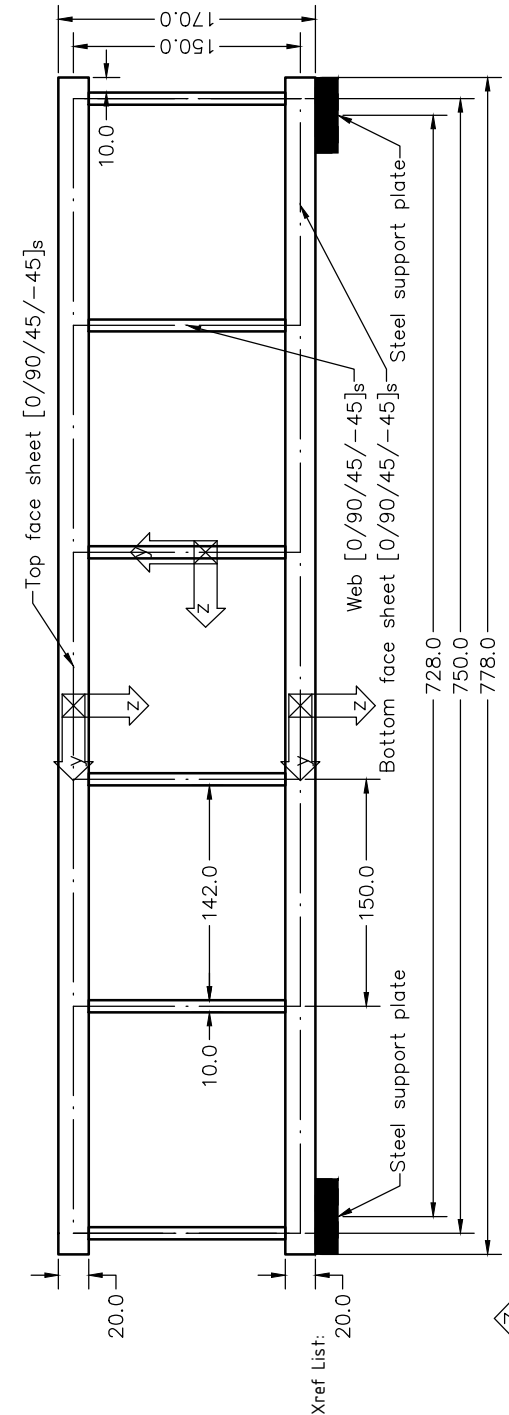
- Fiber direction in local x-direction
- Facesheet cut 10mm next to webs to prevent weakening of the web-flange junction.



Top view



Front view



Side view (span direction)

MAATVOERING IN m TENZIJ ANDERS AANGEGEVEN.
 HOOGTEMATEN IN m T.O.V. N.A.P.
 MATERIAAL MATEN IN mm

Bijbehorende Tekeningen:		Status:	Soort: Ontwerptekening	Afdruk datum: 27-5-2021 monochrome.ctb
Opdrachtgever: TU Delft		Schaal 1:5		
Project: Virtual in-plane fatigue verification		Formaat A3		
Onderwerp: GFRP Sandwich webcore panel for fatigue reduction model validation		Blad Blad 001 van 001		
Getekend door: Mathieu Koetsier 27-5-2021		Datum 27-5-2021		
Gecontroleerd door: -		Tekeningnr. 001		
Geautoriseerd door: -				



Bibliography

- [1] T. Adam, R. F. Dickson, C. J. Jones, H. Reiter, and B. Harris. A power law fatigue damage model for fibre-reinforced plastic laminates. *Proceedings of the Institution of Mechanical Engineers, Part C: Journal of Mechanical Engineering Science*, 200(3):155–166, 1986. ISSN 20412983. doi: 10.1243/PIME_PROC_1986_200_111_02.
- [2] Luigi Ascione, Wouter De Corte, Patrice Godonou, Jean Knippers, Eric Moussiaux, Toby Mottram, Matthias Oppe, Nuno Silvestre, Peter Thorning, Liesbeth Tromp, and S Maria Paganica Church. Prospect for New Guidance in the Design of FRP Structures, 2017.
- [3] ASTM. ASTM Manual on Fitting Straight Lines. Technical Report 313, AMERICAN SOCIETY FOR TESTING AND MATERIALS, Philadelphia, 1962. URL www.astm.org.
- [4] ASTM. Standard Practice for Statistical Analysis of Linear or Linearized Stress-Life (S-N) and Strain-Life (ϵ -N) Fatigue Data. *Annual Book of ASTM Standards*, i(E739 – 10):1–7, 2015. doi: 10.1520/E0739-10R15.2. URL www.astm.org.
- [5] A De Boer, J De Boon, E L Klamer, J A Laak, Rogier P.L. Nijssen, J Peeters, C A Van Der Steen, W D Schutte, E Tromp, H C Van Uden, E Vega, R Verleg, van C J A Ijselmuiden, M A R H Al-Saadi, J Van Der Burg, W Claassen, and van D R V Delft. CUR RECOMMENDATION 96:2017 Fibre-reinforced polymers in buildings and civil engineering structures. Technical Report July, CUR, 2017.
- [6] I. P. Bond. Fatigue life prediction for GRP subjected to variable amplitude loading. *Composites Part A: Applied Science and Manufacturing*, 30(8):961–970, aug 1999. ISSN 1359835X. doi: 10.1016/S1359-835X(99)00011-1.
- [7] J.B. de Jonge. The analysis of load time histories by means of counting methods. Technical report, National Aerospace Laboratory NLR, aug 1982. URL <https://repository.tudelft.nl/islandora/object/uuid%3A24923f1e-6cd9-41f2-9ef0-d78b53357c67>.
- [8] Joris Degrieck and Wim Van Paepegem. Fatigue damage modeling of fibre-reinforced composite materials: Review. *American Society of Mechanical Engineers*, 54(no 4 July 2001), 2001. doi: 10.1115/1.1381395. URL http://asmedigitalcollection.asme.org/appliedmechanicsreviews/article-pdf/54/4/279/5438146/279_1.pdf.
- [9] DNV GL AS. DNV-OS-C501 Composite Components. (November):250, 2013. URL <http://exchange.dnv.com/publishing/codes/docs/2013-11/OS-C501.pdf>.
- [10] Elias N. Eliopoulos and Theodore P. Philippidis. A progressive damage simulation algorithm for GFRP composites under cyclic loading. Part II: FE implementation and model validation. *Composites Science and Technology*, 71(5):750–757, mar 2011. ISSN 02663538. doi: 10.1016/j.compscitech.2011.01.025.
- [11] Elias N. Eliopoulos and Theodore P. Philippidis. A progressive damage simulation algorithm for GFRP composites under cyclic loading. Part I: Material constitutive model. *Composites Science and Technology*, 71(5):742–749, mar 2011. ISSN 02663538. doi: 10.1016/j.compscitech.2011.01.023.
- [12] Anthony G. Evans, Ming Y. He, and John W. Hutchinson. Interface Debonding and Fiber Cracking in Brittle Matrix Composites. *Journal of the American Ceramic Society*, 72(12):2300–2303, dec 1989. ISSN 0002-7820. doi: 10.1111/j.1151-2916.1989.tb06079.x. URL <http://doi.wiley.com/10.1111/j.1151-2916.1989.tb06079.x>.

- [13] Roselita Fragoudakis and Anil Saigal. Predicting the Fatigue Life in Steel and Glass Fiber Reinforced Plastics Using Damage Models. *Materials Sciences and Applications*, 2:596–604, 2011. doi: 10.4236/msa.2011.26080. URL <http://www.scirp.org/journal/msa>.
- [14] E. K. Gamstedt and B. A. Sjögren. Micromechanisms in tension-compression fatigue of composite laminates containing transverse plies. *Composites Science and Technology*, 59(2):167–178, feb 1999. ISSN 02663538. doi: 10.1016/S0266-3538(98)00061-X.
- [15] E. K. Gamstedt and B. A. Sjögren. An experimental investigation of the sequence effect in block amplitude loading of cross-ply composite laminates. *International Journal of Fatigue*, 24(2-4): 437–446, apr 2002. ISSN 01421123. doi: 10.1016/S0142-1123(01)00099-8. URL <https://linkinghub.elsevier.com/retrieve/pii/S0142112301000998>.
- [16] E. K. Gamstedt and R. Talreja. Fatigue damage mechanisms in unidirectional carbon-fibre-reinforced plastics. *Journal of Materials Science*, 34(11):2535–2546, 1999. ISSN 00222461. doi: 10.1023/A:1004684228765. URL <https://link.springer.com/article/10.1023/A:1004684228765>.
- [17] E. Kristofer Gamstedt, Lars A. Berglund, and Ton Peijs. Fatigue mechanisms in unidirectional glass-fibre-reinforced polypropylene. *Composites Science and Technology*, 59(5):759–768, apr 1999. ISSN 02663538. doi: 10.1016/S0266-3538(98)00119-5.
- [18] Rajamohan Ganesan. *Fatigue behavior of thick composite laminates*. Elsevier Ltd., 2 edition, 2020. ISBN 9780081025758. doi: 10.1016/b978-0-08-102575-8.00007-3. URL <http://dx.doi.org/10.1016/B978-0-08-102575-8.00007-3>.
- [19] M.H. Schultz van Haegen-Maas Geesteranus. Vaststelling van de begrotingsstaten van het Ministerie van Infrastructuur en Milieu (XII) voor het jaar 2017, 2016. URL <https://zoek.officielebekendmakingen.nl/kst-34550-XII-60.html>.
- [20] M.H. Schultz van Haegen-Maas Geesteranus. Vaststelling van de begrotingsstaten van het Ministerie van Infrastructuur en Milieu (XII) voor het jaar 2017, 2017. URL https://www.eerstekamer.nl/behandeling/20170710/brief_regering_onderhoud/document3/f=/vkg1d0wfiszw.pdf.
- [21] H. Hamidi, W. Xiong, S. V. Hoa, and R. Ganesan. Fatigue behavior of thick composite laminates under flexural loading. *Composite Structures*, 200:277–289, sep 2018. ISSN 02638223. doi: 10.1016/j.compstruct.2018.05.149.
- [22] Z. Hashin and A. Rotem. A Fatigue Failure Criterion for Fiber Reinforced Materials. *Journal of Composite Materials*, 7(4):448–464, oct 1973. ISSN 0021-9983. doi: 10.1177/002199837300700404. URL <http://journals.sagepub.com/doi/10.1177/002199837300700404>.
- [23] Z. Hashin and A. Rotem. A Fatigue Failure Criterion for Fiber Reinforced Materials. *Journal of Composite Materials*, 7(4):448–464, oct 1973. ISSN 0021-9983. doi: 10.1177/002199837300700404. URL <http://journals.sagepub.com/doi/10.1177/002199837300700404>.
- [24] Andreas Hauße. eLamX² — Chair of Aircraft Engineering — TU Dresden, 2020. URL https://tu-dresden.de/ing/maschinenwesen/ilr/lft/elamx2/elamx?set_language=en.
- [25] L.G.J. Janssen, A.M. van Wingerde, Ch. W. Kensche, T.P. Philippidis, P. Brøndsted, A.G. Dutton, R.P.L. Nijssen, and O. Krause. Reliable Optimal Use of Materials for Wind Turbine Rotor Blades. Technical Report July, OPTIMAT BLADES, 2006.
- [26] Thomas Jollivet, Catherine Peyrac, and Fabien Lefebvre. Damage of composite materials. *Procedia Engineering*, 66:746–758, 2013. ISSN 18777058. doi: 10.1016/j.proeng.2013.12.128.
- [27] Hong C Kim and Lynn J Ebert. Axial Fatigue Failure Sequence and Mechanisms in Unidirectional Fiberglass Composites. Technical report, Case Western Reserve University, Cleveland,, 1978.

- [28] Olaf Krause and Christoph Kensche. Summary Fatigue Test Report OPTIMAT BLADES. Technical report, 2006. URL https://www.wmc.eu/public_docs/10353_000.pdf.
- [29] Prasun K. Majumdar, John J. Lesko, Thomas E. Cousins, and Zihong Liu. Conformable Tire Patch Loading for FRP Composite Bridge Deck. *Journal of Composites for Construction*, 13(6):575–581, dec 2009. ISSN 1090-0268. doi: 10.1061/(asce)cc.1943-5614.0000033.
- [30] M. A. Miner. Cumulative Damage in Fatigue. *Journal of Applied Mechanics*, 12(3):159–164, 1945.
- [31] Bijan Mohammadi, Babak Fazlali, and Davood Salimi-Majd. Development of a continuum damage model for fatigue life prediction of laminated composites. *Composites Part A: Applied Science and Manufacturing*, 93:163–176, feb 2017. ISSN 1359835X. doi: 10.1016/j.compositesa.2016.11.021.
- [32] NEN. NEN-EN 1991-1-4+A1+C2 Eurocode 1: Actions on structures - Part 1-4: General actions - Wind actions. Technical report, European Committee for Standardization, Brussel, 2011.
- [33] Nen. Nen-En 1990 / a1. (september 2006):1–37, 2017.
- [34] NEN. NEN-EN 1991-1 Eurocode 1 - Ontwerp en berekening van bouwconstructies - Deel 1: Grondslagen. Technical report, European Committee for Standardization, Brussel, 2019.
- [35] Nen. NEN-EN 1991-2 + C1 Eurocode 1: Actions on structures - Part 2: Traffic loads on bridges. 2019.
- [36] Rogier P.L. Nijssen. OptiDAT – fatigue of wind turbine materials database. Technical report, Knowledge Centre Wind turbine Materials and Constructions, 2007. URL www.kc-wmc.nl.
- [37] R.P.L. Nijssen. *Fatigue Life Prediction and Strength Degradation of Wind Turbine Rotor Blade Composites*. PhD thesis, Delft University, 2006.
- [38] Martin Noël. Probabilistic fatigue life modelling of FRP composites for construction. *Construction and Building Materials*, 206:279–286 Contents, 2018. doi: 10.1016/j.conbuildmat.2019.02.082. URL <https://doi.org/10.1016/j.conbuildmat.2019.02.082>.
- [39] M. J. Owen and R. J. Howe. The accumulation of damage in a glass-reinforced plastic under tensile and fatigue loading. *Journal of Physics D: Applied Physics*, 5(9): 1637–1649, sep 1972. ISSN 00223727. doi: 10.1088/0022-3727/5/9/319. URL <https://iopscience.iop.org/article/10.1088/0022-3727/5/9/319><https://iopscience.iop.org/article/10.1088/0022-3727/5/9/319/meta>.
- [40] W Van Paepegem, J Degrieck, and P De Baets. Finite element approach for modelling fatigue damage in fibre-reinforced composite materials. *Composites Part B: Engineering*, 32, 2001. URL www.elsevier.com/locate/compositesb.
- [41] A.G. Palmgren. Die Lebensdauer von Kugellagern. *Zeitschrift des Vereines Deutscher Ingenieure*, 14:339–341, 1924.
- [42] Evangelos A Pasipoularidis. *Residual strength and life prediction in composite materials after fatigue*. PhD thesis, UNIVERSITY OF PATRAS MECHANICAL, 2009.
- [43] V. A. Passipoularidis, T. P. Philippidis, and P. Brondsted. Fatigue life prediction in composites using progressive damage modelling under block and spectrum loading. *International Journal of Fatigue*, 33(2):132–144, feb 2010. ISSN 01421123. doi: 10.1016/j.ijfatigue.2010.07.011.
- [44] Theodore P. Philippidis and Anastasios P. Vassilopoulos. Complex stress state effect on fatigue life of GRP laminates. Part I, Experimental. *International Journal of Fatigue*, 24(8):813–823, aug 2002. ISSN 01421123. doi: 10.1016/S0142-1123(02)00003-8.
- [45] Theodore P. Philippidis and Anastasios P. Vassilopoulos. Life prediction methodology for GFRP laminates under spectrum loading. *Composites Part A: Applied Science and Manufacturing*, 35 (6):657–666, jun 2004. ISSN 1359835X. doi: 10.1016/j.compositesa.2004.02.009.

- [46] A. Puck and H. Schürmann. Failure analysis of FRP laminates by means of physically based phenomenological models. *Composites Science and Technology*, 62(12-13 SPECIAL ISSUE): 1633–1662, sep 2002. ISSN 02663538. doi: 10.1016/S0266-3538(01)00208-1.
- [47] A. Puck, J. Kopp, and M. Knops. Guidelines for the determination of the parameters in Puck's action plane strength criterion. *Composites Science and Technology*, 62(3):371–378, feb 2002. ISSN 02663538. doi: 10.1016/S0266-3538(01)00202-0.
- [48] Rijkswaterstaat. Inventarisatie kunstwerken, 2007. URL <https://www.rijksoverheid.nl/binaries/rijksoverheid/documenten/kamerstukken/2007/10/03/br-53977-bijlage-1-inventarisatie-kunstwerken/br-53977-bijlage-1.pdf>.
- [49] Joakim Schön and Tonny Nyman. Spectrum fatigue of composite bolted joints. *International Journal of Fatigue*, 24(2-4):273–279, feb 2002. ISSN 01421123. doi: 10.1016/S0142-1123(01)00082-2.
- [50] W. M. Sebastian, T. Webster, C. Kennedy, and J. Ross. Profiled metal plate - Cork mat loading systems on cellular FRP bridge decks to reproduce tyre-to-deck contact pressure distributions. *Construction and Building Materials*, 49:1064–1082, 2013. ISSN 09500618. doi: 10.1016/j.conbuildmat.2013.07.004.
- [51] Mahmood M. Shokrieh and Larry B. Lessard. Effects of Material Nonlinearity on the Three-Dimensional Stress State of Pin-Loaded Composite Laminates. *Journal of Composite Materials*, 30(7):839–861, may 1996. ISSN 0021-9983. doi: 10.1177/002199839603000705. URL <http://journals.sagepub.com/doi/10.1177/002199839603000705>.
- [52] Mahmood M. Shokrieh and Larry B. Lessard. Multiaxial fatigue behaviour of unidirectional plies based on uniaxial fatigue experiments - I. Modelling. *International Journal of Fatigue*, 19(3):201–207, mar 1997. ISSN 01421123. doi: 10.1016/S0142-1123(96)00074-6. URL <https://www.sciencedirect.com/science/article/abs/pii/S0142112396000746>.
- [53] Mahmood M. Shokrieh and Larry B. Lessard. Progressive Fatigue Damage Modeling of Composite Materials, Part I: Modeling. *Journal of Composite Materials*, 34(13):1056–1080, jul 1998. ISSN 0021-9983. doi: 10.1177/002199830003401301. URL <http://journals.sagepub.com/doi/10.1177/002199830003401301>.
- [54] Mahmood M. Shokrieh and Larry B. Lessard. Progressive Fatigue Damage Modeling of Composite Materials, Part II: Material Characterization and Model Verification. *Journal of Composite Materials*, 34(13):1081–1116, jul 2000. ISSN 0021-9983. doi: 10.1177/002199830003401302. URL <http://journals.sagepub.com/doi/10.1177/002199830003401302>.
- [55] SOFiSTiK. Allgemeine Statik der FE Strukturen. Technical report, SOFiSTiK AG, Oberschleissheim, 2020.
- [56] R. Talreja. Fatigue of composite materials: damage mechanisms and fatigue-life diagrams. *Proceedings of the Royal Society of London. A. Mathematical and Physical Sciences*, 378 (1775):461–475, nov 1981. ISSN 2053-9169. doi: 10.1098/rspa.1981.0163. URL <https://royalsocietypublishing.org/doi/10.1098/rspa.1981.0163>.
- [57] Ramesh Talreja and Janis Varna. *Modeling damage, fatigue and failure of composite materials*. Elsevier Inc., jan 2015. ISBN 9781782422860. doi: 10.1016/c2013-0-16521-x.
- [58] J X Tao, C T Sun, and I X Tao. MATRIX CRACKING ON STIFFNESS OF COMPOSITE LAMINATES EFFECT OF MA'T'R'IX CRACKING ON STIFFNESS OF COMPOSITE LAMINATES. *MECHANICS OF COMPOSITE MATERIALS AND STRUCTURES An INTERNATIONAL JOURNAL*, 3(3):225–239, 1996. ISSN 1521-0596. doi: 10.1080/10759419608945865. URL <https://www.tandfonline.com/action/journalInformation?journalCode=umcm20>.

- [59] Holger Thom. A review of the biaxial strength of fibre-reinforced plastics. *Composites Part A: Applied Science and Manufacturing*, 29(8):869–886, aug 1998. ISSN 1359835X. doi: 10.1016/S1359-835X(97)00090-0.
- [60] D R V Van Delft, G D De Winkel, and P A Joosse. Fatigue behaviour of fibreglass wind turbine blade material under variable amplitude loading. *American Institute of Aeronautics and Astronautics*, 1997. doi: 10.2514/6.1997-951. URL <http://arc.aiaa.org>.
- [61] W. Van Paepegem. Fatigue damage modelling of composite materials with the phenomenological residual stiffness approach. In *Fatigue Life Prediction of Composites and Composite Structures*, pages 102–138. Elsevier Inc., jan 2010. ISBN 9781845695255. doi: 10.1533/9781845699796.1.102.
- [62] W. Van Paepegem and J. Degrieck. Experimental set-up for and numerical modelling of bending fatigue experiments on plain woven glass/epoxy composites. *Composite Structures*, 51(1):1–8, jan 2001. ISSN 02638223. doi: 10.1016/S0263-8223(00)00092-1.
- [63] W. Van Paepegem, I. De Baere, and J. Degrieck. Modelling the nonlinear shear stress-strain response of glass fibre-reinforced composites. Part II: Model development and finite element simulations. *Composites Science and Technology*, 66(10):1465–1478, 2006. ISSN 02663538. doi: 10.1016/j.compscitech.2005.04.018.
- [64] Anastasios P. Vassilopoulos and Rogier P.L. Nijssen. *Fatigue life prediction under realistic loading conditions*. Elsevier Ltd., 2 edition, 2020. ISBN 9780081025758. doi: 10.1016/b978-0-08-102575-8.00011-5. URL <http://dx.doi.org/10.1016/B978-0-08-102575-8.00011-5>.
- [65] Anastasios P. Vassilopoulos, Behzad D. Manshadi, and Thomas Keller. Influence of the constant life diagram formulation on the fatigue life prediction of composite materials. *International Journal of Fatigue*, 32(4):659–669, apr 2010. ISSN 01421123. doi: 10.1016/j.ijfatigue.2009.09.008.
- [66] Technische Weekblad. Rijkswaterstaat: assetmanagement vraagt grotere verscheidenheid aan technische kennis | Technisch Weekblad, 2015. URL <https://www.technischweekblad.nl/partnercontent/rijkswaterstaat-assetmanagement-vraagt-grotere-verscheidenheid-aan-technische-kennis>.
- [67] Haohui Xin. Lecture 12 Fracture Mechanics, Part 3, Fatigue Crack Propagation, 2020.